

Stochastic switching in multistable gene regulatory networks



Inaugural-Dissertation
zur
Erlangung des Doktorgrades
der Mathematisch-Naturwissenschaftlichen Fakultät
der Universität zu Köln

vorgelegt von

Prasanna M. Bhogale

aus Aurangabad (MH), India

Köln, 2024

Berichterstatter (Gutacher):

Prof. Dr. Johannes Berg

Zweite Gutachter und Prüfer:

Prof. Dr. Joachim Krug

Abstract

The *lac*-operon serves as a key model for understanding gene regulation and metabolic adaptation in bacteria. Using theoretical models, computational simulations, and experimental data, this study elucidates the stochastic switching behavior of the *lac*-operon between its induced and uninduced states.

First, a detailed mechanistic model of the *lac*-pathway is established from the extensive literature on the biochemistry of the *lac*-operon, encompassing sugar import, repressor production, importer production, dilution rate, and inducer-repressor-DNA interactions, providing a robust framework for analyzing the system.

The switching behavior to the induced state is analyzed by first calibrating stochastic simulations of a detailed mechanistic model against experimental data on switching rates. This calibration allows for the identification of rate-limiting fluctuations that drive the switching process. Consequently, minimal theoretical models that agree with experimental observations can be derived and subjected to further study. The study employs the Michaelis constant of inducer import as a fitting parameter and introduces a smoothening procedure to identify the key fluctuations influencing the switching curve. This leads to the development of a closed-form expression for the switching rate as a function of external inducer concentration that matches with experiment and simulations across 3 orders of magnitude.

The reverse transition from the induced to the uninduced state has been difficult to study since the induced state is extremely

stable and experimental observations of this transitions are sparse. We start by identifying fluctuations relevant to the transition using the *in silico* smoothing procedure, and constructing simplified theoretical models for each relevant fluctuation. These are then combined to develop a master equation for the *lac* system that can be approximated by a 2D Fokker-Planck equation for pump and repressor protein dynamics. This equation is used to calculate the first passage times to the uninduced state. The theoretical predictions agree qualitatively with experiment demonstrating the extreme stability of the induced state and its dependence on repressor numbers and fluctuations.

By identifying rate-limiting fluctuations and providing a quantitative framework that links molecular interactions to phenotypic switching behavior, this work advances our understanding of stochastic switching in the *lac*-operon and introduces techniques that can be used to analyse other systems.

Zusammenfassung

Das *lac*-Operon dient als ein Modell für das Verständnis der Genregulation und der metabolischen Adaptation in Bakterien. Mithilfe theoretischer Modelle, Computersimulationen und experimenteller Daten beleuchtet diese Studie das stochastische Schaltverhalten des *lac*-Operons zwischen seinem induzierten und nicht-induzierten Zustand.

Zunächst wird basierend auf der umfangreichen Literatur zur Biochemie des *lac*-Stoffwechselwegs ein detailliertes mechanistisches Modell des *lac*-Stoffwechselwegs erstellt, das den Zuckerimport, die Repressorproduktion, die Importerproduktion, die Verdünnungsrate und die Wechselwirkungen zwischen Induktor, Repressor und DNA umfasst und einen robusten Rahmen für die Analyse des Systems bietet.

Das Schaltverhalten in den induzierten Zustand wird analysiert, indem experimentelle Daten zu Schaltraten mit stochastischen Simulationen des mechanistischen Modells verglichen werden. Die Studie verwendet die Michaelis-Konstante des Induktorimports als freier Parameter und führt ein Glättungsverfahren ein, um die wichtigsten Fluktuationen zu identifizieren, die die Schaltkurve beeinflussen. Dies führt zur Entwicklung eines geschlossenen Ausdrucks für die Schaltrate als Funktion der externen Induktorkonzentration, der über 3 Größenordnungen mit Experiment und Simulationen übereinstimmt.

Der umgekehrte Übergang vom induzierten in den nicht-induzierten Zustand ist schwierig zu untersuchen, da der

induzierte Zustand extrem stabil ist und der Übergang somit nur selten beobachtet werden kann. Wir beginnen damit, die für den Übergang relevanten Fluktuationen mithilfe des *in silico* Glättungsverfahrens zu identifizieren und vereinfachte theoretische Modelle für jede relevante Fluktuation zu konstruieren. Diese werden dann kombiniert, um eine Mastergleichung für das *lac*-System zu entwickeln, die durch eine 2D Fokker-Planck-Gleichung für die Dynamik von Pumpen- und Repressorproteinen approximiert werden kann. Diese Gleichung wird verwendet, um die first passage times zum nicht-induzierten Zustand zu berechnen. Die theoretischen Vorhersagen stimmen qualitativ mit dem Experiment überein und demonstrieren die extreme Stabilität des induzierten Zustands und seine Abhängigkeit von der Repressorzahl und Fluktuationen.

Durch die Identifizierung der rate limiting fluctuations und die Bereitstellung eines quantitativen Rahmens, der molekulare Wechselwirkungen mit phänotypischem Schaltverhalten verbindet, verbessert diese Arbeit unser Verständnis des stochastischen Schaltens im *lac*-Operon und führt Techniken ein, die zur Analyse anderer Systeme verwendet werden können.

Acknowledgements

First and foremost, I would like to express my sincere gratitude to my advisor, Prof. Johannes Berg, for his patience, support, and guidance throughout my PhD journey. I thank him for his careful attention to both the scientific content of this thesis and my overall well-being. I would like to thank Prof. J. W. Veening and Dr. R. A. Sorg for a productive and enjoyable collaboration.

Frau Christa Stitz was of immense help from the moment I landed in Cologne, and everything would have been a lot harder without her.

I am deeply grateful to Chau, whose positive and inspiring presence was a source of motivation from the first day of my PhD. My time at the Institute was also enriched by the presence of friends with whom I shared many a coffee, scientific discussions and games of pétanque. I would like to thank Bhavin, Joachim, Simone, Nico, Donate, Filippas, Nandita, and Nina for everything.


Life in Cologne was made more meaningful by the meals, conversations, and arguments shared with friends - Sachita, Ruth, Jayesh, Ulrike, Abhijeet, Rohini, Rahul, Chavvi, and Megha. I am thankful for their companionship and the memories.

Halfway through my time at the Institute, I got married. My wife Ketki has kept me sane through this journey. I also wrote a significant portion of the second paper and the entirety of this thesis after leaving the Institute and after our daughters Kaveri and Iravati were born. I am grateful for my family.

Finally, I would like to thank my parents for their unwavering support, especially over the last two years of change.

Erklärung zur Dissertation

Hiermit versichere ich an Eides statt, dass ich die vorliegende Dissertation selbstständig und ohne die Benutzung anderer als der angegebenen Hilfsmittel und Literatur angefertigt habe. Alle Stellen, die wörtlich oder sinngemäß aus veröffentlichten und nicht veröffentlichten Werken dem Wortlaut oder dem Sinn nach entnommen wurden, sind als solche kenntlich gemacht. Ich versichere an Eides statt, dass diese Dissertation noch keiner anderen Fakultät oder Universität zur Prüfung vorgelegen hat; dass sie - abgesehen von unten angegebenen Teilpublikationen und eingebundenen Artikeln und Manuskripten - noch nicht veröffentlicht worden ist sowie, dass ich eine Veröffentlichung der Dissertation vor Abschluss der Promotion nicht ohne Genehmigung des Promotionsausschusses vornehmen werde. Die Bestimmungen dieser Ordnung sind mir bekannt. Darüber hinaus erkläre ich hiermit, dass ich die Ordnung zur Sicherung guter wissenschaftlicher Praxis und zum Umgang mit wissenschaftlichem Fehlverhalten der Universität zu Köln gelesen und sie bei der Durchführung der Dissertation zugrundeliegenden Arbeiten und der schriftlich verfassten Dissertation beachtet habe und verpflichte mich hiermit, die dort genannten Vorgaben bei allen wissenschaftlichen Tätigkeiten zu beachten und umzusetzen. Ich versichere, dass die eingereichte elektronische Fassung der eingereichten Druckfassung vollständig entspricht.



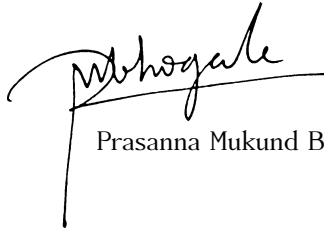
Prasanna Mukund Bhogale

13-11-2024

Teilpublikationen

[1] What makes the lac-pathway switch: identifying the fluctuations that trigger phenotype switching in gene regulatory systems. **P. M. Bhogale**, R. A. Sorg, J-W. Veening, and J. Berg. Nucleic Acids Research, 42(18):11321-11328, 2014.

[2] Switching off: The phenotypic transition to the uninduced state of the lactose uptake pathway. **P. M. Bhogale**, R. A. Sorg, J-W. Veening, and J. Berg. Biophysical Journal, 121:183-192, 2022.

A handwritten signature in black ink, appearing to read 'P. M. Bhogale', with a long horizontal stroke extending to the right.

13-11-2024

Prasanna Mukund Bhogale

Contents

1	Introduction	1
1.1	The <i>lac</i> -operon of <i>E. coli</i>	1
1.1.1	Diauxie	2
1.1.2	Induction	2
1.1.3	A Portrait of the Operon as a Switch	4
1.2	Review of stochastic methods	7
1.2.1	Random variables	8
1.2.2	Stochastic processes	14
1.2.3	Chapman-Kolmogorov equation	16
1.2.4	Master equations and jump processes	18
1.2.5	Simulating master equations - the Gillespie algorithm	22
1.2.6	Fokker-Planck equation	24
1.2.7	First passage times	26
1.3	Structure of this thesis	27
2	The model	29
2.1	Introduction	29
2.1.1	Comparison to previous models	33
2.2	Import of sugar into the cell	35
2.3	Repressor production	36
2.4	Importer production	38
2.5	Inducer-repressor-DNA interactions	39
2.6	Detailed balance	44
2.7	Dilution rate	48
2.8	Other factors	48

2.8.1	Cell Divisions	49
2.8.2	Delays	49
2.8.3	Simulating the model	50
2.9	Summary	50
3	Switching on	53
3.1	Introduction	53
3.2	Switching curves from experiments	54
3.2.1	Simulations and fitting to experiment	54
3.3	The smoothening procedure	56
3.3.1	Smoothening operator state fluctuations	60
3.4	The switching rate γ	62
3.4.1	The threshold period τ	68
3.4.2	Simplified expression for γ	69
3.5	Summary	72
4	Switching off	73
4.1	Introduction	73
4.1.1	Experimental measurements	74
4.1.2	Smoothening curves for different fluctuations	74
4.2	The unbinding rate η	77
4.2.1	Repressor unbinding without inducer interaction – the $\{\eta_j\}$	79
4.2.2	Effective inducer interactions with the repressor-DNA loop	81
4.2.3	Including inducer interactions	82
4.2.4	Probability of forming a repressor-DNA loop with j bound inducers	84
4.3	Calculating the binding rate β	86
4.4	Modelling pump dynamics with β and η	86
4.4.1	Deriving the Fokker-Planck equation for pump proteins	89
4.4.2	Simulating drift and diffusion of pump proteins	92
4.5	Modelling repressor dynamics	94
4.6	Computing the MFPT, results	97
4.6.1	Mean first passage times from the induced to the uninduced state	97
4.6.2	Comparison with experiments	99
4.7	Summary	101

5	Discussion	103
5.1	Identification of rate-limiting fluctuations	103
5.2	Transition to the induced state	104
5.3	Transition to the uninduced state	105
5.4	Experimental tests of the theory	106
5.5	Conclusions and outlook	107
A	Appendix: Experiments	109
A.1	Determining phenotypic switching rates	109
A.2	Experimental conditions	110

1. Introduction

This thesis elucidates the regulatory dynamics of the *lac*-operon in *Escherichia coli*, employing tools from non-equilibrium statistical physics along with simulations and experiments. The *lac*-operon has been a key model system of gene regulation used widely to analyze the mechanisms of gene regulation and bacterial metabolic adaptation. Integrating theory and simulations with experimental data, our investigation aims to provide an understanding of the operon's switching behavior.

1.1. The *lac*-operon of *E. coli*

The work of François Jacob, Jacques Monod, and their colleagues in the 1960s marked a seminal advancement in our understanding of molecular genetics, particularly in gene regulation mechanisms (see [3] for a wonderful account of these early developments by Benno Müller-Hill, who contributed significantly to these advances). This thesis begins with an exploration of the historical context surrounding these breakthroughs, focusing on diauxie – a phenomenon that underscores *E. coli*'s metabolic flexibility in response to different sugars. Our research contributes to the wider discourse on genetic regulatory systems by identifying rate limiting fluctuations and using these to develop quantitative models for the *lac*-operon's transitions between induced and uninduced states.

1.1.1. Diauxie

Originally identified in yeast, diauxie describes a two-phase growth pattern observed in microorganisms when presented with two distinct carbon sources, such as glucose and lactose (for this section, see [3] and references therein). Initially, glucose is consumed preferentially; only upon its exhaustion does the organism adapt to metabolize the alternative sugar, lactose.

Jacques Monod's subsequent research in *E. coli* revealed a similar biphasic growth pattern, with the bacterium initially metabolizing glucose before transitioning to lactose, depicted in Figure 1.1. This shift underscored the bacterium's genetic capacity to prioritize glucose over lactose, adjusting its metabolic pathway according to the available carbon sources.

Monod's findings paved the way for uncovering the *lac*-operon — a gene cluster crucial for lactose metabolism in *E. coli*. The operon encompasses three structural genes (*lacZ*, *lacY*, and *lacA*) and a regulatory gene (*lacI*), which orchestrate lactose breakdown and uptake. The *lac*-operon's expression is regulated by the *lacI* gene product, a repressor that inhibits transcription of the *lac* genes in the absence of lactose, an example of the cellular regulatory mechanisms facilitating metabolic adaptation.

The phenomenon of diauxie, thus, serves as a prelude to the *lac*-operon's intricate regulatory mechanisms, particularly how it transitions from a state of repression to one of induction in the absence of glucose. This transition is critical for the bacterium's survival, ensuring that it efficiently utilizes available carbon sources for energy.

1.1.2. Induction

In the absence of glucose, the *lac*-operon can be induced when lactose is present in the environment. Lactose, specifically its isomer allolactose, serves as an inducer molecule that deactivates the repressor of the *lac*-operon, allowing the bacterium to metabolize lactose.

When glucose is absent, the cellular levels of cyclic AMP (cAMP) increase. cAMP is a secondary messenger that helps in regulating various cellular processes, including the response to changes in carbon source availability. As cAMP levels rise, cAMP binds to a

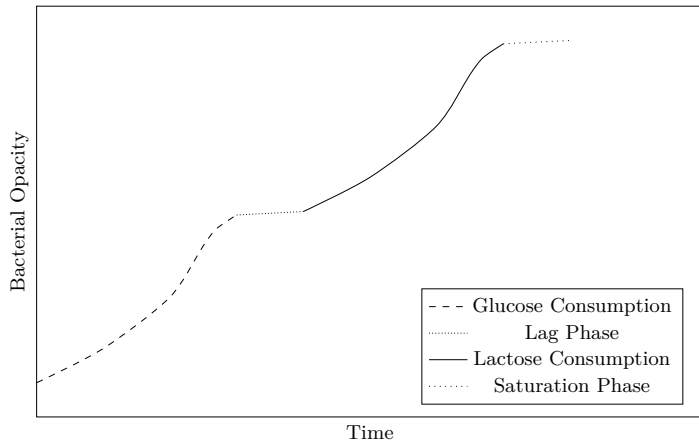


Figure 1.1: Qualitative illustration based on [3] of the diauxic growth phenomenon in bacteria. The graph demonstrates the two distinct growth phases associated with glucose and lactose metabolism. Initially, bacteria preferentially consume glucose, leading to a rapid growth phase. Once glucose is depleted, a lag phase ensues as bacteria adjust their metabolic pathways to utilize lactose, followed by a slower lactose-driven growth phase.

protein called catabolite activator protein (CAP), also known as cAMP receptor protein (CRP). The cAMP-CAP complex then binds to a specific site near the *lac*-operon's promoter. This binding enhances the binding affinity of RNA polymerase to the promoter, making it more likely for transcription to occur.

When lactose is available, a small amount is converted into allolactose, the true inducer of the *lac*-operon. Allolactose binds to the lacI repressor protein, causing a conformational change that prevents the repressor from binding to the operator site. With the repressor protein no longer inhibiting the process, RNA polymerase can bind to the promoter and initiate the transcription of the *lacZ*, *lacY*, and *lacA* genes.

As levels of lactose permease (encoded by the *lacY* gene) rise, more lactose is imported into the cell resulting in increased inducer levels and reducing the probability that a repressor can successfully bind to the lac operator. Thus, induction of the *lac*-operon is a doubly negative feedback mechanism, where induction of the operon represses its repressor.

1.1.3. A Portrait of the Operon as a Switch

The understanding of the switching dynamics between the induced and uninduced states of the *lac*-operon has evolved significantly over the past several decades. This journey began in 1957 with the seminal work of Novick and Weiner [4]. They suggested that the induction of the *lac*-operon is an “all-or-none” phenomenon at the cellular level, where the operon is either fully on or fully off.

Novick and Weiner's hypothesis posited that the operon's switch to the induced state is contingent upon the stochastic appearance of a permease molecule within a bacterium, marking the initiation of an auto-catalytic process. Upon the addition of inducer to a bacterial culture, they observed a linear increase in the rate of enzyme synthesis per bacterium, suggesting that individual cells were transitioning to full induction rapidly, rather than gradually increasing their enzyme production. This “all-or-none” response, further influenced by the concentration of the inducer and the presence of permease, implies a highly sensitive and swift decision-making mechanism at the cellular level. Key to their findings was the recognition that at low

inducer concentrations, a bacterial population consists of cells either fully induced or not at all, with the transition between these states being rapid and complete once initiated. This auto-catalytic induction mechanism explains how a bacterial population can efficiently respond to environmental changes, ensuring that once a threshold level of inducer is reached within a cell, a swift and full switch to enzyme production occurs, adapting the cell's metabolism to its environment.

Fast forward to 2004, and the work of Ozbudak et al. [5] built upon the “all-or-none” hypothesis by exploring the bistability of the *lac*-operon. Employing a blend of experimental and mathematical methods, they delineated the conditions under which the *lac*-operon displays bistability - the ability to exist in either an induced or uninduced state based on the operon's history with specific inducer concentrations. Their findings reveal that in the absence of glucose, the operon switches from uninduced to induced states at specific threshold concentrations of TMG, a non-metabolizable lactose analog. Crucially, this switch exhibits hysteresis; that is, the history of the cell's exposure to TMG concentrations influences its current state. This hysteresis indicates a region of bistability where the operon's state depends on its prior condition, further underpinning the operon's functionality as a molecular switch. Such bistability was predicted by the feedback loops inherent in the *lac*-operon's regulation but is demonstrated definitively in the context of the whole organism by Ozbudak et al. This analysis corroborates the operon's bistability and demonstrates how varying degrees of operon repression impact this dynamic behavior.

In 2008, Choi, Xie, and colleagues made a significant step in clarifying the molecular mechanisms behind the *lac*-operon's switch to the induced state [6], providing an expansion and refinement of the initial concepts proposed by Novick and Weiner. Their investigations revealed that the transition to the induced state is not merely a consequence of a single permease molecule being produced inside the cell, as previously theorized. Instead, they identified that the operon's induction hinges on a singular, stochastic event: the complete dissociation of the tetrameric lactose repressor from all operator sites on the DNA. This critical insight showed that such complete dissociation events are rare

but result in substantial bursts of permease expression, which are essential for crossing the threshold necessary for operon induction.

Through single-molecule fluorescence microscopy, Choi et al. were able to directly observe these rare molecular events in real-time, utilizing a significant advancement in experimental capabilities that were unavailable to Novick and Weiner. They further demonstrated that the basal level expression observed in some cells at intermediate inducer concentrations resulted from partial dissociations of the repressor from one of its operators on looped DNA, whereas the decisive switch to the induced phenotype was triggered by the infrequent but significant events of complete repressor dissociation.

This model contrasts with the earlier hypothesis by Novick and Weiner, which suggested that the random expression of a single permease molecule could suffice to trigger induction. Choi et al.'s findings emphasize the importance of the quantity and manner of permease expression — highlighting that a threshold of several hundred molecules, achieved through large expression bursts following complete repressor dissociation, is necessary for induction.

In this thesis we aim to identify the stochastic steps that drive the phenotypic transition in the *lac*-operon, both from the off state to the on state, and vice versa. In our 2013 study [1], we focused on the transition to the induced state of the *lac*-operon. We introduced a key tool – the smoothing procedure – to identify the critical fluctuation driving the transition. By selectively reducing fluctuations in the regulatory system's components, this method helps in pinpointing their impact on the switching rate, offering a versatile tool for dissecting mechanisms behind stochastic transitions in gene regulatory systems. We find that for the transition to the on state, the detachment of the lac repressor identified by Choi et al. is a necessary condition for the transition, but not a sufficient one. We not only underscored the critical role played by the duration for which the lac repressor remains detached but also introduced a simple model that includes a closed-form formula for the switching rate. This model provides a quantitative tool to predict switching behavior under various conditions, building upon the foundational "all-or-none"

hypothesis by Novick and Weiner and integrating with the insights from single-molecule observations by Choi et al.

In our 2021 work [2], we focused on the transition from the induced to the uninduced state of the *lac*-operon, a process not previously analyzed in the literature. By employing the smoothing procedure introduced in our earlier work, we systematically identified the fluctuations which drive the transition. Our research revealed that this transition is influenced by fluctuations in several components: repressor-operator binding/unbinding, fluctuations in the total number of repressors, and inducer-repressor binding/unbinding. To model this transition, we developed mathematical models for each relevant sub-component of the system, and combined them to construct a 2D Fokker-Planck (FP) equation for permease and repressor numbers from which we could derive the first passage times and thus the switching rates to the uninduced state. Our findings indicate that these transitions occur over very long timescales, in line with experimental observations [2].

1.2. Review of stochastic methods

Stochastic systems refer to processes or models in which uncertainty and randomness are inherently present. These systems can be found across various fields such as physics, biology, economics, and engineering. In a stochastic system, the future state or outcome depends on both the current state and a random element, making precise predictions challenging. Probability theory serves as the mathematical foundation for analyzing and understanding these stochastic systems, providing tools to quantify and model the inherent uncertainty.

In physics - as in life - there are situations which have multiple possible outcomes. Implicitly, there is uncertainty (aleatoric as well as epistemic) as to what the outcome will be. However, to aid decision making, one might attempt to quantify the uncertainty associated with each possibility by attaching to each outcome a number, with larger numbers indicating a higher degree of belief that *that* outcome will in fact be the one that transpires. If those numbers (one for each possible mutually exclusive outcome) are normalized so that they sum to 1, what we have is a probability

distribution.

Probability theory deals with the analysis of random phenomena and the quantification of the likelihood of various eventualities. In this framework, an event, denoted as A , is a subset of a sample space Ω , which represents all possible outcomes of a random experiment. The probability of an event A occurring is represented as $P(A)$, with the probability measure satisfying three main axioms:

1. $0 \leq P(A) \leq 1$ for all events A
2. $P(\Omega) = 1$
3. For any countable collection of mutually exclusive events A_1, A_2, \dots , $P(\bigcup_{i=1}^{\infty} A_i) = \sum_{i=1}^{\infty} P(A_i)$.

These axioms form the basis for understanding and manipulating probabilities in the context of stochastic systems, allowing researchers to model uncertainty and make informed decisions based on the likelihood of various outcomes. In the following sections, we introduce random variables, random events, and stochastic processes.

1.2.1. Random variables

A random variable, denoted by X , is a function that assigns a real number to each outcome in the sample space Ω . It encapsulates the numerical outcome of a stochastic experiment, allowing for the quantitative analysis of random phenomena. The probability distribution of a random variable X characterizes the likelihood of various outcomes, represented as $P(X = x)$ for discrete variables, or the probability density function $f_X(x)$ for continuous variables, where x is a value that X can take. For notational convenience, we will review the theory for continuous random variables. The extension to discrete cases is usually straightforward, see [7, 8].

The expectation value (or expected value) of a continuous random variable X , often denoted as $\mathbb{E}[X]$, is a measure of the central tendency of X . For a random variable X with a probability density function $f_X(x)$, the expectation is defined as,

$$\mathbb{E}[X] = \int_{-\infty}^{\infty} x f_X(x) dx.$$

This integral sums over all possible values of X , weighted by their probability density, providing a single value that represents the average outcome of X if the stochastic experiment were repeated many times. For such a continuous random variable X , we can define the expected value of a function $g(X)$, where g is a real-valued function applied to the random variable. Given the PDF $f_X(x)$, the expected value of $g(X)$ is given by,

$$\mathbb{E}[g(X)] = \int_{-\infty}^{\infty} g(x) f_X(x) dx.$$

Moments are a generalization of the expected value and provide a way to describe the shape and characteristics of the distribution of a continuous random variable. The n -th moment about the origin of a continuous random variable X is defined as the expected value of X^n , and it can be calculated as,

$$\mu_n = \mathbb{E}[X^n] = \int_{-\infty}^{\infty} x^n f_X(x) dx,$$

where n is a positive integer and $f_X(x)$ is the PDF of the random variable X . The n -th central moment is defined as the expected value of the n -th power of the difference between the random variable and its mean:

$$\nu_n = \mathbb{E}[(X - \mathbb{E}[X])^n] = \int_{-\infty}^{\infty} (x - \mathbb{E}[X])^n f_X(x) dx.$$

The first central moment ν_1 is always equal to zero, and the second central moment ν_2 corresponds to the variance of the random variable X . Higher-order central moments provide further insight into the shape and properties of the distribution, such as skewness (measured by the third standardized central moment) and kurtosis.

1.2.1.1. Characteristic function

The characteristic function is an important tool in probability theory and statistics. For a random variable X with probability

1. INTRODUCTION

density function $f_X(x)$, the characteristic function $\phi_X(t)$ is defined as the expected value of e^{itX} , where i is the imaginary unit and t is a real variable,

$$\phi_X(t) = \mathbb{E}[e^{itX}] = \int_{-\infty}^{\infty} e^{itx} f_X(x) dx.$$

The moments of X are obtained through differentiation at $t = 0$. Specifically, the n -th moment of X is retrieved as,

$$\mathbb{E}[X^n] = \left(\frac{d^n}{dt^n} \phi_X(t) \right) \Big|_{t=0}.$$

The characteristic function, as the Fourier transform of the probability density function, provides a complete statistical description of X . It is particularly advantageous for analyzing the distributional aspects and sum of independent random variables because the characteristic function of a sum is the product of their individual characteristic functions. This property simplifies the analysis of sums of random variables, essential in many stochastic processes.

Furthermore, the absolute value of the characteristic function is always bounded by 1, with $\phi_X(0) = 1$, indicating the total probability. This boundedness and continuity in t make it a well-behaved mathematical function, facilitating the derivation of distributional properties and moments. Analyzing the behavior of $\phi_X(t)$ near $t = 0$ provides insights into the variance and higher moments, while its decay rate as $|t|$ increases reveals information about the tails of the distribution.

1.2.1.2. Addition of two random variables

When dealing with the addition of two or more independent continuous random variables, the characteristic function offers a convenient approach. Let X and Y be two independent continuous random variables with characteristic functions $\phi_X(t)$ and $\phi_Y(t)$, respectively. The characteristic function of the sum of these random variables, $Z = X + Y$, can be obtained as the product of their individual characteristic functions,

$$\phi_Z(t) = \phi_{X+Y}(t) = \phi_X(t) \cdot \phi_Y(t).$$

This property makes the characteristic function a powerful tool for analyzing the distribution of sums of independent continuous random variables, as it simplifies the process of determining their combined distribution. Once the characteristic function of the sum $Z = X+Y$ is obtained as the product of their individual characteristic functions, the probability density function $f_Z(z)$ of the sum can be derived using the inverse Fourier transform,

$$f_Z(z) = \frac{1}{2\pi} \int_{-\infty}^{\infty} e^{-itz} \phi_Z(t) dt.$$

The advantage of using the characteristic function becomes more apparent when dealing with multiple independent continuous random variables. Suppose we have n independent continuous random variables X_1, \dots, X_n , with their respective characteristic functions $\phi_{X_1}(t), \phi_{X_2}(t), \dots, \phi_{X_n}(t)$. If we want to find the distribution of their sum, $S_n = X_1 + X_2 + \dots + X_n$, the characteristic function of S_n is given by the product of their individual characteristic functions,

$$\phi_{S_n}(t) = \phi_{X_1}(t) \cdot \phi_{X_2}(t) \cdots \phi_{X_n}(t).$$

Once the characteristic function of the sum S_n is determined, we can derive the probability density function of the sum by applying the inverse Fourier transform.

1.2.1.3. Multivariate Distributions

In the study of stochastic systems, often it is necessary to consider distributions which describe the behavior of multiple random variables simultaneously. For a set of continuous random variables, (X_1, \dots, X_n) , the joint probability density function $f_{X_1, X_2, \dots, X_n}(x_1, x_2, \dots, x_n)$ captures the likelihood of these variables simultaneously taking specific values. Marginal probability density functions are derived from the joint distribution by integrating out the variables that are not of interest. For instance, the marginal distribution of X_1 is obtained by integrating the joint distribution over all variables except X_1 ,

$$f_{X_1}(x_1) = \int_{-\infty}^{\infty} \cdots \int_{-\infty}^{\infty} f_{X_1, X_2, \dots, X_n}(x_1, x_2, \dots, x_n) dx_2 \dots dx_n.$$

This integration process effectively “sums out” the influence of the other variables, providing a distribution that reflects the behavior of X_1 irrespective of the others.

Conditional probability density functions, on the other hand, express the probability distribution of one or more variables given the values of others. For example, the conditional distribution of X_1 given X_2 is defined as,

$$f_{X_1|X_2}(x_1|x_2) = \frac{f_{X_1, X_2}(x_1, x_2)}{f_{X_2}(x_2)},$$

provided that $f_{X_2}(x_2) > 0$. This conditional distribution describes how the distribution of X_1 changes when the value of X_2 is known.

1.2.1.4. Random Events

Imagine receiving text messages at various times throughout the day. This scenario can be modeled as a series of random events, where the exact timing of each message is unpredictable. In the mathematical framework of probability theory these events are defined within the context of a sample space Ω , representing all possible outcomes of a random experiment. A random event A can be considered as a subset of the sample space Ω , where each element of A corresponds to a specific outcome, such as receiving a text message within a particular hour. Mathematically, if we denote the occurrence of an event A at time t as $A(t)$, the waiting time for event A to occur can be modeled as a random variable. The distribution of these waiting times provides insight into the underlying stochastic process governing the events.

1.2.1.5. Poisson Distribution and Exponential Waiting Times

A special case of random events occurs when each event is independent of others and happens at a constant average rate λ , this is called the Poisson process. In this context, the Poisson distribution provides the probability of a given number of events

occurring within a fixed time interval. We want to find the probability of observing k events in a fixed time interval of length t .

Let's divide the time interval t into n equal sub-intervals of length $\Delta t = t/n$. For sufficiently small Δt , the probability of an event occurring in a sub interval is approximately $\lambda\Delta t$, and the probability of more than one event occurring in a sub-interval is negligible. The probability of observing k events in the entire interval t is equal to the probability of observing k successes in n independent Bernoulli trials, each with success probability $p = \lambda\Delta t$. This is given by the binomial distribution,

$$P(k \text{ events in } t) = \binom{n}{k} (\lambda\Delta t)^k (1 - \lambda\Delta t)^{n-k}. \quad (1.1)$$

Taking the limit as $n \rightarrow \infty$ (and consequently $\Delta t \rightarrow 0$), we have:

$$\begin{aligned} \lim_{n \rightarrow \infty} P(k \text{ events in } t) &= \lim_{n \rightarrow \infty} \binom{n}{k} (\lambda t/n)^k (1 - \lambda t/n)^{n-k} \\ &= \frac{(\lambda t)^k}{k!} \lim_{n \rightarrow \infty} \frac{n!}{(n-k)! n^k} (1 - \lambda t/n)^{n-k} \\ &= \frac{(\lambda t)^k}{k!} \lim_{n \rightarrow \infty} \left(1 - \frac{\lambda t}{n}\right)^n \left(1 - \frac{\lambda t}{n}\right)^{-k} \\ &= \frac{(\lambda t)^k}{k!} e^{-\lambda t}. \end{aligned}$$

Thus, the probability of observing k events in a time interval of length t for a Poisson process with rate λ is given by the Poisson distribution,

$$P(k \text{ events in } t) = \frac{(\lambda t)^k}{k!} e^{-\lambda t}. \quad (1.2)$$

For the Poisson process, the waiting times between successive events are exponentially distributed. If T denotes the waiting time for the next event, its probability density function (PDF) reflects the memory-less property of the Poisson process, where the probability of an event occurring is independent of the elapsed time since the last event,

$$f_T(t) = \lambda e^{-\lambda t}.$$

Now, we take a look at more general stochastic processes.

1.2.2. Stochastic processes

In physics, biology, finance, and other fields, stochastic processes play a crucial role in modeling systems where outcomes are inherently uncertain and influenced by random factors. For instance, in physics, the random motion of particles in a fluid, known as Brownian motion, exemplifies a stochastic process where the future position of each particle depends on its current state and a random component reflecting molecular collisions. Similarly, in biology, the process of gene expression in cells, where the timing of transcription and translation events is subject to random fluctuations, can be modeled as a stochastic process. These examples underscore the universality and importance of stochastic modeling in capturing the dynamics of systems influenced by random interactions and events.

Stochastic processes provide a mathematical framework to describe and predict the behavior of such systems over time or space. By considering each possible state of the system as a random variable and indexing these variables by time or space, we can construct a model that reflects the system's evolution under uncertainty. This approach allows for the analysis of complex phenomena where deterministic models fall short, offering insights into the probabilistic behavior and the underlying mechanisms driving the random dynamics observed in physical and biological systems.

A general stochastic process can be defined as a collection of random variables $X_t : t \in T$ and an underlying probability space $(\Omega, \mathcal{F}, \mathbb{P})$, where:

1. X_t is a random variable representing the system's state at time (or position) t .
2. T is the index set, which is often a subset of the real numbers \mathbb{R} or the integers \mathbb{Z} . For instance, if T is a subset of \mathbb{R} , the stochastic process is called a continuous-time stochastic process; if T is a subset of \mathbb{Z} , the process is called a discrete-time stochastic process.
3. Ω is the sample space, which is the set of all possible outcomes or states of the system.

4. \mathcal{F} is a σ -algebra (sigma-algebra) on Ω , representing the collection of all events, where an event is a subset of Ω . \mathcal{F} must satisfy certain properties, such as being closed under complementation and countable unions, and containing the empty set and the sample space itself.
5. \mathbb{P} is a probability measure that assigns probabilities to the events in \mathcal{F} . It must satisfy the axioms of probability: $\mathbb{P}(\emptyset) = 0$, $\mathbb{P}(\Omega) = 1$, and for any countable sequence of mutually exclusive events E_1, E_2, \dots , $\mathbb{P}(\bigcup E_i) = \sum \mathbb{P}(E_i)$.

We can now define a general stochastic process as a family of random variables $\{X_t : t \in T\}$, where each X_t maps outcomes $\omega \in \Omega$ of a probability space $(\Omega, \mathcal{F}, \mathbb{P})$ to states in a state space S ,

$$X_t(\omega) : \Omega \rightarrow S.$$

For this process, the joint probability distribution for a sequence of times t_1, t_2, \dots, t_n within the index set T defines the stochastic process's complete statistical description,

$$\mathbb{P}(X_{t_1} \in A_1, X_{t_2} \in A_2, \dots, X_{t_n} \in A_n),$$

for all $n \in \mathbb{N}$ and for all sets A_1, A_2, \dots, A_n in the σ -algebra of S . Here, each A_i represents a possible state or range of states at time t_i .

The Markov property is a specific characteristic of certain stochastic processes, which states that the future evolution of the process depends only on the present state and is independent of its past history. In other words, a stochastic process with the Markov property has no memory of its past beyond the current state. Stochastic processes that exhibit the Markov property are called Markov processes or Markov chains. Formally, for every s, t in T with $s < t$ and states x, y in S , the Markov property is given by,

$$\mathbb{P}(X_t = y | X_s = x, X_{s_1} = x_1, \dots, X_{s_k} = x_k) = \mathbb{P}(X_t = y | X_s = x).$$

For a continuous-time stochastic process $X_t : t \in \mathbb{R}_{\geq 0}$ with state space S , the Markov property holds if, for any $0 \leq t_1 < t_2 <$

$\dots < t_n < t$ and any sequence of states $x_1, x_2, \dots, x_n, x \in S$, the following conditional probability holds:

$$P(X_t = x \mid X_{t_1} = x_1, X_{t_2} = x_2, \dots, X_{t_n} = x_n) = P(X_t = x \mid X_{t_n} = x_n).$$

In this case, the probability of being in state x at time t depends only on the current state x_n at time t_n and is independent of the process's history. The Markov property is a simplifying assumption in many stochastic models, as it reduces the complexity of analyzing the process by only considering the current state's influence on future states.

1.2.3. Chapman-Kolmogorov equation

The Chapman-Kolmogorov equation is a fundamental relationship in probability theory and stochastic processes. It connects the joint probabilities of a Markov process at different time points and is commonly used in the study of random walks, Brownian motion, and other time-dependent processes.

Suppose we have a Markov process $X(t)$, where t denotes time. The transition probability of the process going from state x at time t to state y at time $t + \tau$ is given by $p(y, t + \tau \mid x, t)$. The Chapman-Kolmogorov equation relates the transition probability over different time intervals, providing a method to compute the probability of transitioning between two states over a time interval $t_1 + t_2$ using the probabilities of transitioning over time intervals t_1 and t_2 separately. Mathematically, the equation is expressed as,

$$p(y, t_2 + t_1 \mid x, 0) = \int p(y, t_2 + t_1 \mid z, t_1) p(z, t_1 \mid x, 0) dz. \quad (1.3)$$

In this equation, $p(y, t_2 + t_1 \mid x, 0)$ represents the transition probability from state x at time 0 to state y at time $t_2 + t_1$. The integral on the right-hand side sums over all possible intermediate states z at time t_1 . The Chapman-Kolmogorov equation thus states that the probability of transitioning from state x to state y over time $t_2 + t_1$ is equal to the sum of probabilities of transitioning from state x to any intermediate state z at time t_1 , and then from state z to state y over the remaining time t_2 .

1.2.3.1. The differential Chapman-Kolmogorov equation

The differential form of the Chapman-Kolmogorov equation provides the clearest bridge from the basic concepts we have already seen, to the master and Fokker-Planck equations that are often used to model stochastic processes. We require the following conditions to be true for all $\epsilon > 0$, in order to express the Chapman-Kolmogorov equation as a differential equation (for simplicity, we consider just 1 dimension throughout this section):

1. Jump transitions are finite:

$$\lim_{\tau \rightarrow 0} \frac{1}{\tau} p(y, t + \tau | x, t) = W(y | x, t) \text{ for } |y - x| \geq \epsilon,$$

2. Drift term is finite:

$$\lim_{\tau \rightarrow 0} \frac{1}{\tau} \int_{|y-x| < \epsilon} dy (y - x) p(y, t + \tau | x, t) = A(x, t) + O(\epsilon),$$

3. Diffusion term is finite:

$$\lim_{\tau \rightarrow 0} \frac{1}{\tau} \int_{|y-x| < \epsilon} dy (y - x)^2 p(y, t + \tau | x, t) = B(x, t) + O(\epsilon),$$

4. All higher order terms disappear.

The details for the derivation of the differential Chapman-Kolmogorov equation are well explained in Section 3.4.1 of Gardiner's book [7], and we will not go over it here. The derivation entails taking the time evolution of the expectation value of some function $f(y)$ which is twice differentiable, applying the Chapman-Kolmogorov equation, then considering the Taylor expansion of $f(y)$ to the second order, and using the three conditions above to get,

$$\begin{aligned} \frac{\partial p(y, t | x, t_1)}{\partial t} = & \underbrace{-\frac{\partial}{\partial y} [A(y, t) p(y, t | x, t_1)]}_{\text{Drift term}} + \underbrace{\frac{1}{2} \frac{\partial^2}{\partial y^2} [B(y, t) p(y, t | x, t_1)]}_{\text{Diffusion term}} \\ & + \underbrace{\int dz [W(y | z, t) p(z, t | x, t_1) - W(z | y, t) p(y, t | x, t_1)]}_{\text{Jump term}}. \end{aligned} \quad (1.4)$$

If we consider the evolution of the probability distribution $p(y, t|x, t_1)$ with respect to the initial variables x, t_1 , we can derive what is known as the *backward* differential Chapman-Kolmogorov equation (see Section 3.6 in Gardiner's text [7]). Using the same methods as used to derive the forward differential Chapman-Kolmogorov equation we get the following form for the backward differential Chapman-Kolmogorov equation,

$$\begin{aligned} \frac{\partial p(y, t|x, t_1)}{\partial t_1} = & -A(x, t_1) \frac{\partial p(y, t|x, t_1)}{\partial x} - \frac{1}{2} B(x, t_1) \frac{\partial^2 p(y, t|x, t_1)}{\partial x^2} \\ & + \int dz W(z|x, t_1) [p(y, t|x, t_1) - p(y, t|z, t_1)]. \quad (1.5) \end{aligned}$$

The forward and backward equations are - in principle - equivalent to each other, but in practice, they are used in different contexts. The forward equation gives us the evolution of measurable quantities in terms of the time of observation. The backward equation on the other hand helps us understand the past of a system given a final state, and these equations are most often used in the study of first passage times. Since a switching rate can be thought of as the mean first passage time to a different meta-stable state, we will look into backward equations and the first passage time in a subsequent section. Now, we delve into the special cases that arise from the different terms of Eq. (1.4), and are commonly used in the analysis of stochastic processes.

1.2.4. Master equations and jump processes

The master equation provides a particularly useful formulation for the evolution of states in jump processes, providing a mathematical description of the time evolution of a probability distribution in a discrete-state, continuous-time Markov process. In particular, it is a specific case of the differential Chapman-Kolmogorov equation when $A(y, t) = 0$ and $B(y, t) = 0$ in Eq. (1.4). We can also derive the master equation from the Chapman-Kolmogorov equation by considering the transition probabilities between states.

Let $p(i, t)$ be the probability of being in state i at time t . The master equation describes the time evolution of $p_i(t)$. Using the

Chapman-Kolmogorov equation, we can write the probability of being in state j at time $t + \tau$ as,

$$p(j, t + \tau | i_0, t_0) = \sum_i p(j, t + \tau | i, t) p(i, t | i_0, t_0).$$

We define the transition rate W_{ji} from $i \rightarrow j$ to be,

$$W_{ji} = \lim_{\tau \rightarrow 0} \frac{p(j, t + \tau | i, t)}{\tau}.$$

Now, we can write the probability to be in state j at time $t + \tau$, $p(j, t + \tau | i, t)$ in terms of the transition rate W_{ji} ,

$$p(j, t + \tau | i, t) = W_{ji}\tau + \delta_{ji},$$

where the term δ_{ji} represents the case when $j = i$ and no transition happens. We can now substitute this expression back into the Chapman-Kolmogorov equation,

$$p(j, t + \tau | i_0, t_0) = \sum_i [W_{ji}\tau + \delta_{ji}] p(i, t | i_0, t_0).$$

Rearranging we have,

$$\frac{p(j, t + \tau | i_0, t_0) - p(j, t | i_0, t_0)}{\tau} = \sum_i W_{ji} p(i, t | i_0, t_0) - \sum_i W_{ij} p(j, t | i_0, t_0).$$

Taking the limit as τ approaches zero,

$$\lim_{\tau \rightarrow 0} \frac{p(j, t + \tau | i_0, t_0) - p(j, t | i_0, t_0)}{\tau} = \frac{\partial p(j, t | i_0, t_0)}{\partial t},$$

which gives us the master equation describing the evolution of the probability in terms of transition rates between states,

$$\frac{\partial p(j, t)}{\partial t} = \sum_i [W_{ji} p(i, t) - W_{ij} p(j, t)],$$

where we have omitted the reference to the initial state (i_0, t_0) everywhere for brevity. In this equation, the first term represents the probability flow out of state i , and the second term represents the probability flow into state i .

1.2.4.1. Revisiting the Poisson process

As an illustration, we consider the master equation approach to one of the simplest stochastic processes - the Poisson process. We have a system where events occur at a constant rate, λ , independent of the current state.

Let us denote $p_n(t)$ as the probability of having n events at time t . For the Poisson process, the rate of change of $p_n(t)$ can be described by the master equation,

$$\frac{dp_n(t)}{dt} = \lambda p_{n-1}(t) - \lambda p_n(t).$$

This equation reflects the fact that the probability of having n events increases due to transitions from $n-1$ to n and decreases due to transitions from n to $n+1$. To solve this, we introduce the generating function,

$$G(z, t) = \sum_{n=0}^{\infty} p_n(t) z^n.$$

Taking the time derivative of $G(z, t)$ and substituting the master equation, we get,

$$\frac{\partial G(z, t)}{\partial t} = \sum_{n=0}^{\infty} \frac{dp_n(t)}{dt} z^n = \lambda \sum_{n=0}^{\infty} p_{n-1}(t) z^n - \lambda \sum_{n=0}^{\infty} p_n(t) z^n.$$

By shifting the index in the summation and recognizing the terms of the generating function, we find,

$$\frac{\partial G(z, t)}{\partial t} = \lambda z \sum_{n=1=0}^{\infty} p_{n-1}(t) z^{n-1} - \lambda G(z, t) = \lambda z G(z, t) - \lambda G(z, t).$$

This leads to a partial differential equation,

$$\frac{\partial G(z, t)}{\partial t} = \lambda(z-1)G(z, t).$$

Solving this differential equation gives the generating function for the Poisson distribution,

$$G(z, t) = G(z, 0)e^{\lambda(z-1)t}.$$

If at $t = 0$ the system starts with zero events, $p_0(0) = 1$, then $G(z, 0) = 1$. Therefore,

$$G(z, t) = e^{\lambda(z-1)t}.$$

Expanding this exponential as a power series in z , we obtain the probabilities $p_n(t)$ as coefficients in the series, leading to the familiar Poisson distribution,

$$p_n(t) = \frac{(\lambda t)^n e^{-\lambda t}}{n!}.$$

1.2.4.2. Constitutive gene expression

As a further illustration of the master equation approach, we set up the master equation for constitutive gene expression. In constitutive gene expression, proteins are produced at a constant rate regardless of the cell's environmental conditions or internal state. We consider a system where the gene product (protein) is synthesized and degraded over time. The master equation for constitutive gene expression is given by (see [9] for other examples),

$$\frac{dp_n(t)}{dt} = \lambda p_{n-1}(t) - (\lambda + n\mu)p_n(t) + (n+1)\mu p_{n+1}(t).$$

Here, $p_n(t)$ is the probability of having n proteins at time t , λ is the rate of protein synthesis, and μ is the rate of protein degradation. The terms in the equation represent the processes affecting the state n :

- $\lambda p_{n-1}(t)$: the rate of entering state n from $n - 1$ (protein synthesis),
- $(\lambda + n\mu)p_n(t)$: the rate of leaving state n due to either synthesis (adding another protein, moving to state $n + 1$) or degradation (removing a protein, moving to state $n - 1$),
- $(n + 1)\mu p_{n+1}(t)$: the rate of entering state n from $n + 1$ (protein degradation).

1.2.5. Simulating master equations - the Gillespie algorithm

The Gillespie algorithm is instrumental in simulating the time evolution of stochastic processes described by master equations. It is particularly valuable in scenarios like chemical kinetics or gene expression, where system dynamics are driven by discrete random events. The Gillespie algorithm effectively manages simulations involving reactions with diverse time scales, allowing for accurate representation of systems where events unfold at markedly different frequencies without necessitating impractically small timesteps that a deterministic model might need to use.

The algorithm operates as follows:

1. **Initialization:** Set the initial state of the system, with $p_i(t = 0)$ representing the probability of each state at the start, and initialize the time $t = 0$.
2. **Reaction Propensity Calculation:** For each possible reaction or transition, calculate the propensity function a_j , which quantifies the likelihood of the reaction occurring per unit time.
3. **Time Step Determination:** Determine the time Δt until the next reaction occurs, typically using an exponential distribution with parameter equal to the total propensity of all reactions, $a_0 = \sum_j a_j$.
4. **Reaction Selection:** Randomly select which reaction will occur next, proportional to the propensity of each reaction.
5. **State Update:** Update the system state to reflect the occurrence of the selected reaction.
6. **Time Update:** Increment the time by Δt .
7. **Iterate:** Repeat steps 2 through 6 until the simulation end time or condition is reached.

We now illustrate this with a concrete example. For the master equation describing constitutive gene expression, the algorithm proceeds by calculating the propensity of each reaction, determining when the next reaction will occur, and deciding

which reaction takes place based on these propensities. The steps of the Gillespie algorithm for constitutive gene expression, where proteins are produced at rate λ and degrade at rate μ , are as follows:

1. Initialize the number of proteins, n , and set time t to zero.
2. Calculate the propensity functions: $\alpha_{\text{prod}} = \lambda$, and $\alpha_{\text{deg}} = \mu n$.
3. Determine the time τ until the next reaction by drawing a random number r_1 and calculating $\tau = (1/\sum \alpha) \ln(1/r_1)$.
4. Choose which reaction will occur next by comparing a second random number r_2 with the relative propensities.
5. Update the number of proteins and time, then repeat from step 2.

In Julia, a simple implementation for constitutive gene expression could look like this:

```
using Random

function gillespie_constitutive(lambda, mu, n0, t_max)
    t = 0.0
    n = n0
    while t < t_max
        alpha_prod = lambda
        alpha_deg = mu * n
        alpha_total = alpha_prod + alpha_deg

        r1, r2 = rand(), rand()
        tau = (1/alpha_total) * log(1/r1)
        t += tau

        if r2 < alpha_prod / alpha_total
            n += 1 # Protein production
        else
            n = max(n - 1, 0) # Protein degradation
        end
    end
end
```

```

println("Time: $t, Protein count: $n")
end
end

```

With that short overview of master equations – how to set them up and how to simulate them – we are well placed to survey the Fokker-Planck equation which can also serve as an approximation to the master equation in some circumstances.

1.2.6. Fokker-Planck equation

The Fokker-Planck equation follows from the differential Chapman-Kolmogorov equation Eq. (1.4) when the jump transition probabilities disappear for all states, $W(y|x, t) = 0$, $\forall x, y, t$. Then, the Fokker-Planck equation takes the form,

$$\frac{\partial p(y, t|x, t_1)}{\partial t} = \underbrace{-\frac{\partial}{\partial y} [A(y, t)p(y, t|x, t_1)]}_{\text{Drift term}} + \underbrace{\frac{1}{2} \frac{\partial^2}{\partial y^2} [B(y, t)p(y, t|x, t_1)]}_{\text{Diffusion term}}.$$

In physical processes, we can often make the approximation that the distribution $p(y, t|x, t_1)$ is sharply peaked enough in y , that y derivatives of $A(y, t)$ and $B(y, t)$ can be ignored when compared to the y derivative of $p(y, t|x, t_1)$. This gives us a more tractable form of the Fokker-Planck equation,

$$\frac{\partial p(y, t|x, t_1)}{\partial t} = -A(y, t) \frac{\partial p(y, t|x, t_1)}{\partial y} + \frac{1}{2} B(y, t) \frac{\partial^2 p(y, t|x, t_1)}{\partial y^2}. \quad (1.6)$$

Similarly, from the backward differential Chapman-Kolmogorov equation we get the backward Fokker-Planck equation,

$$\frac{\partial p(y, t|x, t_1)}{\partial t_1} = A(x, t_1) \frac{\partial p(y, t|x, t_1)}{\partial x} + \frac{1}{2} B(x, t_1) \frac{\partial^2 p(y, t|x, t_1)}{\partial x^2}. \quad (1.7)$$

1.2.6.1. The Fokker-Planck equation as an approximation of the master equation

When a jump process can be approximated by a continuous process (for example a jump from n to $n + 1$ molecules for $n \gg 1$), we can

approximate the master equation by a Fokker-Planck equation. We will illustrate the techniques involved using the master equation for the birth death process, and tackle the slightly more useful master equations for gene expression in later chapters.

The master equation for a birth-death process with a constant (independent of population) birth rate and a death rate proportional to the population is given by,

$$\frac{dP(n, t)}{dt} = \lambda P(n-1, t) + \mu(n+1)P(n+1, t) - (\lambda + \mu n)P(n, t), \quad (1.8)$$

where,

- $P(n, t)$ is the probability of having n individuals at time t .
- λ is the constant birth rate.
- μ is the death rate per individual.

We consider the case when $n \gg 1$, so that jumps are small compared to n . The Taylor series expansion of some function $f(n + \delta n)$ can be written as,

$$\begin{aligned} f(n + \delta n) &= \sum_i \frac{1}{i!} (\delta n)^i (\partial_n)^i f(n) \\ &= e^{\delta n \partial_n} f(n) = E^{\delta n} f(n), \end{aligned} \quad (1.9)$$

where we define $E^{\delta n}$ as the translation operator that takes $f(n)$ to $f(n + \delta n)$. Rewriting the master equation in terms of the translation operator (in $n, \delta n$), we have,

$$\frac{dP(n, t)}{dt} = \lambda(E^{-1} - 1)P(n, t) + \mu(E^1 - 1)nP(n, t). \quad (1.10)$$

From Eq. (1.9) we can expand the translation operator $E^{-\delta n}$ to second order (assuming that higher orders make negligible contributions since $n \gg \delta n$) and substitute it into Eq. (1.10) to yield,

$$\begin{aligned} \frac{dP(n, t)}{dt} &= \lambda \left[\left(1 - \frac{\partial}{\partial n} + \frac{1}{2} \frac{\partial^2}{\partial n^2} \right) - 1 \right] P(n, t), \\ &+ \mu \left[\left(1 + \frac{\partial}{\partial n} + \frac{1}{2} \frac{\partial^2}{\partial n^2} \right) - 1 \right] nP(n, t). \end{aligned} \quad (1.11)$$

Simplifying this expression, we get,

$$\frac{\partial P(n, t)}{\partial t} = -\frac{\partial}{\partial n} A(n) P(n, t) + \frac{1}{2} \frac{\partial^2}{\partial n^2} B(n) P(n, t), \quad (1.12)$$

where,

$$\begin{aligned} A(n) &= \lambda - \mu n \quad (\text{drift term}), \\ B(n) &= \lambda + \mu n \quad (\text{diffusion term}). \end{aligned} \quad (1.13)$$

This expansion of the translation operator is called the Kramers-Moyal expansion and the non-rigorous derivation of the Fokker-Planck equation sketched in this section was first given by Kramers (see [7]). Van Kampen addresses the lack of a clear small parameter in the Kramers-Moyal expansion using a system size expansion (see Chapter X in [8] and see [7, 8] for further discussion). However for our purposes, the naive approximation to the Fokker-Planck equation works very well. It is worth noting that in general, the specific form of the Fokker-Planck equation derived might depend on the specific approximation procedure used on the master equation.

Similar techniques can be used to derive the Fokker-Planck equation for the master equation for constitutive gene expression and other more complex situations that we will encounter while modeling the *lac*-operon.

1.2.7. First passage times

First passage times are relevant to analysis of switching behaviour since the transition rate from some state **1** to another state **2** can also be computed as the inverse of the mean first passage time from state **1** to state **2**. To analyse first passage times for a given stochastic system for which we know the Fokker-Planck equation, we present a concise version of the exposition in Gardiner [7] Section 5.5. Define $G(x, t)$ as the probability that a system starting from state x has not reached the boundary by time t , which implies $G(x, t) = \mathbb{P}(T > t)$ for the first passage time T . The mean first passage time, denoted by $\Gamma(x)$, is the expected time for the system to reach the boundary from x ,

$$\Gamma(x) = \int_0^\infty t \left(-\frac{\partial G(x, t)}{\partial t} \right) dt.$$

Integration this by parts, considering the boundary conditions $G(x, 0) = 1$ and $G(x, t) \rightarrow 0$ as $t \rightarrow \infty$, leads to,

$$\Gamma(x) = \int_0^\infty G(x, t) dt. \quad (1.14)$$

The function $G(x, t)$ satisfies the backward Fokker-Planck equation because it is the backward evolution of the probability distribution given a future final condition of escape at time T . The backward Fokker-Planck equation describes how probabilities diffuse backward in time from the boundary to the starting point in the present, x . Therefore,

$$\frac{\partial G(x, t)}{\partial t} = A(x) \frac{\partial G(x, t)}{\partial x} + \frac{1}{2} B(x) \frac{\partial^2 G(x, t)}{\partial x^2}.$$

Integrating the backward Fokker-Planck equation from 0 to infinity yields a differential equation for the mean first passage time,

$$\int_0^\infty \frac{\partial G(x, t)}{\partial t} dt = - \int_0^\infty \left[-A(x) \frac{\partial G(x, t)}{\partial x} + \frac{1}{2} B(x) \frac{\partial^2 G(x, t)}{\partial x^2} \right] dt. \quad (1.15)$$

In Eq. (1.15), the left-hand side integrates to $G(x, \infty) - G(x, 0)$ and $G(x, 0) = 1$ (as the probability of not crossing the boundary by time 0 is 1), and $G(x, \infty) = 0$ (since eventually, the boundary will be crossed). Therefore, the left hand side of Eq. (1.15) simplifies to -1. On the right hand side, we can use Eq. (1.14) to yield the differential equation for the first passage time,

$$A(x) \frac{\partial \Gamma(x)}{\partial x} + \frac{1}{2} B(x) \frac{\partial^2 \Gamma(x)}{\partial x^2} = -1. \quad (1.16)$$

As long as we can derive a Fokker-Planck equation for a stochastic system, we can use Eq. (1.16) to analyse the switching behavior without having to simulate the entire system.

1.3. Structure of this thesis

With the background provided in this introductory chapter, we are well prepared to tackle the problem of switching of the *lac*-operon.

Chapter 2 gives a detailed overview of the mechanistic model of the operon that underlies this thesis, considering the biochemical reactions relevant to the regulation of the *lac*-operon in the absence of glucose. Once we have identified these reactions along with their rates using the extensive literature on the biochemistry of the *lac*-operon (see for instance [3] and references therein), we use Gillespie's algorithm for simulating stochastic systems to simulate the *lac* system to calibrate the switching rate in our simulations to flow cytometry experiments with single cell resolution (see our work published in [1] and [2], and for an overview of the experiments conducted by Robin A. Sorg from the lab of J. W. Veening see Appendix A). Having established that our simulations of the model of the *lac*-operon described in Chapter 2 match the switching behavior in experiments, we analyze the switching behaviour of this system in Chapters 3 and 4.

In Chapter 3 we analyse the switching behavior from the uninduced to the induced state (also see [1]). We find excellent agreement with experiment, and introduce the smoothing procedure for identifying rate limiting fluctuations that influence the switching behavior. We identify operator state fluctuations via repressor-DNA loop to be the rate limiting fluctuation and use our mechanistic model to derive a simple formula for the switching rate of the *lac*-operon under different external concentrations of the inducer molecule.

In Chapter 4 (also see [2]), we analyse the reverse transition - that from the induced to the un-induced state. We find that this transition is influenced by multiple fluctuations and derive simplified mathematical models for each relevant subsystem to derive a 2D Fokker-Planck equation for pump protein dynamics. We use the Fokker-Planck equation to numerically calculate the first passage times to the uninduced state, and find that this switch occurs on timescales far longer than the lifetime of a cell which agrees qualitatively with experimental results.

Finally in Chapter 5, we summarize and discuss these results.

2. The model

In this chapter we establish a mechanistic model of the *lac*-pathway. The material presented in this chapter is based on published work done by this author, see [1, 2]. For the purposes of this thesis we use the model we described in [2] which is an updated version of the model we described in [1].

2.1. Introduction

In order to analyse the switching behavior of the *lac*-pathway, we must first identify some set of chemical reactions as constituting the system that we want to study. In particular, we must consider all chemical reactions relevant to the regulation of the *lac*-pathway in the absence of glucose.

Table 2.1: Summary of the detailed mechanistic model of the *lac*-system presented in this chapter.

I	The number of inducer molecules inside the cell. The inducer TMG is an analog of galactose that is imported by LacY but cannot be metabolized by <i>E. coli</i> .		
E	The external concentration of the inducer TMG.		
Y	LacY, the surface protein that imports inducer into the cell.		
Inducer transport	$E \xrightarrow{\alpha(Y)} I$ $\alpha(Y) = m \frac{E}{E_h + E} Y$	$m = 1260 / \text{min}$ $E_h = 1.05 \times 10^5 [\mu\text{M}]$	from [10] fitting parameter
Inducer diffusion	$I \xrightarrow{f^{\text{out}}} E$	$f^{\text{out}} = 3.4 \times 10^{-4} / \text{min}$	based on [11]

2. THE MODEL

	$E \xrightarrow{f^{\text{in}}} I$	$f^{\text{in}} = 0.14 / \text{min}$	based on [6, 12, 13, 14, 11]
<i>lacI</i> <i>mRNA_I</i>	the gene which encodes for the LacI protein. Messenger RNA for the produced after transcription of the <i>lacI</i> gene.		
LacI	Monomer of the <i>lacI</i> -repressor. Four of these come together to form the repressor.		
LacI production	$lacI \xrightarrow{c^R} lacI + mRNA_I$ $mRNA_I \xrightarrow{l^R} mRNA_I + LacI$	$c^R = 0.1336 / \text{min}$ $l^R = 3.33 / \text{min}$	[15] est. by setting burst parameter to 5
LacI2	Dimer of LacI molecules.		
LacI dimerization	$LacI + LacI \xrightarrow{u^{2R}} LacI2$	$u^{2R} = 10^3 / \text{min}$	est. [16] for fast dimerization
R	$LacI2 \xrightarrow{v^{2R}} LacI + LacI$ The <i>lacI</i> -repressor which is a dimer of LacI2 molecules.	$v^{2R} = 10^{-5} / \text{min}$	based on [16]
Repressor production	$LacI2 + LacI2 \xrightarrow{u^{4R}} R$	$u^{4R} = 10^3 / \text{min}$	est. [16] for fast dimerization
	$R \xrightarrow{v^{4R}} LacI2 + LacI2$	$v^{4R} = 10^{-5} / \text{min}$	based on [16]
<i>lacY</i> <i>mRNA_Y</i>	The gene which encodes for the LacY protein. Messenger RNA produced after transcription of the <i>lacY</i> gene.		
Plac	The operator region of the <i>lac</i> -genes when it is free of repressors.		
LacY production	$Plac \xrightarrow{c^Y} Plac + mRNA_Y$ $PlacI \xrightarrow{c^Y} PlacI + mRNA_Y$ $mRNA_Y \xrightarrow{l^Y} mRNA_Y + LacY$	$c^Y = 6 / \text{min}$ $\bar{c}^Y = 6 \times 10^{-3} / \text{min}$ $l^Y = 20 / \text{min}$	based on [17] based on [17, 6] based on [17] and burst parameter 30
$R_j, \forall j \in \{0, 1, 2, 3, 4\}$	Each repressor molecule has four binding sites for the inducer. In R_j , the subscript j refers to the number of free binding sites on the repressor. So, R_4 is a repressor with no inducers bound to it, while R_0 has four inducers bound.		
Inducer-repressor binding	$R_j + I \xrightarrow{0.25j \bar{b}} R_{j-1}, \forall j \in \{4, 3, 2, 1\}$	$\bar{b} = 2.29 \times 10^{-3} / \text{min}$	from [18]
Inducer-repressor unbinding	$R_j \xrightarrow{(4-j)d} R_{j+1} + I, \forall j \in \{0, 1, 2, 3\}$	$d = 12 / \text{min}$	from [18]
$PlacI_{R_j}$	The operator region of the <i>lac</i> -genes when a repressor (with $(4-j)$ inducers bound to it) is bound to any one of its binding sites.		
$Plac2_{R_j}$	The DNA-repressor loop formed when a repressor (with $(4-j)$ inducers bound to it) is bound to two binding sites on the DNA.		
Inducer binding to DNA bound repressor	$PlacI_{R_j} + I \xrightarrow{0.25j \bar{\bar{b}}} PlacI_{R_{j-1}}, \forall j \in \{4, 3, 2, 1\}$	$\bar{\bar{b}} = 4.98 \times 10^{-4} / \text{min}$	from [18]
Inducer binding to DNA-repressor loop	$Plac2_{R_j} + I \xrightarrow{0.25j \bar{\bar{b}}} Plac2_{R_{j-1}}, \forall j \in \{4, 3, 2, 1\}$	$\bar{\bar{b}} = 2.707 \times 10^{-5} / \text{min}$	set by detailed balance, see Section 2.6
Inducer unbinding from DNA bound repressor	$PlacI_{R_j} \xrightarrow{(4-j)\bar{d}} PlacI_{R_{j+1}} + I, \forall j \in \{0, 1, 2, 3\}$	$\bar{d} = 48 / \text{min}$	from [18]
Inducer unbinding from DNA-repressor loop	$Plac2_{R_j} \xrightarrow{(4-j)\bar{\bar{d}}} Plac2_{R_{j+1}} + I, \forall j \in \{0, 1, 2, 3\}$	$\bar{\bar{d}} = \bar{d}$	same as \bar{d}
Repressor binding to DNA	$R_j + Plac \xrightarrow{g} PlacI_{R_j}, \forall j \in \{0, 1, 2, 3, 4\}$	$g = 0.166 / \text{min}$	from [19]
Repressor unbinding from single operator site	$PlacI_{R_0} \xrightarrow{w_0} Plac + R_0$	$w_0 = 274710.82 / \text{min}$	set by detailed balance, see Section 2.6

Repressor unbinding from either end of DNA loop	$\text{Plac1R}_1 \xrightarrow{w_1} \text{Plac} + \text{R}_1$	$w_1 = 14935.15 / \text{min}$	=	set by detailed balance , see Section 2.6
	$\text{Plac1R}_2 \xrightarrow{w_2} \text{Plac} + \text{R}_2$	$w_2 = 811.97 / \text{min}$		set by detailed balance , see Section 2.6
	$\text{Plac1R}_3 \xrightarrow{w_3} \text{Plac} + \text{R}_3$	$w_3 = 44.14 / \text{min}$		set by detailed balance , see Section 2.6
	$\text{Plac1R}_4 \xrightarrow{w_4} \text{Plac} + \text{R}_4$	$w_4 = 2.4 / \text{min}$		from [18]
	$\text{Plac2R}_0 \xrightarrow{2w_0} \text{Plac1R}_0$			
DNA loop formation from singly bound repressor	$\text{Plac2R}_1 \xrightarrow{2w_1} \text{Plac1R}_1$			
	$\text{Plac2R}_2 \xrightarrow{2w_2} \text{Plac1R}_2$			
	$\text{Plac2R}_3 \xrightarrow{2w_3} \text{Plac1R}_3$			
	$\text{Plac2R}_4 \xrightarrow{2w_4} \text{Plac1R}_4$			
	$\text{Plac1R}_j \xrightarrow{c} \text{Plac2R}_j, \forall j \in \{0, 1, 2, 3, 4\}$	$c = 568.8 / \text{min}$		from [17, 1]
Dilution	$\text{Y} \xrightarrow{\varphi} \emptyset$ $\text{LacI} \xrightarrow{\varphi} \emptyset$ $\text{LacI2} \xrightarrow{\varphi} \emptyset$ $\text{R}_4 \xrightarrow{\varphi} \emptyset$ $\text{R}_3 \xrightarrow{\varphi} \emptyset$ $\text{R}_2 \xrightarrow{\varphi} \emptyset$ $\text{R}_1 \xrightarrow{\varphi} \emptyset$ $\text{R}_0 \xrightarrow{\varphi} \emptyset$ $\text{I} \xrightarrow{\varphi} \emptyset$	$\varphi = 0.0167 / \text{min}$		from [1], Appendix A
mRNA degradation	$mRNA_I \xrightarrow{\phi} \emptyset$ $mRNA_Y \xrightarrow{\phi} \emptyset$	$\phi = 0.6666 / \text{min}$		from [17]
<hr/>				
$\xi = \frac{c}{\phi} \text{I} \text{Y}$	Effective production rate for pump proteins when the operator is free of repressors			
$\bar{\xi} = 0$	Effective production rate for pump proteins when the repressor is bound to operator forming the DNA-repressor loop			
$\langle \text{Y} \rangle = \frac{\eta}{\eta + \beta} \frac{\xi}{\varphi}$	Mean number of pump proteins			

The *lac*-pathway is formed by the *lac*-genes *lacY*, *lacZ*, and *lacA*, which are under joint regulatory control, thus forming a so-called operon. In the induced state of the *lac*-pathway, lactose (‘inducer’) is imported across the cell membrane by the LacY protein (‘pumps’) and metabolized by the enzyme LacZ into glucose and galactose. Allolactose, a lactose variant originating from LacZ activity, binds to the repressor of the *lac*-genes and drastically reduces the affinity of the *lac*-repressor to its DNA binding sites [3, 6]. The *lac*-repressor is formed by a dimer of LacI dimers which are expressed constitutively. The reduced affinity causes the repressor to unbind from the *lac*-regulatory region, enabling the transcription of the *lac*-genes and production of the Lac proteins and further import of lactose. In the uninduced

2. THE MODEL

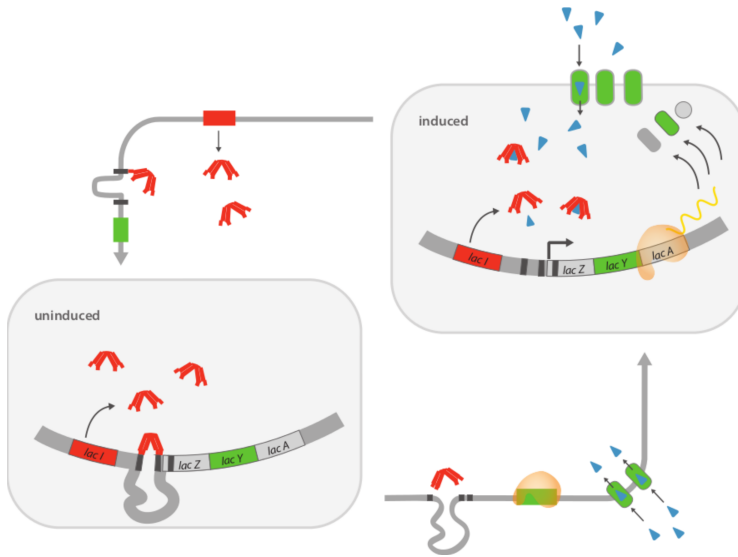


Figure 2.1: Feedback in the lactose-uptake pathway. Three genes under common regulatory control constitute the lactose-uptake pathway: *lacZ* encodes the enzyme to break down lactose, *lacY* encodes a permease (importer of lactose, shown in green), which actively imports lactose from the environment (here: the non-metabolizable lactose-analogue TMG, blue wedge), and *lacA* encodes a transacetylase. Bi-stability is achieved by a positive feedback-loop; the imported TMG acts as an inducer of the *lac*-genes by increasing the unbinding rate of LacI tetramers (red) from the so-called operator binding sites in the *lac*-regulatory region. LacI tetramers inhibit the expression of the *lac*-genes. As a result, the induced state shown on the right, with the *lac*-genes expressed, is stable if the permease imports enough inducers to deactivate the repressors. The uninduced state shown on the left can also be stable, since in the absence of *lac*-expression, the repressors prevent expression of the *lac*-genes by binding to the regulatory region and forming a DNA loop. However, this regulatory circuit is built from stochastic components and can be interrupted by random fluctuations of the number of mRNA, proteins, inducer, repressors, or the binding state of repressors to DNA. These fluctuations lead to transitions between the induced and uninduced states. *This figure is reproduced from published work by the author [1]. I would like to thank M. Markus for help preparing this figure.*

state on the other hand, the repressor frequently binds to two DNA sites in the regulatory region of the *lac*-operon and forms a DNA-repressor loop that effectively blocks transcription of the *lac*-genes and thus the import of lactose into the cell. For a graphical representation, see Fig. 3.6.

Our model describes the transcription and translation of mRNA and protein, both of LacY proteins (lactose importer or ‘pumps’) and of LacI proteins (the monomers of the *lac*-repressor), repressor binding to DNA at its binding sites, DNA looping, the uptake of lactose (inducer) or its analog into a cell, inducer interactions with the repressor in solution and bound to DNA, and the passive diffusion of inducers into the cell [1]. Almost all rates of these processes are taken from the experimental literature (see the following sections and Table 2.1). The exceptions are the Michaelis constant of inducer import by LacY, which we use to calibrate our model against the experimental measurements of switching rates from the uninduced to the induced state presented in [1], and some of the dissociation rates of DNA and repressors, which we determine using the principle of detailed balance (see Section 2.6 and [1]).

2.1.1. Comparison to previous models

Along with experimental work that has been cited throughout this chapter, many computational studies have examined different aspects of the *lac*-system. A small sample of this rich literature is outlined here.

Modeling the dynamics of the *lac*-system, Mettetal et al. [20] formulate a deterministic model of the *lac*-system which they fit to experiment using several fitting parameters (using the deterministic framework published earlier in [5]) and then experimentally estimate protein number fluctuations and burst sizes (number of proteins produced per mRNA molecule) for LacY, LacI and GFP. Using these parameters, they formulate a stochastic model consisting of bursts of protein production (mRNA production followed by instantaneous protein production and mRNA degradation), protein degradation and extrinsic noise which is modeled using a single noise parameter. Repressor binding to regulatory DNA is not modeled explicitly. However, Choi et al. [6]

show that repressor dissociation from its binding sites on DNA plays a crucial role in the switch from the uninduced to the induced state.

Roberts et al. [21] construct a detailed spatially resolved model of the *lac*-operon. They examine the switching behavior and the effects of such phenomena as spatial crowding. Their results are consistent with the findings of Choi et al. but they further conclude that both mRNA and protein thresholds are crossed during the phenotypic switch.

Stamatakis et al. [22] also construct a detailed, computational, spatially homogeneous stochastic model of the *lac*-operon, including sources of stochasticity such as cell division, operator fluctuations, mRNA and protein number fluctuations and the effect of dilution. They focus on describing mathematically the effects of this stochasticity at the single cell level on population dynamics and compare it with a deterministic model of the *lac*-system. None of the previous models have attempted to identify the rate limiting fluctuation of the switch to the induced state of the *lac*-system. Details of our model and literature sources for parameters follow below

We do not model the spatial heterogeneity of the bacterial cell. Experiments by Kuhlman and Cox [23] show that repressor concentration – and thus the binding probability – depends on the distance between the *lacI* genes and the *lac*-operon. As this distance is fixed in our experiments, a constant rate of binding per repressor molecule is appropriate (this rate would change if the distance between genes were changed). A different effect arising from spatial heterogeneity is that a particular repressor molecule that has just been released from the regulatory region might rebound more quickly than one of the other repressor molecules in the system, on account of its spatial proximity to the regulatory region. This is a competition between spatial proximity to the regulatory region (of the originally bound repressor) and the larger number of other repressors (potentially more distant, but more numerous). Roberts et al. [21] estimate the probability that a given repressor molecule binding to the regulatory region is the same molecule that has just unbound (rebinding probability) to be in the range of 0.15 and 0.24, comparable to the result under perfect mixing (0.1 for 10 repressor molecules). This suggests that

spatial effects do not make a large difference to the rebinding probability of a repressor that has just dissociated from DNA. In our case, this effect would lead to an increased binding rate that would be absorbed into the one fitting parameter of our model.

In the following sections, we look at the chemical reactions in each subsystem of the *lac*-operon and its regulation.

2.2. Import of sugar into the cell

First, we examine the passive and active import of the inducing sugar into the cell.

We refer to the concentration of TMG present outside the cell as E and the number of sugar molecules inside the cell as I . TMG can enter the cell in two ways : (i) active import by importers LacY and (ii) passive diffusion. For sugar transport by importers we can write



where Y denotes the number of LacY molecules in the cell. We base our model of active sugar transport (characterized by the function $\alpha(Y)$) on [24], where the transport of a lactose-like sugar by importers is found by *in vitro* measurements to follow a hyperbolic function

$$\alpha(Y) = m \frac{E}{E_h + E} Y, \quad (2.2)$$

where the maximum rate of sugar transport by inducer $m = 1260 \text{ /min}$ is measured in [10] and we use the Mich elis-Menten coefficient E_h as a fitting parameter to calibrate our simulations to experiments described in [1, 2] and Appendix A. To the best of our knowledge, measurements of the quantity E_h are not available for TMG, the lactose analog used in our experiments [1]. From Eq. (4.25) (which relates the internal inducer number to external inducer concentration and pump number, from Eq. (2.2), $I = \alpha(Y)/\varphi$) it is clear that assumptions about the value of m will strongly affect the fitting value for E_h . In our mechanistic model, we use the value of m reported in [25] by Smirnova et. al for the sugar NPG (1260 /min). We determine the Mich elis constant E_h by fitting simulations of the detailed

2. THE MODEL

mechanistic model to experimental data on the switching from the uninduced to the induced state from [1] (the reverse transition to the one considered here, see SI Section S3 for details). The best fit was obtained for $E_h = 1.05 \times 10^5 \mu\text{M}$. For comparison, values of the Michaelis constants E_h for lactulose transport by LacY ($2.4 \times 10^2 \mu\text{M}$), and sucrose ($6.7 \times 10^3 \mu\text{M}$), fructose ($3.5 \times 10^4 \mu\text{M}$) transport by CscB are reported by Sugihara et. al in [24]. Since there are significant variations between different sugars, the fitted value of E_h for TMG is not implausible, however it is sensitive to other parameters of the model for which TMG-specific measurements are not available. Specifically, for large values of E_h , Eq. (4.25) depends on m and E_h only through their ratio. The value obtained for E_h might thus reflect simply a value of the parameter m that is not correct for the inducer TMG used here. However, while $E_h \gg 100 \mu\text{M}$ the ratio of m and E_h will be independent of inaccuracies in the value of m .

For passive diffusion of sugars in and out of the cell we have

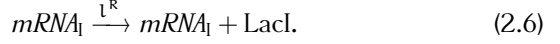
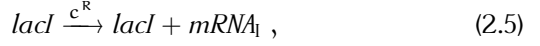


We take $f^{\text{in}} = 0.14 / \text{min}$ based on [11]. Using the cellular dimensions of *E. coli* from [13, 14] we estimate the surface area of *E. coli* to be $\approx 4 \times 10^{-12} \text{m}^2$ while *E. coli* cell volume is taken to be $6 \times 10^{-19} \text{m}^3$ [13]. Using these, we can calculate the rate of sugar diffusing out (per sugar molecule in the cell) as $f^{\text{out}} = 3.4 \times 10^{-4} / \text{min}$ [6, 12, 13, 14, 11].

2.3. Repressor production

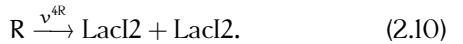
Having seen how sugar/inducer is imported into the cell, we now look at the *lac*-repressor. The repressor is a dimer of LacI dimers and has 4 binding sites for inducers (one on each LacI molecule).

The *lacI* gene is expressed constitutively, and when transcribed, it produces the messenger RNA $mRNA_I$ that when translated produces the LacI protein, the monomer of the tetrameric repressor that can bind to the *lac*-regulatory region,



Measurements reported in [15] indicate that the typical *E. coli* cell produces around 10 complete repressors in one cell cycle. Since the repressor is a tetramer, we have around 40 monomers in the cell. We denote the rate of mRNA degradation by ϕ . Based on mRNA lifetimes reported in [26, 17], we have $\phi = 0.6666$ min. The burst sizes (the ratio of translation rate to mRNA degradation rate) and burst frequencies (ratio of transcription rate to dilution rate) for the *lac*-operon and other genes in *E. coli* have been extensively studied, for example in [27, 28, 29, 17, 30]. We take a burst size of 5 and burst frequency of 8 (estimated for a low abundance protein) from [28, 30] to obtain the transcription rate ($c^R = 0.1336$ /min) and the translation rate ($l^R = 3.33$ /min) for *lacI*.

Using the symbol LacI2 for the dimer, and R for the tetrameric repressor, we represent the tetramerization process through the following reactions



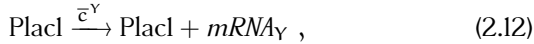
While the rates at which the tetramerization proceeds are not well known, the affinity of the dimer to tetramer reactions is known to be 10^8 /M [16]. Thus, it is reasonable to expect that most LacI molecules will occur as the tetrameric repressor R rather than in the monomeric or dimeric states. To reflect this, we take the association rates $u^{2R} = u^{4R} = 10^3$ /min and the dissociation rates $v^{2R} = v^{4R} = 10^{-5}$ /min.

2.4. Importer production

Having dealt with inducers and repressors in the previous two sections, in this section we consider the third intracellular molecule relevant to our system - the pump LacY. TMG is imported into the cell by the LacY protein acting as a importer (pump). LacY is produced by a *lac*-gene controlled by the *lac*-regulatory region of the *lac*-genes we refer to as Plac. It is known that the repressor can form a DNA loop by binding to two operator sites, thus effectively hindering transcription of the *lac*-genes [6]. We refer to a *lac*-regulatory region with the DNA-loop formed as Plac2.

Using the measurements from [17], which indicate that the number of LacY proteins in the cell (if there are no active repressors present) is 10000, we take the rates of *lacY* transcription $c^Y = 6$ /min and translation $l^Y = 20$ /min to obtain a burst size (ratio of translation rate to mRNA degradation rate) of 30 consistent with [27, 31].

However, when the repressor is bound to DNA forming the repressor-DNA loop (the Plac2 state), one end of the repressor can come undone causing the DNA loop to open, leading to leaky production of importers [6], a state we refer to as Plac1. With the *lac*-genes repressed, the cell is expected to have approximately 10 importer proteins [17], giving a transcription rate of $\bar{c}^Y = 6 \times 10^{-3}$ /min,



Here, the mRNA_Y is the messenger RNA that when translated produces the importer protein LacY. The degradation rate of mRNA is taken to be $\phi = 0.6666$ /min from [26]



2.5. Inducer-repressor-DNA interactions

In this section we deal with the chemical reactions that complete the doubly negative feedback loop that causes the bi-stability of the *lac*-operon - the interactions of inducer molecules with repressors, both in the cell and while bound to DNA.

Once the sugar (lactose, here TMG) has been imported into the cell it can bind to the repressor at four sites, one on each monomer. The sugar-bound repressors are less effective at curbing production of importers (see below) and thus the sugar is also referred to as an inducer (of importer production). Each repressor has four binding sites for inducer molecules. We represent the number of *free* binding sites on the inducer with the subscript. So, R_4 is just a free repressor R , where as a repressor with one inducer bound is R_3 , and so on. In general, a repressor denoted by R_j has $(4 - j)$ repressors bound to it. We take b to be the rate at which an inducer binds to a repressor molecule with four free binding sites, while d is the dissociation rate of one inducer molecule from its binding site on the repressor,



The rates of inducer-repressor binding and unbinding were investigated *in vitro* by Dunaway et al. [18]. They give the binding rate as $b = 2.29 \times 10^{-3}$ /min and the dissociation rate as $d = 12$ /min.

Dunaway et al. also find that interactions between inducers and DNA-bound repressors are weaker than the interactions between

2. THE MODEL

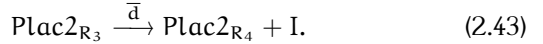
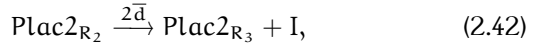
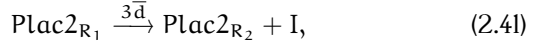
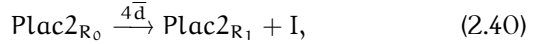
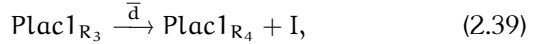
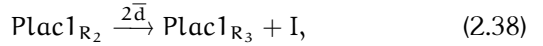
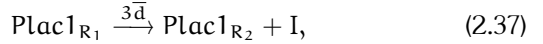
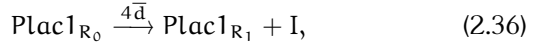
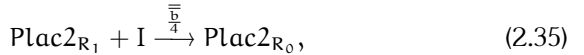
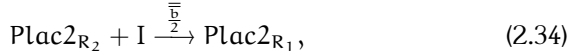
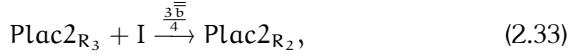
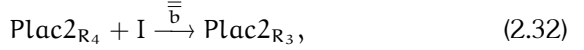
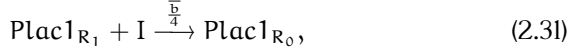
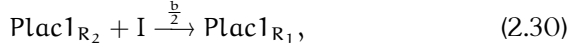
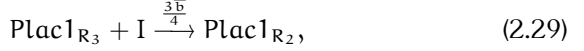
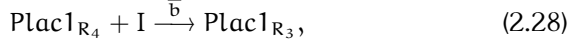
inducers and free repressors. In particular, DNA-bound repressors bind to inducers at a rate \bar{b} that is 4.6 times more slowly, and dissociate at a rate \bar{d} that is 4 times faster. We represent the DNA-repressor-inducer complex by Plac1_{R_j} if the repressor is bound to one operator site and Plac2_{R_j} if the repressor is bound to two operator sites forming a DNA loop. As before, the subscript in R_j stands for the number of unoccupied inducer binding sites on the repressor. We take \bar{b} to be the rate at which an inducer binds to an inducer free repressor bound to one binding site on the DNA, while \bar{d} is the dissociation rate of an inducer molecule from its binding site on a DNA bound repressor. The rate $\bar{\bar{b}}$ at which an inducer binds to a repressor DNA loop is set by detailed balance (see Section 2.6) where as we take the rate $\bar{\bar{d}}$ at which an inducer dissociates from the DNA repressor loop to be the same as the rate \bar{d} , with the reduced affinity of the repressor in a DNA loop to the inducer being wholly reflected in the difference between the rates \bar{b} and $\bar{\bar{b}}$. Dunaway et al. measure the rates d , b , \bar{d} , \bar{b} , while the rate $\bar{\bar{b}}$ is set by detailed balance (see Section 2.6),

$$d = 12 \text{ /min}, \quad (2.24)$$

$$\bar{d} = 48 \text{ /min}, \quad (2.25)$$

$$\bar{b} = 4.98 \times 10^{-4} \text{ /min}, \quad (2.26)$$

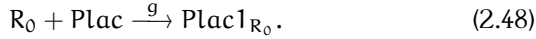
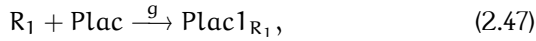
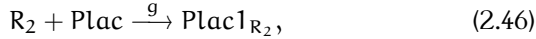
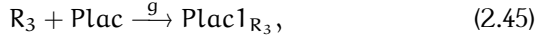
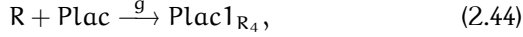
$$b = 2.29 \times 10^{-3} \text{ /min}. \quad (2.27)$$



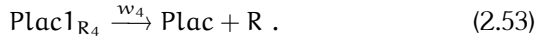
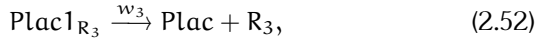
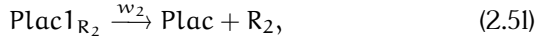
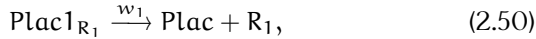
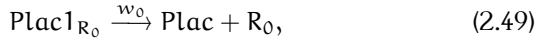
The interactions between the *lac*-regulatory region and the repressor depend on the number of inducers bound to the repressor. In general, repressors with different number of inducers bound to them might bind and unbind from the *lac*-regulatory region at different rates. However Winter et al. [32] find that inducer binding states do not significantly change the rate of repressor-*lac*-regulatory region binding. This is consistent with the idea that the binding rate of the repressor to

2. THE MODEL

the operator (g) is limited by the 3D and 1D random searches that the repressor conducts to find its binding site [33, 34]. Thus, we have

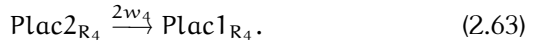
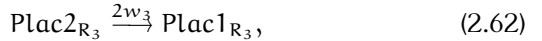
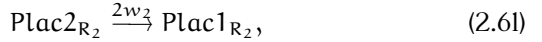
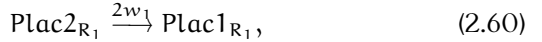
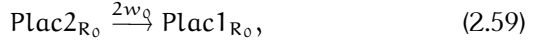
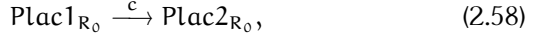
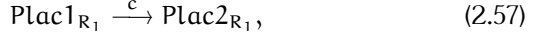
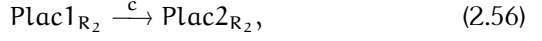
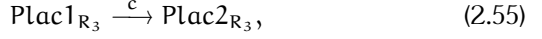
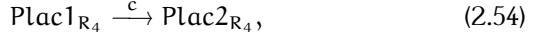


The binding rate of a single repressor to its binding sites has been measured in [19, 17] and they put an upper bound of 6 minutes for a single repressor to find one of its binding sites. This corresponds to $g = 0.166$ /min. We represent the dissociation rate of a repressor with j free binding sites ($4 - j$ inducers bound) from one of its binding sites on the DNA by w_j ,



When one end of the repressor is bound, the rate at which the other end binds to a second site to form the repressor-DNA loop is represented by c . Either of two ends of the repressor can unbind from the DNA to open the loop. DNA loop formation is

then described by



The rate $w_4 = 2.4$ /min (the dissociation rate of repressor molecule from its binding site) has been measured by Dunaway et al. in [18]. The rates w_3, w_2, w_1, w_0 are determined by the condition of detailed balance as described in Section 2.6.

The rate at which the repressor unbinds from both its binding sites and dissociates completely from the *lac*-regulatory region in the absence of inducer molecules is estimated in [17] to be ≈ 0.02 /min. Following the reasoning of Choi et al., total unbinding of the repressor from the DNA occurs when there are two consecutive unbinding events. The repressor-DNA loop is broken by the first unbinding event and if the second unbinding event occurs before the loop is re-formed, the repressor completely unbinds from the *lac*-regulatory region. The rate of complete dissociation of the repressor (η) from the DNA depends on the rate at which the repressor unbinds from one of its binding sites (w_4) and the rate at which the loop reforms if the repressor is bound to one operator site represented by c . As discussed earlier in this section, w_4 and η have been measured in [18, 17]. To compute c , we must determine the relationship between η , c and w_4 .

We assume that the two ends of the repressor bound to DNA unbind independently of each other at rate w_4 and that successive

unbinding events are also independent of earlier binding, unbinding events. Thus, we can treat the unbinding of the repressor from each of its binding sites as independent Poisson processes both characterized by the rate w_4 . Similarly, we can treat the re-formation of the loop when one end of the repressor is bound to DNA as a Poisson process characterized by the rate c .

We can write down simple linear equations that express the lifetime of the repressor in the DNA-repressor loop τ_L , and of the repressor with one leg bound to DNA τ_l in terms of the microscopic rates w_4 and c , as well as the experimentally measured effective rate of dissociation η . We have,

$$\tau_L - \left(\frac{1}{2w_4} + \tau_l \right) = 0, \quad (2.64)$$

$$\tau_l - \left(\frac{w_4}{(w_4 + c)^2} + \frac{c}{w + c} \left(\frac{1}{w_4 + c} + \tau_L \right) \right) = 0. \quad (2.65)$$

Solving these equations

$$\tau_L = \frac{c + 3w_4}{2w_4^2}, \quad (2.66)$$

$$\tau_l = \frac{c + 2w_4}{2w_4^2}, \quad (2.67)$$

where we know,

$$\eta = \frac{1}{\tau_L} = 0.02. \quad (2.68)$$

Thus, we can write down the expression for c in terms of the known rates η and w_4 ,

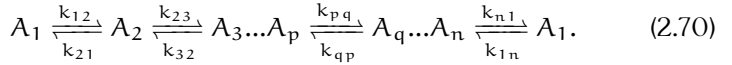
$$c = \frac{2w_4^2}{\eta} - 3w_4 = 568.8. \quad (2.69)$$

2.6. Detailed balance

While the *lac*-operon has been studied extensively, several microscopic rates in the network of DNA-repressor-inducer binding/unbinding reactions remain unavailable in the literature,

see Figure 4.4. Fortunately, we can estimate these using the principle of detailed balance.

In a system composed of many elementary processes (such as chemical reactions), the principle of detailed balance applies when every elementary process is time reversible. At equilibrium, this microscopic reversibility implies that every elementary process must be balanced by its reverse process. While detailed balance does not apply to irreversible processes such as transcription and translation, we can use it to constrain rates in reaction networks involving binding and unbinding of ligands and their substrates. Tree-like reaction networks (which do not have any cycles) in equilibrium always obey detailed balance. For reaction networks which do include cycles, detailed balance provides a relationship between the rates of the reactions involved in each cycle [35]. As an illustration, consider the following cycle:



Then, the relationship between the rates is given by

$$k_{12}k_{23} \dots k_{pq} \dots k_{n1} = k_{21}k_{32} \dots k_{qp} \dots k_{1n}. \quad (2.71)$$

Thus, the principle of detailed balance can be used to determine one rate in each reaction cycle in terms of the others.

In Figure 4.4, the timescales implied by microscopic reactions rates (denoted by lowercase letters next to the relevant transitions, see Table 2.1) are all a lot shorter than the timescales over which inducer concentrations change appreciably (the lifetimes of the quasi-stable induced and uninduced states). So, it is reasonable to assume that this reaction system is always in a local equilibrium, letting us use the principle of detailed balance to deduce unknown reaction rates.

We use the reaction loops in Figure 4.4 to derive the rates of some of the reactions in our model (for more on the various rates involved, see Table 2.1). While the dissociation rate of a repressor with one leg bound to the operator in the absence of inducers (w_4) has been measured in [18], the dissociation rates when one or more inducers are bound to the repressor have not. These we can derive by the principle of detailed balance.

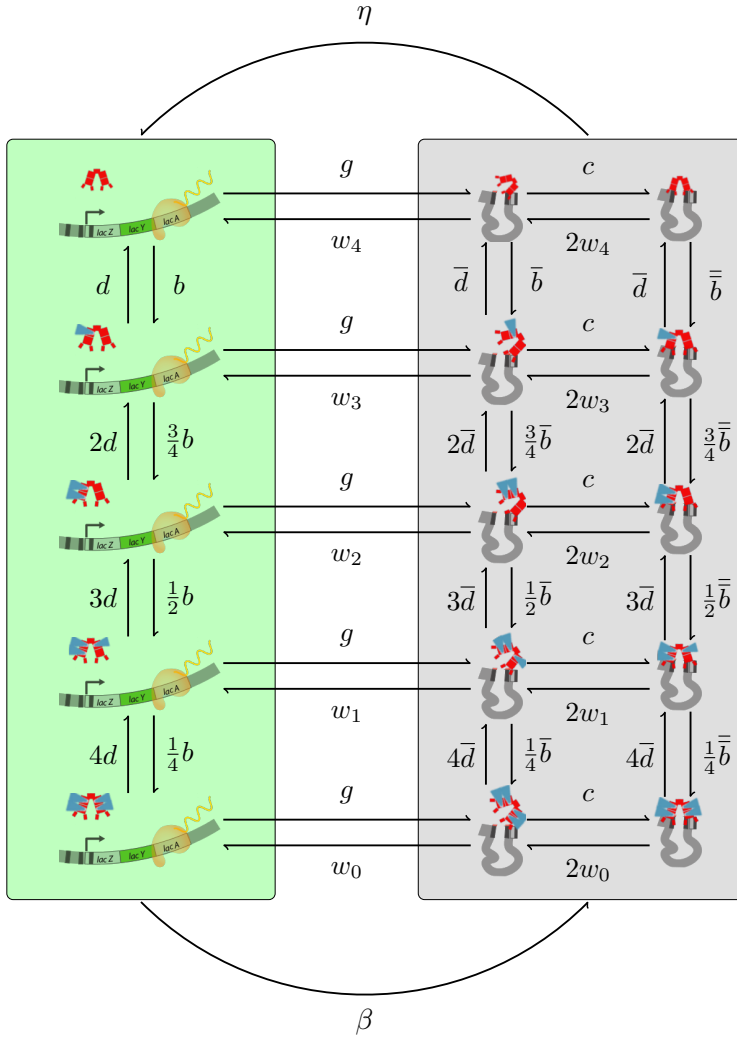


Figure 2.2: The repressor-DNA-inducer reaction system. *This figure is reproduced from published work by the author [2].*

Considering the topmost loop on the left in Figure 4.4 the principle of detailed balance implies,

$$w_3 = \frac{w_4 \cdot \bar{d} \cdot b}{d \cdot \bar{b}}. \quad (2.72)$$

Considering the topmost loop on the right, we establish the relationship between the rate of inducer dissociation from repressor with one leg bound to DNA (\bar{b}) and two legs bound to DNA $\bar{\bar{b}}$,

$$\bar{\bar{b}} = \bar{b} \frac{w_4}{w_3}. \quad (2.73)$$

Similarly,

$$w_2 = \frac{w_3 \cdot \bar{d} \cdot b}{d \cdot \bar{b}}, \quad (2.74)$$

$$w_1 = \frac{w_2 \cdot \bar{d} \cdot b}{d \cdot \bar{b}}, \quad (2.75)$$

$$w_0 = \frac{w_1 \cdot \bar{d} \cdot b}{d \cdot \bar{b}}. \quad (2.76)$$

We consider the reactions involving inducer (TMG) binding to the repressor and the repressor binding to the operator (Eq. (17) to Eq. (60)). The rates of total repressor dissociation η , repressor dissociation from one binding site w_4 , inducer binding to repressor bound and unbound from DNA (\bar{b}, b) and inducer unbinding from repressor bound and unbound from DNA (\bar{d}, d) have been measured in experiments (see Table 2.1). Dunaway et al. [18] report that rates at which repressors with one or more inducers bound to them dissociate from DNA (w_3, w_2, w_1, w_0), are too fast to measure. We use the detailed balance condition to deduce these rates along with the rate at which inducers dissociate from a repressor bound to the DNA at both ends ($\bar{\bar{b}}$).

Substituting the numeric values of the relevant rates (see Table 2.1 for a summary) in the expressions for the $w_j \forall j < 4$ derived

2. THE MODEL

above, we obtain,

$$w_3 = 44.144 \text{ /min} , \quad (2.77)$$

$$\bar{b} = 2.707 \times 10^{-5} \text{ /min} , \quad (2.78)$$

$$w_2 = 811.97 \text{ /min} , \quad (2.79)$$

$$w_1 = 14935.15 \text{ /min} , \quad (2.80)$$

$$w_0 = 274710.82 \text{ /min.} \quad (2.81)$$

2.7. Dilution rate

All molecular species inside the cell are subject to dilution via cell growth,



In our experiments the dilution rate is $\varphi = 0.0167 \text{ /min}$, see Appendix A.

2.8. Other factors

Apart from the chemical reactions and the stochasticity intrinsic to them and to the small numbers of molecules they produce, there are other sources of noise that could be salient to switching behavior. We consider a couple of these below.

2.8.1. Cell Divisions

Cell growth and division involve random partitioning of molecules between the daughter cells which is a source of mRNA and protein number fluctuations. If there are n molecules of a particular type inside the cell just before division and each molecule is equally likely to go to either of the two daughter cells, the probability that m molecules go to one daughter cell while $(n - m)$ go to the other is distributed binomially [36] as

$$P_n(m) = \binom{n}{m} 2^{-n}. \quad (2.91)$$

Every doubling period (60 minutes, in our case) and for each type of molecule (j) in our system (sugars, mRNA, proteins) with abundances n_j , we use the distribution given by Eq. (2.91) to draw a number m_j . In Eq. (2.91) cell division is assumed to be symmetrical and thus the mean $\langle m_j \rangle$ is given by $\langle m_j \rangle = n_j/2$. To normalize the number of molecules per unit volume (the daughter cell has half the volume of the mother cell) we take the abundance of molecule (j) in the daughter cell to be $2m_j$. The variance in m_j implied by Eq. (2.91) is $n_j 2^{-2}$. Since the variance is proportional to abundance n_j , the coefficient of variance (the ratio of the standard deviation to the mean) is proportional to $1/\sqrt{n_j}$ showing that partitioning noise is more significant for molecules with low abundances.

2.8.2. Delays

Delays between different events in a gene regulatory model can be used to effectively describe mechanisms that are not modeled explicitly. For instance, in a model describing gene expression by a single step (omitting RNA production) one can use a delay between transcription factor binding and protein production to account for the intermediate steps of transcription and translation. Such delays, whose duration is a random variable drawn from some distribution, can affect the switching behavior between phenotypic states [37]. In our approach we aim at first for a highly detailed model, which explicitly includes intermediate steps such as transcription and translation. Each of these steps happens at a finite rate, hence delays e.g. between transcription factor

2. THE MODEL

binding and protein production emerge naturally from the model, rather than being put in by hand via an *ad-hoc* delay distribution. It might be that our detailed model is still not sufficiently detailed, requiring the inclusion of either further explicit reactions, or alternatively delays. An example for such a step is the folding of proteins. However, the good match between experimentally determined switching rates and the switching rates observed in the model suggest that we have already captured the relevant processes.

2.8.3. Simulating the model

We performed stochastic simulations of the detailed mechanistic model using the Gillespie algorithm [38] in FORTRAN and Julia. To measure first passage times to the induced state at a given inducer concentration, we first initialized the cells in the uninduced state (0 μ M TMG) for 60 minutes, and then changed the concentration to the one at which switching behavior was being measured. We simulate each cell until a threshold close to the number of pumps in the induced state ≈ 10000 (see [17]) has been crossed. Conversely, to measure the first passage times to the uninduced state, we initialize the cells at 250 μ M TMG, and then change the concentration to the one at which switching behavior is to be measured, and simulate each cell until a threshold close to the number of pumps in the uninduced state ≈ 10 (see [17]) has been crossed.

2.9. Summary

In this chapter we considered various subsystems involved in the *lac*-operon and its regulation. We associated microscopic rates measured in the literature to each chemical reaction, thus establishing the detailed mechanistic model of the *lac*-system that our analysis of switching behavior will be based on. In particular, we considered sugar import, repressor production, pump protein production and the network of inducer-repressor-DNA binding and unbinding reactions.

While the model has a large number of parameters, we identified the Michaelis coefficient of inducer import by pumps as the single parameter we will use to calibrate our simulations

against experiments based on the switch to the induced state that is considered in the next chapter.

2. THE MODEL

3. Switching on

In this chapter analyse the switch to the induced state of the *lac*-pathway. The material presented in this chapter is based on published work done by this author [1]. Experiments referred to in this chapter were performed by Robin A. Sorg from the lab of J. W. Veening and published in joint work with this author [1, 2].

3.1. Introduction

In the previous chapter, we saw a detailed model of the *lac*-pathway that includes the transcription and translation of LacY (lactose importer or ‘pumps’) and LacI proteins (the monomers of the *lac*-repressor), repressor binding to DNA, DNA looping, the uptake of lactose (inducer) or its analog into a cell, inducer interactions with the repressor in solution and bound to DNA, and the passive diffusion of inducers into the cell. As has been discussed before in Chapters 1 and 2, the *lac*-system has two metastable states. In the induced state the *lac*-genes are expressed, the pump molecule LacY exists in the cell in large quantities, the inducer (in our case TMG) is being imported into the cell, and most repressors are bound to one or more inducer molecules making them unlikely to remain on their binding sites on DNA for very long. On the other hand, in the uninduced state, a repressor is tightly bound to its two binding sites forming a stable repressor-DNA loop that effectively inhibits any production

of the pump molecule, and there are very few inducers in the cell.

In this chapter, we will elucidate the mechanism of switching from the uninduced state to the induced state. First, in Section 3.2, we illustrate the analysis of experimental data from experiments reported in joint work with this author (see [1]) to compute the dependence of the switching rate to the induced state on external TMG concentration. We show that stochastic simulations of the model described in Chapter 2 match the experimental rate curve using the Michaelis constant of inducer transport as a free parameter. Then, in Section 3.3, we describe the smoothing procedure introduced by this author and collaborators in [1] to identify what fluctuations influence the switching curve. In Section 3.4 we develop a closed form expression for the switching to the induced state and describe the match with experiment and simulation.

3.2. Switching curves from experiments

To assess expression of the *lac*-genes at the single-cell level flow cytometry was used on a population of *E. coli* strain CH458, which contains a *gfp-cat* cassette inserted downstream of the *lac*-operon [39] (see Appendix A for details). The switching rate from the uninduced state to the induced state is the number of cells per unit time which switch from low numbers of *lac*-proteins to a state with high number of *lac*-proteins. To determine the rate of switching to the induced state, a population of uninduced cells was prepared and the fraction of cells in the uninduced state at subsequent times was fit to an exponential decay. Examples are shown in Figure 3.1. Switching rates are determined at different external inducer concentrations, resulting in a rate curve of the switching rate against inducer concentration (see Figure 3.7).

3.2.1. Simulations and fitting to experiment

We simulate the mechanistic model defined in Table 2.1, and use the parameter E_h (the Michaelis constant of inducer import by LacY) to fit to experimental measurements of the transition to the induced state presented in [1]. The best fit is obtained for $E_h = 1.05 \times 10^5$. As

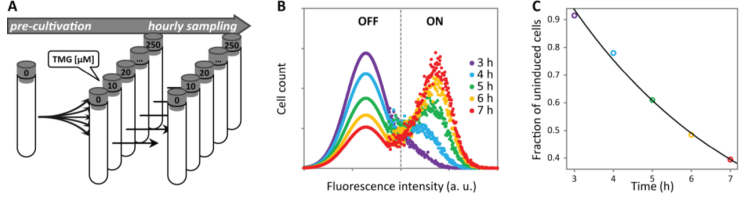


Figure 3.1: Single-cell analysis and the rate of phenotype switching.

A: (Schematic) We take hourly samples from populations of *E. coli* cells growing at different concentrations of the external inducer. Through dilution at regular intervals we keep the populations under constant conditions, see Appendix A and [1]. A fluorescent reporter indicates the expression levels of the *lac*-genes in individual cells. **B:** Fluorescence data taken at 30 μM of TMG (smoothened with a moving average filter for visual clarity) showing the bimodal distribution of reporter expression with high and low levels corresponding to cells in uninduced (OFF) and induced (ON) states. Initially, all cells are in the uninduced state. With time, the fraction of cells in the induced state increases and the fraction of cells in the uninduced state decreases (shown here: purple 3h, blue 4h, green 5h, yellow 6h, red 7h, other time points not shown). **C:** The fraction of cells in the uninduced state decays approximately exponentially with time. Fitting an exponential function (black line) to the data points gives the switching rate to the induced state. For this particular concentration of TMG the switching rate is $3.9 \times 10^{-3} \pm 3.3 \times 10^{-4} / \text{min}$. This figure was jointly made with Robin A. Sorg and is reproduced from published work by the author [1].

3. SWITCHING ON

Figure 3.2 shows, this one fitting parameter is enough to capture the switching rates seen in experiments over several orders of magnitude.

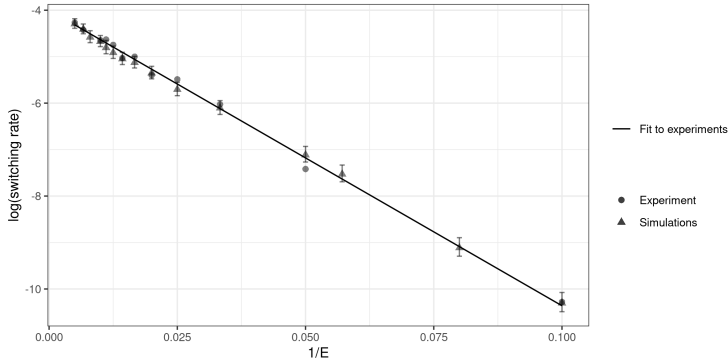


Figure 3.2: Fitting simulations to experiments: Simulations of the mechanistic model with the single fitting parameter $E_h = 1.05 \times 10^5$ match experimental observations taken from [1] over several orders of magnitude of the switching rate, and external TMG concentrations (denoted by E) ranging from $10\mu\text{M}$ to $200\mu\text{M}$. The straight line fit to experiments is shown as a visual guide.

3.3. The smoothening procedure

In the previous section we described how the switching curve is measured in flow cytometry experiments and how we calibrate the free parameter of our model of the *lac*-operon against the experimental rate curve using stochastic simulations. In this section, we will describe smoothening procedure we introduced in [1] and use it to identify the fluctuations that influence the transition to the induced state.

Multistable gene regulatory systems use specific mechanisms like feedback to stabilize expression patterns defining different phenotypic states [5, 40, 41, 42, 43, 44, 45, 46]. However, no natural system is strictly multistable since it will not persist in any one of its states indefinitely. Instead, the lifetimes of stable

states are finite, with random fluctuations causing transitions between different states. In gene regulatory systems the copy numbers of mRNA molecules, proteins, and ligands fluctuate over time due to the random timing of transcription, translation, transport, and binding [47, 29, 48, 49, 20, 50, 51, 52]. These fluctuations can trigger a switch from one phenotype to another [53, 54, 6, 55, 56]. However, when all components of a multistable system fluctuate, what are the fluctuations causing the transition? In other words, what are the rate-limiting fluctuations?

Such rate-limiting fluctuations are difficult to identify experimentally, because it is hard to monitor and control variation in molecular copy numbers inside a cell. In an ideal scenario, one would take a multistable system and reduce the amplitude of fluctuations of each of its components in turn. If reducing the fluctuations of a particular component affects the switching rate between different states, then one can consider fluctuations in that component rate-limiting to the transition. This strategy has been implemented experimentally by Maamar *et al.* [53] for a single component of a bi-stable signaling pathway in *Bacillus subtilis*. The *comK*-pathway enables *B. subtilis* to take up new genetic material, which may offer fitness advantages [57]. Maamar *et al.* increased the transcription rate of *comK* and simultaneously decreased its translation rate. Average protein levels were left unaffected, but fluctuations around this mean due to the random timing of mRNA production were reduced. Maamar *et al.* observed a decrease in the switching rate between the states with low levels of ComK and high levels of ComK, showing that mRNA-fluctuations affect the switching rate. But are these the only rate-limiting fluctuations in the system? Repeating this procedure for all components in a pathway is cumbersome for small pathways and unfeasible for larger pathways. Moreover, transitions could be driven by fluctuations in ligand numbers, protein conformations or binding state, which are even harder to control in experiments.

If rate-limiting fluctuations are hard to identify experimentally, they cannot be identified purely on the basis of regulatory network models and computer simulations either. Any model describes a restricted number of molecular species and replaces the rest with effective reaction rates. The formulation of a model thus already

constitutes an *a priori* assumption on the relevant constituents. Being rare events, transitions between stable states are strongly influenced by the molecular details. Two models can thus exhibit the same bi-stable expression patterns as a function of external parameters, e.g. hysteresis plots [5], yet differ markedly in the mechanisms and rates of switching between states. Indeed the rate-limiting fluctuation is thought to differ drastically across pathways: mRNA fluctuations in the *comK*-pathway [53], fluctuations in initial pump numbers in the arabinose-uptake pathway [54], and gene activity bursts in the λ -phage lysogeny [56]. Hence, transitions between stable states can act as a sensitive probe into molecular details of a pathway.

We described a detailed mechanistic model of the *lac*-system in Chapter 2. To assess the effect of fluctuations in specific components of the *lac*-pathway on the switching rate, we put forward a simple scheme to control fluctuation amplitudes *in silico*. Take a particular component, e.g. *lacY*-mRNA that is produced in units of 1 molecule at some rate. (This rate changes over time due to repressor binding and unbinding to the *lac* regulatory region.) We now change the number of molecules produced in each transcription event by a smoothening factor $s < 1$, and simultaneously divide the transcription and degradation rates by the same factor. For a smoothening factor $s = 0.1$, mRNA molecules are produced in units of $1/10$ but at 10 times the rate. In general this leads to non-integer numbers of molecules in the system. Nevertheless, a well-defined stochastic system results from this procedure: for instance, the Gillespie algorithm simulates transitions between states a, b, c, \dots . For $s = 1$ these states correspond to $(0, 1, 2, 3, \dots)$ molecules in the system, while at $s = 0.1$ they are $(0, 0.1, 0.2, 0.3, \dots)$. The application of this procedure to molecular species like importers and repressors is straightforward, but smoothening the *lac*-regulatory region state requires separate consideration (see Section 3.3.I).

This is impossible to do experimentally but feasible *in silico*; downstream, the rate of protein production will now simply be proportional to a non-integer number of mRNA molecules, and analogously for other molecules and binding states. The effect of this procedure is illustrated in Fig. 3.3. The mean number of

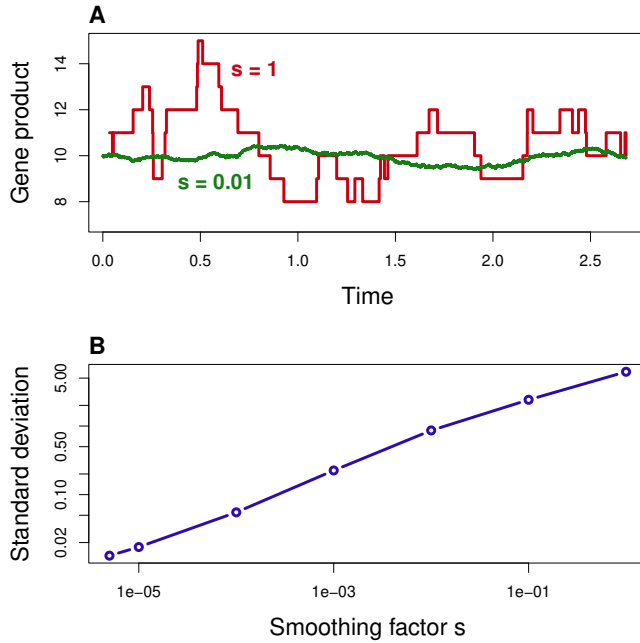


Figure 3.3: The smoothening procedure is illustrated with a birth-death process where some molecule is created and degraded at constant rates. Plot (A) shows the time series of molecular copy numbers with a mean of 10 molecules (red line). For the smoothened dynamics (green line), step sizes are multiplied by the smoothening factor $s = 0.01$ and rates are divided by s , leaving the mean unchanged. Plot (B) shows the standard deviation of molecular copy numbers against the smoothening factor s . The amplitude of fluctuations around the mean increases with s . *This figure is reproduced from published work by the author [1].*

molecules is preserved, but the fluctuations about this mean are reduced by a factor of s . Deterministic dynamics (which can be described by ODEs) corresponds to $s = 0$, while finite values of s result in some degree of stochasticity. If smoothening fluctuations in a particular component affects the switching rate between phenotypic states, we conclude that these fluctuations are rate limiting to the particular transition. On the other hand, if smoothening fluctuations in a particular component is found not to affect the switching rate, its dynamics can be modeled by an ordinary (deterministic) differential equation. In this way, the minimal model describing a particular transition can be determined systematically.

We also found that the noise introduced by random partitioning at cell division does not play a role in the switch to the induced state. We eliminated the noise from cell division by skipping the random partitioning step (see Section 2.8.1) and found no effect on the switching rate curve. As has been pointed out earlier (in Section 2.8.1), fluctuations due to random partitioning are more significant for molecules with low abundances. While there are only about 10 repressors in the *E. coli* cell, the *lac*-system is unaffected by changes in repressor numbers as long as a repressor is bound to the *lac*-regulatory region. Since the lifetime of the repressor-DNA loop is large (approximately 40 min) as compared to the time scale of repressor mRNA transcription (approximately 7 min), the switching rate is insensitive to smoothening of repressor number fluctuations including those caused by cell division.

3.3.1. Smoothening operator state fluctuations

The regulatory region of a gene has only two states with respect to its repressors, *occupied* and *unoccupied*. We aim to smoothen the fluctuations in the operator state without changing the mean production rate of gene product. For this discussion, we assume that the regulatory region undergoes the transition *occupied* \rightarrow *unoccupied* at a rate u and the reverse transition at a rate b . If the rate of production of gene product when the operator is unoccupied is r while the rate of production when operator is occupied by the repressor is approximately zero, the mean rate of production of gene product is $\frac{ru}{u+b}$.

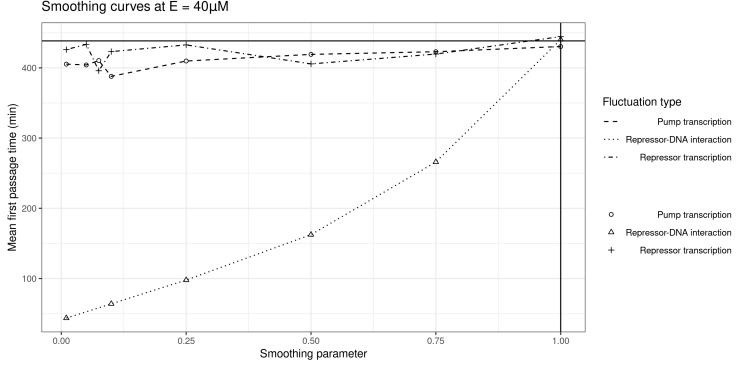


Figure 3.4: Shown is the change in mean first passage time to the induced state as different fluctuations are smoothened. We see that the dominant influence is from operator state fluctuations (repressor-DNA interactions) rather than fluctuations in repressor or pump numbers. Values of the smoothening parameter $s < 1$ indicate reduced fluctuations, where as $s = 1$ reproduces the mechanistic model detailed in Chapter 2.

To smoothen the fluctuations in *lac*-regulatory region state by a factor s , we picture a population of pseudo-promoters which can reach a maximum number of $\frac{1}{s}$ pseudo-promoters, each producing gene product at a rate rs . Now, we define the birth rate of pseudo-promoters

$$u(n) = u \left(\left(\frac{1}{s} \right) - n \right), \quad (3.1)$$

where n is the current population of pseudo-promoters. Note that the birth rate is dependent on n and goes to 0 as n approaches its maximum value of $1/s$. The death rate is the usual population dependent death rate

$$b(n) = bn. \quad (3.2)$$

Thus, the mean population of pseudo-promoters is

$$n_{\text{mean}} = \frac{\frac{u}{s}}{u + b} \quad (3.3)$$

and the mean rate of production of gene product

$$rs \frac{\frac{u}{s}}{u + b} = r \frac{u}{u + b} \quad (3.4)$$

as expected. For $s \rightarrow 0$ the fluctuations around the mean tend to zero.

For this binary system (*occupied* and *unoccupied* state), a simpler smoothening procedure is also feasible [58], namely to increase of both binding and unbinding rates keeping their ratio constant. However, the limit of this procedure is not a deterministic process, whereas the method based on a population of pseudo-operators generalizes the smoothening described above to binary systems. Nevertheless we expect the two methods to yield identical results in practice.

We find that for our system the only relevant fluctuations for the *uninduced* \rightarrow *induced* switch are fluctuations in the operator state. smoothening the fluctuations in other species does not affect the rate of switching, while smoothening fluctuations in the operator state slows down the rate of phenotypic switching to the point of being unobservable over the timescale of our simulations.

3.4. The switching rate γ

In the previous section, we applied the smoothening procedure to various components of our model of the *lac*-system and found that the switching rate curve is unaffected by reducing fluctuations in all components except the operator state. Notably, fluctuations arising from the finite number of *lacY* mRNA and protein, partitioning due to cell division, or the random timing of transcription and translation do not affect the switch to the induced state. Only the random timing of repressors binding to and unbinding from the *lac*-operator affects the switching rate. Reducing these fluctuations, the switching rate decreases until no more transitions to the induced state are observed on the timescale of our simulations. The stochastic dynamics of all other components can be replaced by a smoothen deterministic dynamics without affecting the switching rate (see Section 3.3). Fluctuations in the operator state are thus the rate-limiting fluctuations for the transition to the induced state.

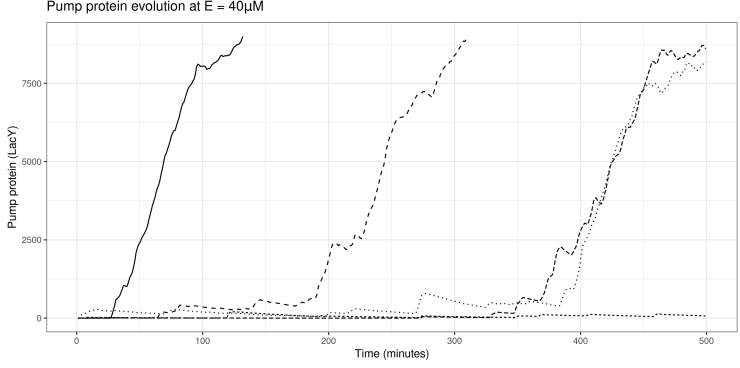


Figure 3.5: Sample time series of the transition to the induced state at an external TMG concentration of $40\mu\text{M}$.

In the *lac*-system, LacI molecules can tetramerize and bind simultaneously to two different operator sites, forming a DNA loop that results in a very effective repression of transcription. A mechanism proposed by Choi *et al.* [6] is that the repressor unbinds from both operator sites, triggering a burst of mRNA production taking the *lac*-pathway to the induced state. However, we find that full repressor unbinding takes place at a far higher rate than the transition to the induced state (see Fig. 3.7). An additional mechanism must be involved.

Once the repressor has released the *lac*-operon, the same repressor molecule (or a different one) might quickly bind again. Alternatively, the operator might remain unbound for a time period τ long enough for sufficient numbers of LacY to be produced and for sufficient inducer molecules to be pumped into the cell to deactivate repressors and switch the cell to the induced state.

Accounting for this threshold period gives a simple but accurate theory of the transition to the induced state of the *lac*-system, analogous to the theory developed by Walczak, Onuchic and Wolynes for a simple model of a self-activating gene [59]. The effect of *lac* expression on the repressors of the *lac*-genes is mediated by the inducing sugars imported by the

3. SWITCHING ON

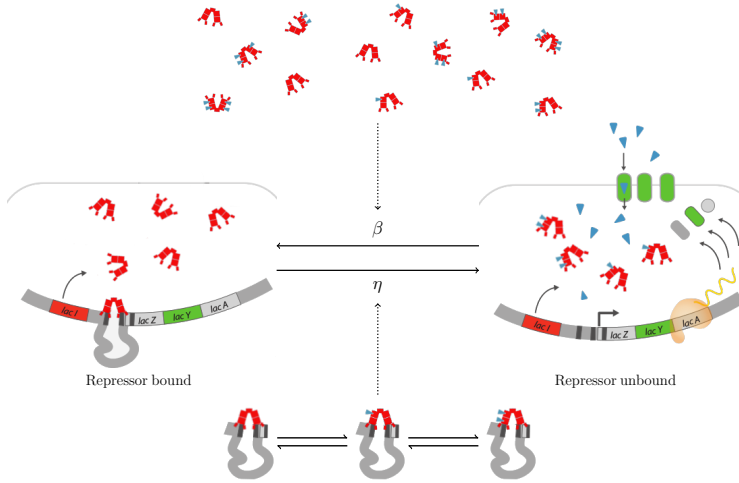


Figure 3.6: Repressor binding and unbinding. The *lac*-repressor (red) binds the *lac* regulatory region with two of its 'legs' forming a DNA loop that prevents transcription of the *lac*-genes (center left). Without a repressor bound, the *lac*-genes are expressed, and the pumps LacY (green) import the inducer lactose (blue triangles). The rate of repressor binding β depends on the number of repressors present in the cell (top), the rate of unbinding η depends on the number of inducers bound to the DNA bound repressor (bottom). *This figure is reproduced from published work by the author [2]. I would like to thank M. Markus for help preparing this figure.*

importer LacY. The threshold period τ is then given by the time required to express a number of importers sufficient to maintain a certain concentration of inducers in the cell. This critical number of importers is set by the requirement that repressors are deactivated by binding to the imported inducers. Thus, the time period τ is a function of external inducer concentration.

The time period for which the operator is free of repressors depends on the binding and unbinding rates of repressor to the operator. In the uninduced state, there are very few inducers in the cell, so the rate η at which the repressor completely unbinds is known (see Table 2.1). In Chapter 2 we had denoted the rate at which a single repressor will bind to the operator by g (see Table 2.1). If R is the number of repressors in the cell, then the rate at which the *lac*-regulatory region will be found by some repressor is $\beta = Rg$. In the *lac*-system there are approximately 10 repressors in the cell [15], giving $\beta = 10 \times g = 1.66$.

First, we derive an expression for the switching rate γ in terms of the rates η , β and the threshold period τ . In a subsequent step, we will calculate the expression for the threshold period τ , and calibrate it against data from experiments and simulations.

We derive an expression for the threshold rate γ in two steps. First, we compute the expected time taken for one complete binding-unbinding cycle between the repressor and the DNA, assuming that the operator *does not* stay free of repressors longer than the threshold period τ . Then, we calculate the expected number of such cycles until the operator *does* stay free of repressor for τ minutes, and the system switches to the induced state. Multiplying these two quantities together gives us the expected waiting time to the switch to the induced state, the inverse of which is the switching rate γ .

We treat binding and unbinding of the repressor from the *lac*-regulatory region as independent Poisson processes characterized by the rates g and η respectively. We note again that the time intervals t between successive events in a Poisson process with a rate parameter λ are independently distributed according to an exponential distribution $p(t) = \lambda e^{-\lambda t}$.

Let $p_b(t_b)$ denote the probability distribution of time periods t_b over which the *lac*-regulatory region remains occupied by a repressor, i.e. t_b is the time interval between a binding and a

successive complete unbinding event. Similarly, we denote by t_u the time intervals for which the *lac*-regulatory region remains free of repressors, i.e. t_u is the time period between a complete unbinding event and a binding event that follows it.

Let the probability distribution of times $t_u < \tau$ for which the *lac*-regulatory region remains free of repressors for a period less than the threshold period τ be $p_{t_u < \tau}(t_u)$. We denote the Laplace transform of $p_b(t_b)$ by $P_b(s)$ and the Laplace transform of $p_{t_u < \tau}(t_u)$ by $P_u(s)$. Then we have

$$p_b(t_b) = \eta \cdot e^{-\eta \cdot t_b} \quad (3.5)$$

$$P_b(s) = \frac{\eta}{s + \eta} \quad (3.6)$$

$$p_{t_u < \tau}(t_u) = \begin{cases} \frac{\beta \cdot e^{-\beta \cdot t_u}}{1 - e^{-\beta \cdot \tau}} & \text{if } t_u < \tau, \\ 0 & \text{if } t_u > \tau. \end{cases} \quad (3.7)$$

$$P_u(s) = \frac{\beta}{e^{\beta \cdot \tau} - 1} \cdot \frac{e^{\beta \cdot \tau} - e^{-s \cdot \tau}}{\beta + s}. \quad (3.8)$$

We now consider a cycle of binding, complete unbinding and rebinding before the threshold period τ has elapsed, taking the time t_b plus $t_u < \tau$. We denote the Laplace transform of the distribution of the time taken by each cycle ($t_u + t_b$) by $P_{cy}(s)$. Since the time taken by each unbinding-binding cycle is just the addition of two random variables (time intervals over which the operator region is bound t_b and unbound t_u) with known distributions $p_b(t_b)$ and $p_{t_u < \tau}(t_u)$, in the Laplace domain we have

$$P_{cy}(s) = P_b(s) \cdot P_u(s). \quad (3.9)$$

Using $P_{cy}(s)$ we can calculate the average time taken for one unbinding-rebinding cycle $E(t_{cy})$,

$$E(t_{cy}) = \left[-\frac{d}{ds} P_{cy}(s) \right]_{s \rightarrow 0} \quad (3.10)$$

$$= \left[\frac{1}{\beta} + \frac{1}{\eta} \right] - \frac{\tau}{e^{\beta \cdot \tau} - 1}. \quad (3.11)$$

The number of unbinding-rebinding cycles before the *lac*-regulatory region finally remains unoccupied for a time

greater than τ is a random number. Let $p_{cy}(n)$ be the probability that n such unbinding-binding cycles occur before the *lac*-regulatory region finally remains unoccupied for time greater than τ and let $G_{cy}(s)$ be the corresponding probability generating function,

$$p_{cy}(n) = (1 - e^{-\beta \cdot \tau})^n \cdot e^{-\beta \cdot \tau} \quad (3.12)$$

$$G_{cy}(s) = \frac{1}{(1 - e^{-\beta \cdot \tau})} \sum_{n=0}^{\infty} (1 - e^{-\beta \cdot \tau})^n \cdot e^{-\beta \cdot \tau} \cdot s^n \quad (3.13)$$

$$= \frac{e^{-\beta \cdot \tau}}{(1 - e^{-\beta \cdot \tau})} \frac{1}{1 - s \cdot (1 - e^{-\beta \cdot \tau})} \cdot \quad (3.14)$$

If $E(n)$ is the average number of unbinding-rebinding cycles before the operator region remains unoccupied for a time τ , we can calculate $E(n)$

$$E(n) = \left[\frac{d}{ds} G_{cy}(s) \right]_{s \rightarrow 1} \quad (3.15)$$

$$= \left[\frac{e^{-\beta \cdot \tau}}{(1 - e^{-\beta \cdot \tau})} \frac{d}{ds} \left(\frac{1}{1 - s \cdot (1 - e^{-\beta \cdot \tau})} \right) \right]_{s \rightarrow 1} \quad (3.16)$$

$$= \left[\frac{e^{-\beta \cdot \tau}}{(1 - e^{-\beta \cdot \tau})} \left(\frac{(1 - e^{-\beta \cdot \tau})}{(1 - s \cdot (1 - e^{-\beta \cdot \tau}))^2} \right) \right]_{s \rightarrow 1} \quad (3.17)$$

$$= \frac{e^{-\beta \cdot \tau}}{e^{-2\beta \cdot \tau}} \quad (3.18)$$

$$= e^{\beta \cdot \tau}. \quad (3.19)$$

Given that successive binding and unbinding events are statistically independent, the expected time of switching $E(t_{sw})$ is the average time taken by every binding-unbinding-rebinding cycle $E(t_{cy})$ multiplied by the average number of such cycles $E(n)$

$$E(t_{sw}) = E(n) \cdot E(t_{cy}). \quad (3.20)$$

We then calculate the rate of switching $\gamma = 1/E(t_{sw})$ using $E(t_{cy})$ from Eq. (3.11) and $E(n)$ from Eq. (3.19) to obtain

$$\frac{1}{\gamma} = e^{\beta \cdot \tau} \cdot \left[\left(\frac{1}{\beta} + \frac{1}{\eta} \right) - \frac{\tau}{e^{\beta \cdot \tau} - 1} \right]. \quad (3.21)$$

Equation (3.21) gives the switching rate from the uninduced state to the induced state γ as a function of τ . The terms $1/\eta$ and $1/\beta$ represent the average periods for which the *lac*-regulatory region is occupied and unoccupied by the repressor respectively (t_b , t_u as defined previously in this section), while the $\frac{\tau}{e^{\beta \cdot \tau} - 1}$ term accounts for the fact that the operator region is never unoccupied for a period greater than τ until the switch occurs.

In the next section, we derive an expression for the threshold period τ in terms of the external inducer concentration E .

3.4.1. The threshold period τ

The threshold period connects the switching rate γ to external inducer concentration. The time interval τ needs to be long enough to produce enough pumps (LacY) such that positive feedback kicks in and the system switches to the induced state. As has been discussed in earlier chapters, the LacY protein modulates its own production via two intermediaries - a sugar (TMG in this case) which is imported by LacY, and a repressor whose activity is reduced upon being bound by the sugar. The sugar thus acts as an inducer for LacY production,

$$Y_\tau = I_\tau \frac{\varphi + f^{\text{out}}}{m} \left(1 + \frac{E_h}{E} \right), \quad (3.22)$$

where E_h is the Michaelis constant for inducer import by pumps, m is the rate of inducer import by 1 pump in the presence of an infinite concentration of external inducers (see Table 2.1), φ is the dilution rate, f^{out} is the diffusion rate of inducer out of the cell through the cell membrane and I_τ is a free parameter of effective switching to be calibrated against experiment and simulation.

At low external inducer concentrations more pumps are required to maintain a certain inducer level inside the cell. The threshold time period τ is the time needed to make Y_τ proteins if the operator remains free of repressors. Thus, τ is related to Y_τ via the rates of transcription (c^Y), translation (l^Y) and the mRNA lifetime (ϕ),

$$\tau = Y_\tau \frac{\phi}{c^Y l^Y}. \quad (3.23)$$

Using Eq. (3.22) and Eq. (3.23) we obtain for the threshold period

$$\tau = \underbrace{I_\tau \frac{\phi}{c^\gamma l^\gamma} \frac{\varphi + f^{\text{out}}}{m}}_{\omega} \left(1 + \frac{E_h}{E} \right) \quad (3.24)$$

$$= \omega \left(1 + \frac{E_h}{E} \right), \quad (3.25)$$

where,

$$\omega = I_\tau \frac{\phi}{c^\gamma l^\gamma} \frac{\varphi + f^{\text{out}}}{m}. \quad (3.26)$$

We substitute Eq. (3.25) in the equation for the switching rate Eq. (3.21), and then with I_τ as the free parameter of effective switching rate, calibrate against experiment to obtain $I_\tau = 5292$, which implies $\omega = 3.9 \cdot 10^{-4}$. Figure 3.7 shows the match between experiment, simulation and the effective theory for the switching rate.

3.4.2. Simplified expression for γ

The switching rate γ is high when τ is small (high external concentration of inducers) and when the rate of repressors binding to the operator β is small. Thus, the threshold period theory explains the observation in theoretical models that speeding up the rate of repressor-operator binding and unbinding leads to a decrease of the switching rate [60, 9, 61]. Fig. 3.7 shows excellent agreement between the experimentally determined switching rate, the mechanistic model, and the theoretical switching rate curve Eq. (3.21). If the gene is in the repressed state for most of the time ($\beta \gg \eta$), the switching rate (3.21) simplifies to

$$\gamma = \eta e^{-\beta\tau} = \eta e^{-\beta\omega \left(1 + \frac{E_h}{E} \right)}, \quad (3.27)$$

which is the rate of repressor unbinding η divided by the expected number of unbinding-rebinding events $e^{\beta\tau}$ per switch derived earlier in this section. This expression predicts a linear relationship between the logarithm of the switching rate and the inverse external inducer concentration, see Fig. 3.8.

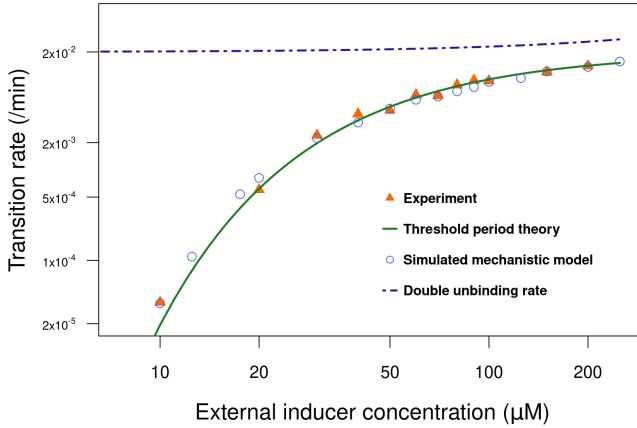


Figure 3.7: The transition from uninduced to induced state of the *lac*-system. The unshaded region indicates the range of external inducer (TMG) concentration where switching rates from the uninduced to the induced state of the *lac*-system could be determined experimentally. Orange triangles give the switching rates as determined in Fig. 3.1 for different inducer concentrations. The experimentally determined switching rates agree closely with the switching rates observed in computer simulations of the mechanistic model (blue circles). The rate of unbinding of the repressor from both its binding sites (simulations, dashed blue line) which was established by Choi *et al.* [6] as a necessary condition for a switch to occur, is up to 3 orders of magnitude greater than the switching rate. The full green line gives our theoretical result Eq. (3.21) for the switching rate, which takes into account the threshold time period between repressor unbinding and rebinding. *This figure is reproduced from published work by the author [1].*

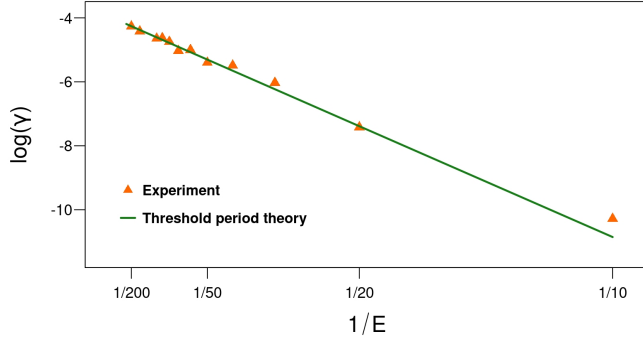


Figure 3.8: Linear relationship between switching rate and inducer concentration on a logarithmic/inverse plot. We re-plot data from Fig. 3.7 in the form suggested by equation (3.27). The logarithm of the switching rate turns out to be in good approximation a linear function of the inverse external inducer concentration. The slope $-\omega\beta E_h$ and the intercept $\ln(\eta) - \omega\beta$ of this plot allow to directly read off the parameters E_h and $\omega\beta$ from the experimentally measured switching rates (given the unbinding rate η). *This figure is reproduced from published work by the author [1].*

3.5. Summary

In this chapter we combined data from experiments and stochastic simulations, and identified the rate limiting fluctuation driving the switch to the induced state of the *lac*-operon by smoothening out each source of fluctuation in turn to observe *in silico* the effect each fluctuation had on the switching behavior. We found that the fluctuations in the operator state drove the switch to the induced state.

Then, we derived an expression for the switching rate γ and linked it to the external inducer concentration via the notion of the threshold period for which the operator needed to be free of repressor to cause a switch to the induced state, and matched this with experiments and simulation with one free parameter representing the number of inducers needed to tip the cell over to the induced state.

Finally, we simplified the expression for the switching rate to predict that there would be a linear relationship between the logarithm of the switching rate and the inverse of the external inducer concentration, and found that this matches very well with observations from experiments.

4. Switching off

In this chapter, we analyse the switch to the uninduced state of the *lac*-pathway. The material presented in this chapter is based on published work done by this author [2]. Experiments referred to in this chapter were performed by Robin A. Sorg from the lab of J. W. Veening and published in joint work with this author [1, 2].

4.1. Introduction

After examining the transition from the uninduced to the induced state of the *lac*-operon, we turn to the reverse transition - the transition from the induced to the uninduced state. The induced state of the *lac*-system is long lived and the transition to the uninduced state is hard to observe (see Section 4.1.1 and Appendix A).

In this chapter, we will first present analysis of data from flow cytometry experiments to infer switching rates at different levels of external inducer concentrations (see Sections (3.2, 4.1.1 and Appendix A). Then, we present the results of the smoothening process introduced in [1] and Section 3.3 to identify the key fluctuations influencing the transition to the uninduced state. We find that several different sub-systems are involved in this transition, and we consider these in order to derive effective rates of repressor binding and unbinding to the operator. We then use these effective rates to write master equations for protein

production, from which we derive the Fokker-Planck equation for protein evolution following the methodology outlined in [9, 7]. We also derive a Fokker-Planck equation for repressor numbers and use both of these to set up the 2D backward Fokker-Planck equation in repressor and pump numbers. Using the backward Fokker-Planck equation, we derive the differential equation for mean first passage times to the uninduced state. We solve this equation numerically and compare the results to experiments.

4.1.1. Experimental measurements

First, we consider the experimental data for the transition to the uninduced state. See [1, 2] for details. Following the methodology outlined in [1], we estimate the first passage times (the inverse of the switching rate) from the induced to the uninduced state by fitting exponential curves to experimental measurements of the fraction of cells in the induced state as a function of time.

For TMG concentrations below $5\mu\text{M}$, we see a population-wide collapse to the uninduced state - implying that the induced state is not viable at these concentrations. This graded dynamic response has been called “ballistic” [20] (as opposed to the stochastic switching that occurs in the bi-stable regime). At TMG concentrations of $5\mu\text{M}$ and $7.5\mu\text{M}$ we can measure the switching rates (see Fig. 4.1), whereas for concentrations of $10\mu\text{M}$ and over, no switching events are observed at all.

Since we have approximately 10^6 cells in our experiment (see [1]), the lack of a single transition over the 480 minutes of experimental observations leads to an estimate of the lifetime of the induced state (approximately 2×10^9) minutes with a probability of 0.8, for concentrations of external TMG of $10\mu\text{M}$ and above.

4.1.2. Smoothening curves for different fluctuations

Before we attempt to analyse the transition to the uninduced state we must identify the key fluctuations that play a role in determining the switching rate. Following the methodology established in [1] and Section 3.3, we “smoothen” various fluctuations of interest to see if this affects the MFPT to the induced state for the *lac*-system.

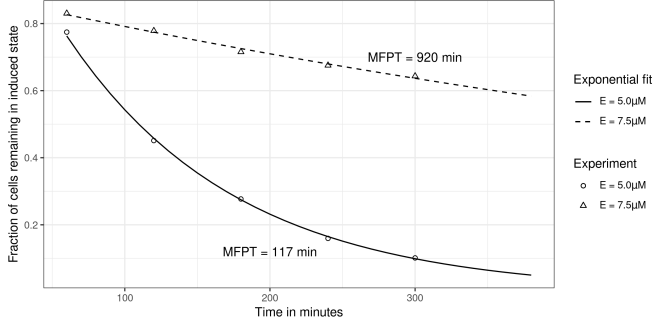


Figure 4.1: Inferring switching rates: Shown above are fits for external TMG concentrations $5\mu\text{M}$ and $7.5\mu\text{M}$, which give us switching rates of 8.51×10^{-3} and 1.08×10^{-3} respectively.

Fluctuations in binding-unbinding interactions were smoothened by dividing the binding as well as unbinding rates by the smoothening parameter s (so, $s = 0.1$ would mean that the binding-unbinding process happens on a time scale that is 10x faster). On the other hand, fluctuations in production processes (transcription, translation) were modeled by dividing the rate or production by s , and multiplying the quantum of production by s . So, if a transcription process produced one mRNA per minute on average, a smoothening of $s = 0.1$ would mean that mRNA is produced in “units” of 0.1, but ten times faster. The mean level of mRNA would remain the same, but the fluctuations in mRNA levels would decrease.

For the transition to the uninduced state of the *lac*-system, Figure. 4.2 shows the evolution of the MFPT as various fluctuations are smoothened. We find that operator state fluctuations have the largest influence on switching to the uninduced state, but repressor numbers and inducer-repressor interactions also play a role, see Figure. 4.2 and Figure. 4.8.

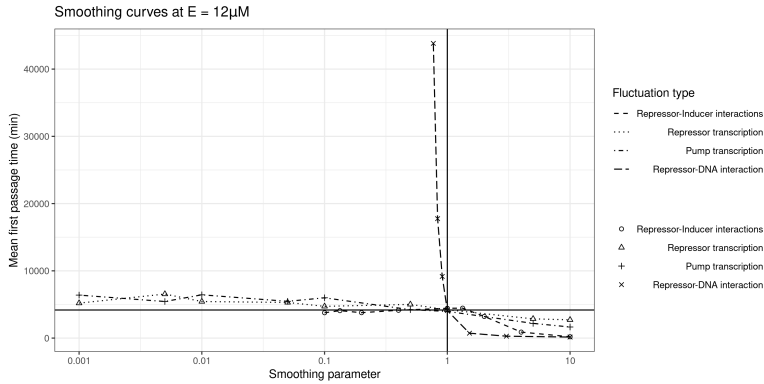


Figure 4.2: We plot the mean first passage time to the uninduced state as a function of the smoothening parameter s when the smoothening of fluctuations is applied to different types of fluctuations. Values of the smoothening parameter s less than 1 represent smoothened fluctuations (reduced fluctuations) compared to the baseline parameters of the model, whereas values of s greater than 1 represent artificially enhanced fluctuations. Fluctuations in the binding state between repressor and DNA (caused by the formation and breakage of the repressor-DNA loop) have the strongest influence on the mean first passage time; the mean first passage time rapidly increases for s less than one. Fluctuations in transcription events of repressors and pumps affect the mean first passage time comparatively weakly (the *lacI* gene is expressed constitutively, so there are no operator state fluctuations).

4.2. The unbinding rate η

In the previous section, we determined that operator state fluctuations play a major role in the transition to the uninduced state. The state of the operator depends on two effective rates, the rate at which a repressor binds to the operator β , and the rate at which a repressor completely unbinds from the operator - η . In this section we analyse the network of reactions that define interactions between DNA, repressor, and inducer molecules to calculate an effective rate $\eta(E, Y)$ as a function of pump numbers Y and external inducer concentration E .

The unbinding of the *lac*-repressor from the regulatory region of the *lac*-operon is a composite event for two reasons: First, the repressor consists of two ‘legs’, both of which need to unbind from their binding sites. Second, the unbinding rate of each leg depends on the number of inducers bound to the repressor, and that number can change even while the repressor is bound to the *lac*-operon.

Each *lac*-repressor can bind up to 4 inducer molecules (one per LacI protein, four of which make a single repressor) and the repressor-operator affinity decreases with each successive inducer bound to the repressor. For instance, a repressor with two inducers bound to it will dissociate from one operator site at the rate of 811/min (see Table 2.1), while a repressor with no inducers bound to it has a much lower dissociation rate of 2.4/min[18].

The repressor-operator system can thus be characterized by the number of inducers bound to a repressor, and the number of legs bound to the regulatory region. These configurations are shown in Fig. 4.3, along with the transitions between them. Unfortunately, not all rates of repressor binding and unbinding in the presence of different numbers of inducers have been measured experimentally (to the best of our knowledge). We use the detailed balance condition to infer some of these rates, see Section 2.6.

The *lac*-repressor can bind to 3 different sites on DNA - the primary operator O1, and two so-called *pseudo operators* O3 (which is 92 bp upstream from O1) and O2 (401 bp downstream of O1). In [62], C hler et. al report that in the presence of O1 and O2, O3 does not seem to play any role in DNA loop formation. So, we assume that the DNA-repressor loop formation is between O1 and

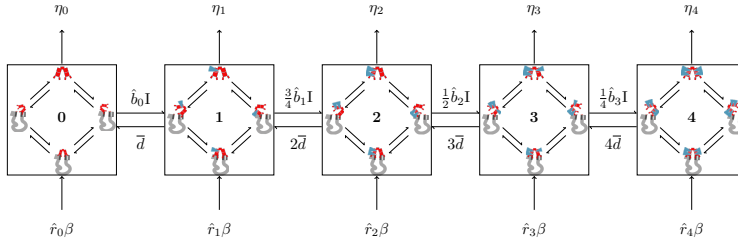


Figure 4.3: Repressor unbinding. The repressor unbinding rate depends on the number of inducers bound to the repressor, which changes over time. From left to right, 0, 1, 2, 3 or 4 inducers are bound to the repressor, with the changes in the number of inducers are indicated by horizontal arrows. The effective rates of inducer binding to the inducer-DNA system are given by \hat{b}_i and the dissociation rate for a single inducer is given by \bar{d} (see Table 2.1 and Section 2.5 for details). The two legs of the repressor can unbind individually (diagonal arrows in each subplot). When both legs have unbound, the repressor dissociates from the regulatory region. *This figure is reproduced from published work by the author [2].*

O2, and we do not consider the marginal role O3 might play.

Assuming that the repressor is bound to DNA in the O1-repressor-O2 loop, the model for the effective dissociation rate η can be broken up into a series of simpler computations, which will be implemented in the sub-sections that follow:

1. First, we compute the dissociation rates from DNA $\{\eta_j\}$ of repressors with j inducers bound to them under the simplifying assumption that there are no inducer interactions with the DNA bound repressors. See Section 4.2.1.
2. Then, we calculate the effective inducer interaction rates for DNA bound repressors with j inducers bound to them, which we denote by $\{\hat{b}_j\}$. See Section 4.2.2.
3. We add the inducer interactions to the DNA bound repressor system and use the $\{\eta_j\}$ s and the $\{\hat{b}_j\}$ s calculated in Sections 4.2.1 and 4.2.2 to compute the DNA residence times $\{\tau_j\}$ of repressors that from a DNA-repressor loop with j inducers bound. See Section 4.2.3.
4. From the fractions of repressors in the cell with j inducers bound to them $\{r_j\}$, we calculate the probability for a DNA-repressor loop form with j inducers bound to it, $\{\hat{r}_j\}$. See Section 4.2.4.

The dissociation rate η is then the inverse of the expectation of lifetimes $\{\tau_j\}$ over the probabilities $\{\hat{r}_j\}$.

4.2.1. Repressor unbinding without inducer interaction - the $\{\eta_j\}$

We want to investigate the rate of dissociation of a repressor with j inducers bound to it if no further inducer-repressor binding-unbinding events are possible. This means (in Figure 4.4) traversing the horizontal row from the brown box to the green box, right to left.

Let the time to escape if we start in the repressor-inducer loop be denoted by τ_L and the time to escape if we start in the single leg bound state be denoted by τ_1 . Since we know the microscopic

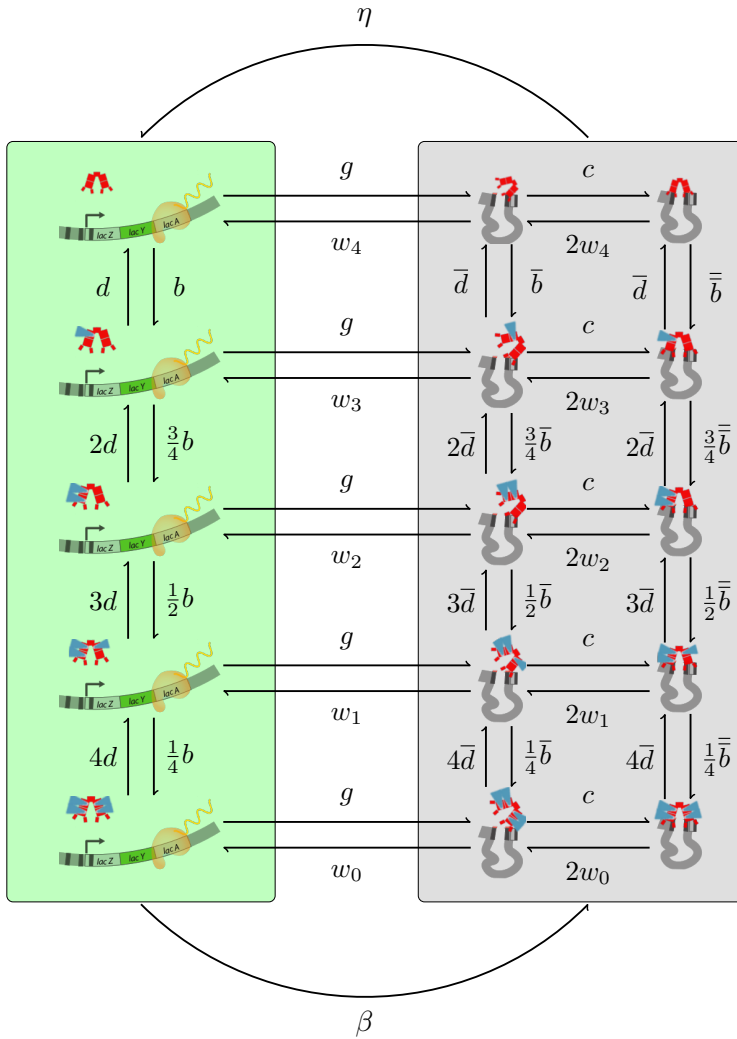


Figure 4.4: The repressor-DNA-inducer reaction system. *This figure is reproduced from published work by the author [2].*

rates of every reaction in the system shown in Figure 4.4, we can express the residence times in each state of the reaction system in terms of residence times at other states, and the microscopic reaction rates. This yields linear equations relating the residence times in different states of one horizontal row in Figure 4.4,

$$\tau_L^j - \left(\frac{1}{2w_{4-j}} + \tau_L^j \right) = 0, \quad (4.1)$$

$$\begin{aligned} \tau_L^j - \left(\frac{w_{4-j}}{(w_{4-j} + c)^2} \right. \\ \left. + \frac{c}{w_{4-j} + c} \left(\frac{1}{w_{4-j} + c} + \tau_L^j \right) \right) = 0. \end{aligned} \quad (4.2)$$

Solving these equations we have,

$$\tau_L^j = \frac{c + 3w_{4-j}}{2w_{4-j}^2}, \quad (4.3)$$

$$\tau_L^j = \frac{c + 2w_{4-j}}{2w_{4-j}^2}, \quad (4.4)$$

$$(4.5)$$

and

$$\eta_j = \frac{1}{\tau_L^j}. \quad (4.6)$$

We have computed the dissociation times for repressors with different numbers of inducers bound to them if no further inducer binding or unbinding events take place.

4.2.2. Effective inducer interactions with the repressor-DNA loop

Now, we analyse the interactions of inducers with the DNA bound repressor so that we can include these and combine them with the $\{\eta_j\}$ calculated in Section 4.2.1 in order to compute the effective dissociation rate. In the DNA-repressor loop, the rate at which inducers bind is \bar{b} whereas with just one leg bound to DNA, it is \bar{b} . The effective rate of inducer-repressor interactions is thus an average between these rates taking into account (for j inducers

bound to the repressor) the lifetimes of the states (with two and one legs bound to the DNA), and the probability that an inducer binds to the repressor in each of those states.

The lifetime of a repressor with j inducers bound to it in the DNA-repressor loop (time until one leg unbinds or an inducer binds or unbinds) is

$$t_j^I = \frac{1}{\left(2w_{4-j} + j\bar{d} + \frac{4-j}{4}\bar{b}I\right)}, \quad (4.7)$$

whereas the probability that it will exit this state when an inducer binds to it is

$$p_j^I = \frac{\frac{4-j}{4}\bar{b}I}{\left(2w_{4-j} + j\bar{d} + \frac{4-j}{4}\bar{b}I\right)}. \quad (4.8)$$

Similarly, for the state with one leg of the repressor bound to the inducer we have

$$t_j^I = \frac{1}{\left(w_{4-j} + c + j\bar{d} + \frac{4-j}{4}\bar{b}I\right)}, \quad (4.9)$$

and

$$p_j^I = \frac{\frac{4-j}{4}\bar{b}I}{\left(w_{4-j} + c + j\bar{d} + \frac{4-j}{4}\bar{b}I\right)}. \quad (4.10)$$

Using these, we can write the effective rate of inducer interaction with the DNA-repressor loop as,

$$\hat{b}_j = \left(\frac{t_j^I p_j^I (1/\bar{b}) + t_j^I p_j^I (1/\bar{b})}{t_j^I p_j^I + t_j^I p_j^I} \right)^{-1} \quad \forall j \in \{0, 1, 2, 3\}. \quad (4.11)$$

4.2.3. Including inducer interactions

Armed with the dissociation rates without further inducer interaction $\{\eta_j\}$ and the effective rates $\{\hat{b}_j\}$ of inducer binding to DNA bound repressors, we can set up equations for the dissociation times of the repressors with j inducers bound to them. See Figure 4.3. As before, we write linear equations relating lifetimes in different states (see Figure 4.3) and the $\{\tau_j\}$ - the

average residence times on the operator for repressors with j inducers bound to them starting in the DNA-repressor loop,

$$\tau_0 - \frac{\eta_0}{(\eta_0 + \hat{b}_0 I)^2} - \frac{\hat{b}_0 I}{\eta_0 + \hat{b}_0 I} \left(\frac{1}{\eta_0 + \hat{b}_0 I} + \tau_1 \right) = 0, \quad (4.12)$$

$$\begin{aligned} \tau_1 &= \frac{\eta_1}{(\eta_1 + \bar{d} + 0.75\hat{b}_1 I)^2} \\ &- \frac{\bar{d}}{\eta_1 + \bar{d} + 0.75\hat{b}_1 I} \left(\frac{1}{\eta_1 + \bar{d} + 0.75\hat{b}_1 I} + \tau_0 \right) \\ &- \frac{0.75\hat{b}_1 I}{\eta_1 + \bar{d} + 0.75\hat{b}_1 I} \left(\frac{1}{\eta_1 + \bar{d} + 0.75\hat{b}_1 I} + \tau_2 \right) = 0, \end{aligned} \quad (4.13)$$

$$\begin{aligned} \tau_2 &= \frac{\eta_2}{(\eta_2 + 2\bar{d} + 0.5\hat{b}_2 I)^2} \\ &- \frac{2\bar{d}}{\eta_2 + 2\bar{d} + 0.5\hat{b}_2 I} \left(\frac{1}{\eta_2 + 2\bar{d} + 0.5\hat{b}_2 I} + \tau_1 \right) \\ &- \frac{0.5\hat{b}_2 I}{\eta_2 + 2\bar{d} + 0.5\hat{b}_2 I} \left(\frac{1}{\eta_2 + 2\bar{d} + 0.5\hat{b}_2 I} + \tau_3 \right) = 0, \end{aligned} \quad (4.14)$$

$$\begin{aligned} \tau_3 &= \frac{\eta_3}{(\eta_3 + 3\bar{d} + 0.25\hat{b}_3 I)^2} \\ &- \frac{3\bar{d}}{\eta_3 + 3\bar{d} + 0.25\hat{b}_3 I} \left(\frac{1}{\eta_3 + 3\bar{d} + 0.25\hat{b}_3 I} + \tau_2 \right) \\ &- \frac{0.25\hat{b}_3 I}{\eta_3 + 3\bar{d} + 0.25\hat{b}_3 I} \left(\frac{1}{\eta_3 + 3\bar{d} + 0.25\hat{b}_3 I} + \tau_4 \right) = 0, \end{aligned} \quad (4.15)$$

$$\begin{aligned}\tau_4 &= \frac{\eta_4}{(\eta_4 + 4\bar{d})^2} \\ &- \frac{4\bar{d}}{\eta_4 + 4\bar{d}} \left(\frac{1}{\eta_4 + 4\bar{d}} + \tau_3 \right) = 0,\end{aligned}\quad (4.16)$$

which can be solved simultaneously for the $\{\tau_j\}$ with Mathematica. To calculate the effective dissociation rate η , we need to combine these $\{\tau_j\}$ with the probabilities for an repressor-DNA loop to form with j inducers bound to it.

4.2.4. Probability of forming a repressor-DNA loop with j bound inducers

Now that we know the lifetime of the repressor with j inducers bound to it in a DNA-repressor loop, the expected lifetime of such a loop is an average over the probabilities that the DNA-repressor loop with j inducers bound exists in the first place. This is what we will tackle in this section.

Let the number of inducers inside the cell be I . The details regarding rates of inducer-repressor binding and unbinding are discussed in Section 2.5. For convenience, we define

$$a = \frac{Ib}{d}, \quad (4.17)$$

where b is the rate at which an inducer binds to a repressor free of inducers and d is the rate at which an inducer dissociates from a repressor with all its inducer binding sites occupied as described in Section 2. If we represent the fraction of repressors bound to j sugars by r_j , at equilibrium we have

$$\frac{r_1}{r_0} = a, \quad (4.18)$$

$$\frac{r_2}{r_1} = \frac{3}{8}a, \quad (4.19)$$

$$\frac{r_3}{r_2} = \frac{a}{6}, \quad (4.20)$$

$$\frac{r_4}{r_3} = \frac{a}{16}. \quad (4.21)$$

Since $\sum_{j=0}^4 r_j = 1$, we can calculate the fraction of repressor molecules which are free from inducers to be

$$r_0 = \frac{1}{1 + \alpha + \frac{3}{8}\alpha^2 + \frac{\alpha^3}{16} + \frac{\alpha^4}{256}}. \quad (4.22)$$

In order to form a DNA repressor loop, when the repressor is bound to one operator site, it must bind to the other operator site before it unbinds from the first one. The unbinding rates for repressors with j inducers bound to them are w_{4-j} (see Table 2.1), whereas the looping rate is c . Thus, the probability of forming a repressor-DNA loop with j inducers bound is proportional to $r_j \frac{c}{c+w_{4-j}}$. Normalizing to get the probabilities we have,

$$\hat{r}_j = \frac{r_j \frac{c}{c+w_{4-j}}}{\sum_{j=0}^4 r_j \frac{c}{c+w_{4-j}}}. \quad (4.23)$$

Then, the repressor unbinding rate is given by the expectation value,

$$\eta = \left(\sum_{j=0}^4 \hat{r}_j \tau_j \right)^{-1}. \quad (4.24)$$

In Eq. (4.24), the residence times $\{\tau_j\}$ and the probabilities $\{\hat{r}_j\}$ are functions of the number of inducers in the cell, which in turn is a function of number of pump proteins and external inducer concentration. At a fixed number of pumps, an equilibrium between inducer import and inducer dilution through cell growth is established. The mean number of inducers I can then be written as a function of pump number Y , see Table 2.1,

$$I(Y) = \frac{m}{\varphi} \frac{E}{E_h + E} Y, \quad (4.25)$$

where φ is the dilution rate, m is the rate of inducer import per pump, E_h is the Michaelis constant which we use as a fitting parameter (see Section 2.2).

Equations (4.24) and (4.25) jointly establish a relationship between the number of pumps and the repressor dissociation rate. This is an effective rate, which results from inducers

repeatedly binding/unbinding from repressors and influencing the residence time of repressors on the regulatory region. Equations (4.24) and (4.25) quantify the amount of feedback in the *lac*-pathway: The more pumps there are, the faster the *lac*-repressor will unbind from the regulatory region, enabling the production of further pumps. In Fig. 4.5 we compare the results from Equations (4.24) and (4.25) for the effective dissociation rate to the rate at which repressors unbind from the regulatory region in simulations of the detailed mechanistic model and find very good agreement. This effective repressor dissociation rate will be used below as the rate at which the *lac*-operon turns from the transcriptionally inactive to the active state, which enters the diffusion model of the pump numbers.

4.3. Calculating the binding rate β

It is clear from the discussion above that repressors with different numbers of inducers bound to them have very different probabilities of forming a repressor-DNA loop, since the rates w_{4-j} are very different for different values of j . For R repressors present in the cell, the rate at which a repressor-DNA loop might form is given by,

$$\beta = gR \sum_{j=0}^4 r_j \frac{c}{c + w_{4-j}}, \quad (4.26)$$

where g is the rate of a repressor finding its binding site on DNA. The quantity $R \sum_{j=0}^4 r_j \frac{c}{c + w_{4-j}}$ could be interpreted as the “effective” number of repressors in the cell. The $\{r_j\}$ are functions of pump numbers and external inducer concentration, and thus we can compute $\beta(Y, E)$ for any pump numbers Y and inducer concentration E .

4.4. Modelling pump dynamics with β and η

Pump protein dynamics are overwhelmingly influenced by the binding and unbinding of the repressor to DNA, where it forms a repressor DNA loop (see Figure 4.2) and completely suppresses transcription of the *lac*-genes. We can thus ignore the

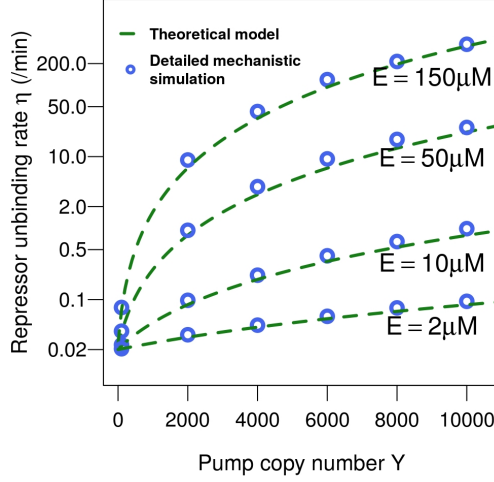


Figure 4.5: Rate of repressor dissociation from the operator.

This figure shows the rate of repressor dissociation from the regulatory region at different copy numbers of the pumps. Pump numbers affect the dissociation rate via the number of inducers, as an inducer-bound repressor dissociates quickly from the regulatory region. Blue circles show the dissociation rate under the detailed mechanistic model, the green line shows the results of equations (4.24) and (4.25) without any parameter fitting. *This figure is reproduced from published work by the author [2].*

complexities of the DNA-repressor loop formation and breakage, and use the effective unbinding rate η and binding rate β as functions of pump numbers Y and the external inducer concentration E to represent the rates of transition between two states of the *lac*-system in which the genes are expressed and repressed respectively. With this approximation and using these effective rates, we can write the master equations for pump protein dynamics in terms of operator fluctuations.

We start with a master equation for protein production with repressors binding and unbinding from the operator at rates β and η respectively [9]. This is a standard model of gene regulation; later we will add the dependencies of β and η on repressor numbers and inducer numbers which are specific to the *lac*-pathway. $p_Y^0(t)$ denotes the probability that the *lac*-genes are transcriptionally inactive (the operator is bound by a repressor, a state denoted **O**), and there are Y pump proteins in the cell, while $p_Y^1(t)$ denotes the probability that the *lac*-genes are transcriptionally active (the operator is free of a repressor; state **I**) and there are Y pump proteins in the cell. The master equation of this process is,

$$\frac{dp_Y^0}{dt} = -(Y\varphi + \bar{\xi} + \eta) p_Y^0 + (Y+1)\varphi p_{Y+1}^0 + \bar{\xi} p_{Y-1}^0 + \beta p_Y^1 \quad (4.27)$$

$$\frac{dp_Y^1}{dt} = -(Y\varphi + \xi + \beta) p_Y^1 + (Y+1)\varphi p_{Y+1}^1 + \xi p_{Y-1}^1 + \eta p_Y^0, \quad (4.28)$$

where ξ and $\bar{\xi}$ are the effective pump protein production rates when the operator is free of repressors and bound to a repressor respectively, η and β have been computed in previous sections, and the other rates are given in Table 2.1. Then, using Table 2.1, we can write

$$\xi = \frac{c^Y}{\phi} l^Y = 180/\text{min}, \quad (4.29)$$

$$\bar{\xi} = 0, \quad (4.30)$$

where c^Y is the transcription rate, ϕ is the rate of mRNA degradation and l^Y is the translation rate.

4.4.1. Deriving the Fokker-Planck equation for pump proteins

Operator fluctuations happen much faster than the time scale of switching since the induced state is very stable compared to repressor binding and unbinding rates (see Table 2.1), and the number of pump proteins in the induced state is large enough that the discreteness in pump dynamics can be ignored. These approximations (detailed below) help us go from the discrete master equation to the continuous Fokker-Planck equation. In order to derive the Fokker-Planck equation corresponding to equations (4.27) and (4.28), we follow the framework introduced by Kepler and Elston in [9]. First, we cast equations in a more tractable form. Let us denote the operator state by $s \in \{0, 1\}$, with 0 being the state when the repressor is bound to DNA, while 1 denotes the state when DNA is free of repressor. Let \hat{s} denote the other state from s . Let $K = \eta + \beta$ be the sum of the effective DNA-repressor binding and unbinding rates, while $k_0 = \frac{\eta}{K}$ and $k_1 = \frac{\beta}{K}$. To make the notation uniform, denote the protein production rate when repressor is bound by ξ_0 and the protein production rate when repressor is unbound by ξ_1 . Then, equations (4.27) and (4.28) can be written as,

$$\begin{aligned} \frac{dp_Y^s}{dt} = & \varphi [(Y+1)p_{Y+1}^s - Yp_Y^s] + \xi_s(p_{Y-1}^s - p_Y^s) \\ & + K [k_s p_Y^{\hat{s}} - k_s p_Y^s] \text{ for } s \in \{0, 1\}. \end{aligned} \quad (4.31)$$

There are two approximations needed in order to derive a single Fokker-Planck equation for this system:

1. The fast-operator-fluctuation approximation: We assume that the time scale for operator fluctuations (given by K^{-1}) is much shorter than the time scale for protein number evolution. This enables us to combine the two coupled equations (4.31) into a single master equation.
2. The diffusion approximation to the master equation: As outlined and illustrated in Section 1.2.6.1 of the introductory chapter, we can assume that pump numbers are large compared to jumps in pump numbers, and so re-write the master equation in terms of an exponential translation

operator, and then truncate the expansion of this operator at the second order to derive a Fokker-Planck equation corresponding to the master equation.

We now proceed to make these two approximations in turn to derive the Fokker-Planck equation.

4.4.1.1. The fast operator approximation

Let us consider the marginal distribution, and the difference distribution,

$$p_Y = p_Y^0 + p_Y^1, \quad (4.32)$$

$$q_Y = k_0 p_Y^0 - k_1 p_Y^1. \quad (4.33)$$

Equations (4.32) and (4.33) imply,

$$p_Y^1 = k_0 p_Y - q_Y, \quad (4.34)$$

$$p_Y^0 = k_1 p_Y + q_Y. \quad (4.35)$$

Using equations (4.32)-(4.35), we can re-write the master equations (4.31) in terms of p_Y and q_Y ,

$$\begin{aligned} \dot{p}_Y = & (\xi_0 k_1 + \xi_1 k_0)(p_{Y-1} - p_Y) + \varphi[(Y+1)p_{Y+1} - Yp_Y] \\ & + (\xi_0 - \xi_1)(q_{Y-1} - q_Y), \end{aligned} \quad (4.36)$$

$$\begin{aligned} \dot{q}_Y = & -Kq_Y + (k_0 \xi_0 + k_1 \xi_1)(k_0 - k_1)(q_{Y-1} - q_Y) \\ & + \varphi(k_0 - k_1)^2[(Y+1)q_{Y+1} - Yq_Y] \\ & + k_0 k_1 (\xi_1 - \xi_0)(p_{Y-1} - p_Y). \end{aligned} \quad (4.37)$$

The fast operator approximation can be made when K is larger than the other rates in the system. Noting that k_1 and k_0 are both small when K is large, we can ignore all the q terms in the LHS of Eq. (4.37) not multiplied by K can be ignored. This gives us an equation for q_Y in terms of the p_Y when $\dot{q}_Y = 0$,

$$q_Y = \frac{k_0 k_1}{K} (\xi_1 - \xi_0)(p_{Y-1} - p_Y). \quad (4.38)$$

We can then use substitute for q_Y and q_{Y-1} in equation (4.36) to obtain the following approximate equation for p_Y ,

$$\begin{aligned} \dot{p}_Y &= (\xi_0 k_1 + \xi_1 k_0)(p_{Y-1} - p_Y) + \varphi[(Y+1)p_{Y+1} - Yp_Y] \\ &\quad + \frac{1}{K} k_0 k_1 (\xi_0 - \xi_1)^2 (p_{Y-2} - 2p_{Y-1} + p_Y). \end{aligned} \quad (4.39)$$

Next, we apply the diffusion approximation (also known as the expansion of the master equation) to derive the corresponding Fokker-Planck equation.

4.4.1.2. The diffusion approximation

Since $Y \gg 1$, and so $(Y+1) \approx Y$, we can use the diffusion approximation to treat pump numbers as continuous as outlined in the introductory chapter in Section 1.2.6.1. Replacing the time derivative with a partial derivative, and let Y now denote the continuous variable corresponding to the integer valued variable (the meaning is always clear from the context), we first re-write the master equation (4.39) in terms of the translation operator E to give

$$\begin{aligned} \partial_t p(Y, t) &= [E^{-1} - 1](\xi_0 k_1 + \xi_1 k_0)p(Y, t) + [E^1 - 1]\varphi Y p(Y, t) \\ &\quad + [E^{-2} - 2E^{-1} + 1]\frac{1}{K} k_0 k_1 (\xi_0 - \xi_1)^2 p(Y, t). \end{aligned} \quad (4.40)$$

Now, we can take a naive expansion of the translation operator up to second order (as illustrated in the Introduction, Section 1.2.6.1) to obtain

$$\begin{aligned} \partial_t p(Y, t) &= \left[1 - \partial_Y + \frac{1}{2} \partial_Y^2 - 1 \right] (\xi_0 k_1 + \xi_1 k_0)p(Y, t) \\ &\quad + \left[1 + \partial_Y + \frac{1}{2} \partial_Y^2 - 1 \right] \varphi Y p(Y, t) \\ &\quad + \left[1 - 2\partial_Y + \frac{4}{2} \partial_Y^2 - 2 + 2\partial_Y - \frac{2}{2} \partial_Y^2 + 1 \right], \end{aligned} \quad (4.41)$$

which simplifies to

$$\begin{aligned} \partial_t p(Y, t) = \partial_Y \left[\underbrace{\varphi Y - (\xi_0 k_1 + \xi_1 k_0)}_{-A_Y(Y)} \right] p(Y, t) \\ + \frac{\partial_Y^2}{2} \left[\underbrace{(\xi_0 k_1 + \xi_1 k_0) + \varphi Y + \frac{2}{K} k_0 k_1 (\xi_0 - \xi_1)^2}_{B_Y(Y)} \right] p(Y, t). \end{aligned} \quad (4.42)$$

Equation (4.42) is the Fokker-Planck equation for pump protein dynamics as defined by equations (4.27) and (4.28). We can read off the drift term $A(Y)$ and $B(Y)$ from equation (4.42). To obtain the drift and diffusion coefficients more explicitly in terms of the parameters of the *lac*-operon and the effective rates we have derived in previous sections, we substitute for $K = \eta + \beta$, $k_0 = \eta/K$, $k_1 = \beta/K$, $\xi_0 = \bar{\xi} = 0$ and $\xi_1 = \xi$ to obtain,

$$A_Y(Y) = \frac{\eta}{\eta + \beta} \xi - \varphi Y, \quad (4.43)$$

$$B_Y(Y) = \frac{\eta}{\eta + \beta} \xi + \varphi Y + 2 \frac{\eta \beta}{(\eta + \beta)^3} \xi^2, \quad (4.44)$$

see Table 2.1 for details of the parameters. In Figure 4.6, we compare the theoretical drift and diffusion given by equations (4.43)-(4.44) and find that our effective theory describes the results from simulation very well.

4.4.2. Simulating drift and diffusion of pump proteins

In order to compare the theoretical expressions for drift and diffusion with the simulation (as shown in Figure 4.6), we simulate a large number of cells starting from the same protein number (having given other quantities time to settle into their equilibrium values with protein values held constant) for 1 minute, and measure the resulting value of the pump protein. The mean of the differences between the start and end points gives us drift (shown in the upper panel of Figure 4.6) whereas the square root of the second moment of the displacement in pump proteins gives us an estimate of the diffusion coefficient $D = \langle \delta Y^2 \rangle / 2t$, where t is the time for which the system is simulated and δY the displacement in pump numbers in that time.

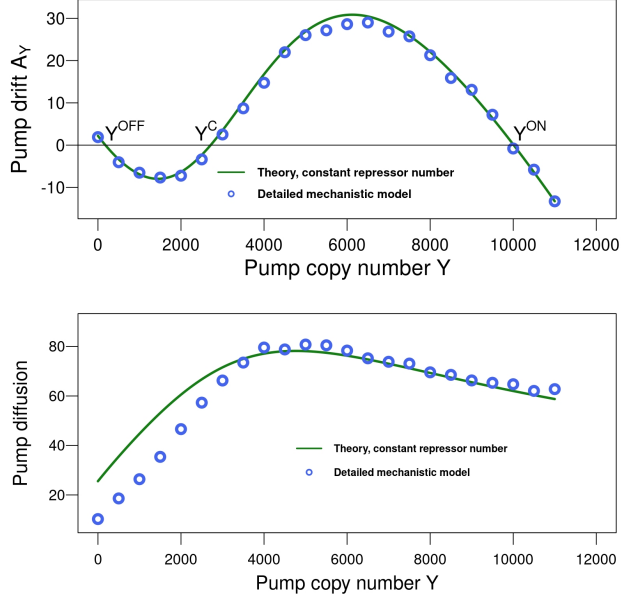


Figure 4.6: Protein drift and diffusion. With repressor numbers held constant, protein dynamics can be approximated by a univariate Fokker-Planck equation, Eq. (4.42). In the top panel, we plot the drift for pump proteins in simulations of our detailed mechanistic model of the *lac*-operon (at an external inducer concentration of $15\mu\text{M}$ where the system is still bi-stable) along with the theoretical drift term from our calculations, Eq. (4.43) (without any parameter fitting). We observe a very good match between the detailed mechanistic model and the results of (4.43). The points of zero drift, Y^{ON} and Y^{OFF} , represent the stable points of the induced and uninduced states respectively, while Y^C is the separatrix between them. In the panel below, we plot the diffusion from simulations of our detailed mechanistic model along with the theoretical diffusion obtained from from Eq. (4.44). The agreement is good at intermediate and high pump copy numbers, while at low pump copy numbers some discrepancy arises. *This figure is reproduced from published work by the author [2].*

4.5. Modelling repressor dynamics

Apart from operator fluctuations and repressor-inducer interactions, fluctuations in repressor numbers also play a role in the transition to the uninduced state. In this section, we make a simple approximation to build an analogy between the repressor system and the equations for gene product production described in Section 4.4. The *lacI* gene is expressed constitutively, but from Table 2.1 we see that transcription is much slower (rate $c^R = 0.1336/\text{min}$) than translation (rate $l^R = 3.33/\text{min}$). For analytical tractability, we make the assumption that only one mRNA molecule corresponding to the LacI protein exists in the cell at any given moment, however to account for the rare occasions when there are 2 mRNA molecules present, we modify the translation rate to

$$\hat{l}^R = l^R \left(1 + \frac{c^R}{c^R + \phi} \right), \quad (4.45)$$

ignoring higher order terms that reflect more than 2 mRNA molecules present. The system thus has two states, one with 0 mRNA molecules and one with a single mRNA molecule present translating LacI at the rate \hat{l}^R . The master equations for the dynamics of LacI can be written as,

$$\begin{aligned} \frac{dp_{\text{LacI}}^0}{dt} = & -(\text{LacI}\phi + c^R) p_{\text{LacI}}^0 \\ & + (\text{LacI} + 1)\phi p_{\text{LacI}+1}^0 + \phi p_{\text{LacI}}^1, \end{aligned} \quad (4.46)$$

$$\begin{aligned} \frac{dp_{\text{LacI}}^1}{dt} = & -(\text{LacI}\phi + \hat{l}^R + \phi) p_{\text{LacI}}^1 \\ & + (\text{LacI} + 1)\phi p_{\text{LacI}+1}^1 + \hat{l}^R p_{\text{LacI}-1}^1 + c^R p_{\text{LacI}}^0, \end{aligned} \quad (4.47)$$

where the transition from $0 \rightarrow 1$ happens at the transcription rate c^R , whereas the transition from $1 \rightarrow 0$ happens at the rate of mRNA degradation $\phi = 0.6666/\text{min}$. Thus, making the approximation that there is only one mRNA molecule that can produce the LacI protein at any moment has enabled us to express the system in terms exactly analogous to the system described in Section 4.4.1.

Proceeding along exactly the same lines as in Section 4.4.1, we can derive the drift and diffusion coefficients for the Fokker-Planck

equation corresponding to the master equations (4.46) and (4.46) which describe repressor dynamics in the approximation that the transcription rate is much lower than the transcription rate, so there is only one repressor mRNA in the cell at any given time. The drift and diffusion coefficients obtained are

$$A(\text{LacI}) = \frac{\hat{l}^R c^R}{(c^R + \phi)} - \text{LacI}\phi, \quad (4.48)$$

$$B(\text{LacI}) = \frac{\hat{l}^R c^R}{(c^R + \phi)} + \text{LacI}\phi + 2 \frac{c^R \phi}{(c^R + \phi)^3} (\hat{l}^R)^2. \quad (4.49)$$

In equations (4.48) and (4.49), LacI numbers are taken to be continuous. This makes it easy to recover the dynamics of repressor molecules (which consist of 4 LacI molecules) which can be treated as being produced at a rate $(s \cdot \hat{l}^R)$ while still being diluted at the same rate ϕ , where the smoothening factor $s = 1/4$. Substituting for \hat{l}^R in equations (4.48) and (4.49) and taking into account the smoothening factor, we can write down the drift and diffusion for repressor dynamics,

$$A_R(R) = s \frac{\hat{l}^R \left(1 + \frac{c^R}{c^R + \phi}\right) c^R}{(c^R + \phi)} - R\phi, \quad (4.50)$$

$$B_R(R) = s \frac{\hat{l}^R \left(1 + \frac{c^R}{c^R + \phi}\right) c^R}{(c^R + \phi)} + R\phi + 2s^2 \frac{c^R \phi}{(c^R + \phi)^3} \left(\hat{l}^R \left(1 + \frac{c^R}{c^R + \phi}\right) \right)^2. \quad (4.51)$$

The steady state distribution is then given by the standard result for Fokker-Planck equations (see [7, 8] for details),

$$p(R) = \frac{C}{B_R(R)} \exp\left(\frac{1}{2} \int_0^R \frac{A_R(r)}{B_R(r)} dr\right), \quad (4.52)$$

where C is a normalization constant.

In Figure 4.7 we compare the theoretical distribution given by Eq. (4.52) to the distribution observed in simulation.

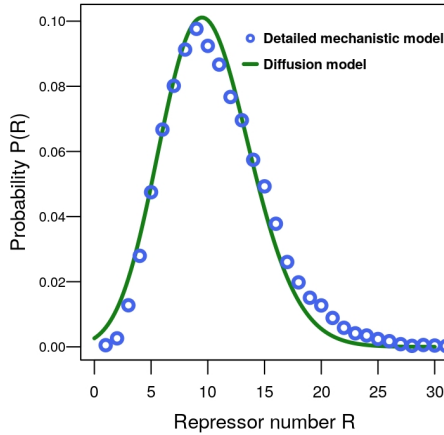


Figure 4.7: Distribution of repressor numbers. Repressor number fluctuate since the *lacI*-gene is expressed at such low levels that typically there are none or one copy of *lacI*-mRNA in the cell. Green lines show the probability distribution function from the diffusion model defined by drift (4.50) and diffusion (4.51), blue circles give the corresponding quantities observed in the detailed mechanistic model. *This figure is reproduced from published work by the author [2].*

4.6. Computing the MFPT, results

Having obtained the Fokker-Planck equations for pumps and repressors, we can compute the mean first passage time to the uninduced state. Drift and diffusion of the pump numbers given by equations (4.43) and (4.44) depend on the repressor unbinding rate η and the binding rate β . The unbinding rate depends on the pump copy number via equations (4.24) and (4.25), and the binding rate fluctuates along with the number of repressors given by equations (4.50) and (4.51). These results specify how drift and diffusion of the protein numbers Y and the repressor numbers R depend on each other. The bivariate Fokker-Planck equation (4.53) defined by this drift and diffusion thus couples the stochastic dynamics of protein numbers Y and the repressor numbers R ,

$$\begin{aligned} \partial_t p(Y, R) = & -\partial_Y A_Y p(Y, R) + \frac{1}{2} \partial_Y^2 B_Y p(Y, R) \\ & - \partial_R A_R p(Y, R) + \frac{1}{2} \partial_R^2 B_R p(Y, R). \end{aligned} \quad (4.53)$$

4.6.1. Mean first passage times from the induced to the uninduced state

Starting in the induced state, with pump number Y set equal to $Y^{\text{ON}} = 10^4$, the transition to the uninduced state occurs when the number of pump proteins reaches the vicinity of the zero-drift point defining the uninduced state Y^{OFF} , with $\mathcal{O}(100)$ pump proteins. In the absence of repressor fluctuations, the dynamics of the number of pump protein can be described by the univariate Fokker-Planck equation Eq. (4.42). The values of the protein numbers where the drift Eq. (4.43) equals zero, Y^{ON} and Y^{OFF} , are the stable fixed points of the Fokker-Planck equation in the noiseless (deterministic) limit. In the presence of noise, they correspond to the long-lived induced and uninduced states respectively, while Y^{C} corresponds to the separatrix between them (the unstable fixed point, see Figure 4.6). Such a visualization of the stationary points in terms of zeros of a closed-form drift function is not possible for dynamics of pump proteins in the presence of repressor fluctuations. In this case, the dynamics of the system is described by the two-dimensional

Fokker-Plank equation (4.53). The mean first passage (MFP) time Γ from one stable fixed point (Y^{ON}) to another (Y^{OFF}) can still be calculated based on the backward Fokker-Planck equation (see [9, 7] and Section 1.2.7 for details),

$$-1 = A_Y \partial_Y \Gamma + \frac{1}{2} B_Y \partial_Y^2 \Gamma + A_R \partial_R \Gamma + \frac{1}{2} B_R \partial_R^2 \Gamma, \quad (4.54)$$

subject to the boundary conditions

$$\Gamma(Y^{\text{OFF}}) = 0, \quad (4.55)$$

$$\left. \frac{d\Gamma}{dt} \right|_{Y^{\text{ON}}} = 0. \quad (4.56)$$

These boundary conditions state that mean first passage time is 0 when the dynamics starts already at the destination Y^{OFF} , while near the induced state Y^{ON} , the first passage time is insensitive to small perturbations in the starting point. Inducer numbers in the cell at start and end points do not affect the first passage time since they quickly reach the steady state determined by the number of pump proteins given by Eq. (4.25).

To determine the mean first passage time, we solve the differential equation for the mean first passage time ((4.54)) numerically. Fig. 4.8 shows the results as a function of the external inducer concentration. We compare the first passage times to the uninduced state obtained from Eq.((4.54)) to simulations of the detailed mechanistic model and find a good match between the diffusion model and the detailed mechanistic model. We find that the mean first passage time increases exponentially with external inducer concentration once the induced state is viable. As a result, for concentrations larger than approximately $10\mu\text{M}$, the induced state is extraordinarily stable, with mean-first passage times exceeding 10^9 minutes. The induced state can thus persist over many generations, and is actually transmitted more stably to subsequent generations than genetic information: A generation time of 60 min implies a transition rate to the uninduced state of $\mathcal{O}(10^{-7})$ per generation, compared to a point mutation rate of $\mathcal{O}(10^{-6})$ per generation. A similar situation has been found in the dormant state of the λ -phage [63].

On the other hand, at external inducer concentrations below $5\mu\text{M}$, there is no long-lived induced state, as the lactose that can be imported at such low external concentrations is not sufficient to deactivate all repressors and sustain an induced state. Thus, even if initial pump numbers are large, they quickly decay and the cells collectively transition to the uninduced state. This dynamics has been called a ‘ballistic transition’ [20].

Fluctuations in the number of repressors contribute in different ways to the transition to the uninduced state. Performing simulations of the detailed mechanistic model at constant number of repressors (with repressor number equal to their mean $R = 10$ under the full model), increases the mean first passage time significantly at high inducer concentrations. Higher-than-average repressor numbers lead to long periods where the *lac*-genes are transcriptionally silenced, making it easier for the pump number to reach lower levels, which can effectively lower the barrier to be crossed by diffusion.

4.6.2. Comparison with experiments

Due to the long mean-first-passage time, the transition to the uninduced state is challenging to observe experimentally. Specifically, the rapid increase of the MFPT with external inducer concentration means that the transition can only be observed in a narrow window where the induced state is stable but the MFPT is shorter than time scale over which the experiment is performed. The experiments were performed by Robin A. Sorg in joint work with the author as described in [1]. We found the induced state to be unstable at TMG concentrations below $5\mu\text{M}$, and observed a ‘ballistic collapse’ of the entire cell population to the uninduced state. At concentrations greater than $10\mu\text{M}$, we did not observe any transitions over 8 hours in a population of approximately 10^6 cells, implying that the mean first passage time is greater than 2×10^9 minutes (see Fig 4.8 inset). On the other hand, at an intermediate concentration of $7.5\mu\text{M}$, we did observe transitions to the uninduced state occurring at a rate of $1.08 \times 10^{-3}/\text{min}$. This behavior qualitatively matches the numerical simulations. For a quantitative comparison far higher population sizes of cells would be needed to observe more transitions to the uninduced

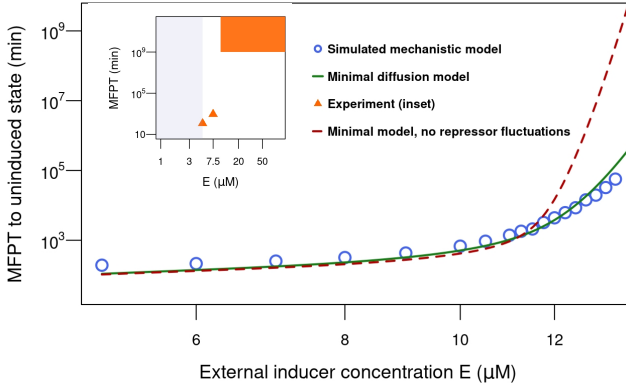


Figure 4.8: Mean first passage times. The mean first passage time starting from the induced state with Y^{ON} pumps to the uninduced state with Y^{OFF} pumps is plotted against the external inducer concentration. The results from the minimal diffusion model (4.54) agree very well with simulations of the detailed mechanistic model (blue circles and green line, respectively). We also show the results from the detailed mechanistic model when repressor numbers are kept constant (red dashed line). Neglecting repressor fluctuations slows down the transition at high inducer concentrations. The super-exponential growth of mean first passage times with external TMG concentration is consistent with observations from our experiments (inset). The transition can only be observed at a concentrations of $5\mu\text{M}$ and $7.5\mu\text{M}$ (estimated MFPT of 117 minutes and 920 minutes respectively, see Section 4.1.1) due to the the first passage times for concentrations above $10\mu\text{M}$ being too high to be observable in our experiments. The duration of our experiments gives a lower bound of $\mathcal{O}(10^9)$ minutes for the mean first passage time (see main text). This lower bound is indicated by the rectangle in the top right of the inset. *This figure is reproduced from published work by the author [2].*

state even when the MFPT is large.

4.7. Summary

In this chapter we examined the transition from the induced to the uninduced state of the *lac*-operon. We first used the smoothening procedure to identify the key fluctuations driving the transition, and then derived effective rates of repressor binding and unbinding to the operator as functions of pump numbers and external inducer concentrations, by formulating mathematical models of appropriate subsystems. We then used these effective rates to build master equations for repressor and pump dynamics, which, in the diffusion approximation, let us compute the Fokker-Planck equation for the evolution of pump and repressor distributions. We then derived the differential equation for the mean first passage time from the backward Fokker-Planck equation, and solved it numerically to obtain the mean first passage time to from the induced to the uninduced state.

4. SWITCHING OFF

5. Discussion

In this thesis, we have presented a comprehensive investigation of the switching behavior of the lactose uptake pathway in *Escherichia coli*, a canonical example of a bi-stable gene regulatory system. By integrating detailed mechanistic modeling with stochastic simulations and quantitative experiments, we have elucidated the key factors governing the transitions between the induced and uninduced states of the *lac*-operon. Our results provide novel insights into the stochastic mechanisms of phenotypic switching and offer a general framework for dissecting the dynamics of multistable gene regulatory systems.

5.1. Identification of rate-limiting fluctuations

A central challenge in understanding the stochastic dynamics of gene regulatory systems is to identify the fluctuations that drive transitions between distinct phenotypic states. Experimentally, this is difficult due to the limited ability to selectively control fluctuations in individual molecular components *in vivo*. In this work, we introduced a computational approach, termed “smoothing”, to systematically modulate the amplitude of fluctuations in different parts of a regulatory network *in silico* [1].

By applying the smoothing procedure to a detailed mechanistic model of the *lac*-system, we identified the repressor-DNA binding and unbinding events as the critical

fluctuations triggering the transition from the uninduced to the induced state. Notably, this transition was found to be insensitive to fluctuations in other cellular components such as mRNA and protein levels. Our finding highlights the importance of the stochastic operator state in driving the phenotypic switch, consistent with single-molecule experiments [6].

The smoothening procedure offers a general and powerful tool to probe the stochastic mechanisms of phenotypic transitions in complex regulatory networks. By selectively suppressing fluctuations in different network components, it allows us to pinpoint the rate-limiting fluctuations without the need for challenging experimental manipulations. Moreover, as the smoothening can be applied to any model component, it is not limited to experimentally accessible quantities such as mRNA or protein numbers, but can also probe the role of fluctuations in molecular conformations, binding states, or reaction rates.

Rate-limiting fluctuations can be highly specific to a particular system and transition. For example, while operator fluctuations drive the *lac*-switch, transitions in other systems have been attributed to fluctuations in mRNA numbers [53], initial protein numbers [54], or gene activity states [56]. This specificity underscores the importance of developing detailed mechanistic models that capture the relevant molecular processes and sources of stochasticity for each system of interest. The smoothening procedure can then be used to systematically identify the rate limiting fluctuations.

5.2. Transition to the induced state

Building upon the identification of repressor-operator binding as the key fluctuation driving the *lac*-switch, we derived an analytic expression Eq. (3.21) for the switching rate from the uninduced to the induced state [1]. This expression relates the switching rate to three key parameters: the rates of repressor binding and unbinding, and a critical time interval that the operator must remain unbound to accumulate sufficient inducer molecules to drive the transition.

The derivation of the analytic switching rate proceeds in two steps. First, we compute the mean time for a single repressor binding-unbinding cycle, conditioned on the operator remaining

unbound for less than the critical time interval. Second, we calculate the mean number of such cycles before a successful transition event, where the operator remains unbound for a time exceeding the critical interval. Combining these two quantities yields a concise expression for the mean first passage time to the induced state, which is inversely related to the switching rate.

Our theory provides a quantitative explanation for the experimentally observed dependence of the switching rate on the external inducer concentration. In particular, it predicts that the logarithm of the switching rate should decrease linearly with the inverse inducer concentration, with a slope determined by the critical time interval and the repressor binding rate. This prediction is in excellent agreement with our experimental measurements, which span several orders of magnitude in both the switching rate and inducer concentration. The derivation of the analytic switching rate illustrates how a complex gene regulatory network can be reduced to a tractable stochastic model that captures its key dynamical features.

5.3. Transition to the uninduced state

While the transition to the induced state is driven primarily by operator fluctuations, the reverse transition from the induced to the uninduced state involves a more complex interplay of multiple stochastic processes. By applying the smoothening procedure to our mechanistic model, we found that fluctuations in repressor-DNA binding, repressor numbers, and inducer-repressor interactions all contribute significantly to the transition dynamics [2].

To model this multi-dimensional stochastic process, we first derived effective rates of repressor binding and unbinding that depend on the regulatory state of the cell and the intracellular inducer concentration. These effective rates capture the feedback between the repressor and inducer dynamics: repressor binding inhibits inducer import, while inducer binding promotes repressor unbinding. By averaging over the fast timescales of inducer-repressor association and dissociation, we obtained a simplified model of the inducer-repressor dynamics that retains the essential features of the feedback loop.

We derive the master equation for pump production and dilution

using the effective binding and unbinding rates calculated earlier, and use the fast operator fluctuation and diffusion approximations to derive the Fokker-Planck equation for pump dynamics. To model repressor number dynamics, we use the fact that translation rates are much larger than transcription rates of the LacI protein, enabling us to make the approximation that there at most one mRNA for LacI at an given time. This enables us to derive the Fokker-Planck equation for the repressor numbers in the cell in a manner exactly analogous to pump numbers. We combine these equations to derive the 2D Fokker-Planck equation for repressor and pumps.

Using the backward Fokker-Planck equation, we derive the differential equation for mean first passage time and solving it numerically, we obtained predictions for the stability of the induced state as a function of the external inducer concentration. Our results show that the mean lifetime of the induced state grows super-exponentially with the inducer concentration, reaching values of 10^9 minutes or more for modest inducer levels. This extreme stability, exceeding the typical timescale of cell division, suggests that the induced state of the *lac*-system can function as a robust form of cellular memory.

The analysis of the transition to the uninduced state highlights the complex, multi-dimensional nature of phenotypic switching in gene regulatory networks. Unlike the transition to the induced state, which is driven by a single rate-limiting step (operator unbinding), the reverse transition involves the concerted action of multiple stochastic processes.

5.4. Experimental tests of the theory

A key strength of our approach is the close integration of theoretical modeling with quantitative experiments. Throughout this work, we have sought to test our models and predictions against measurements of the switching dynamics at the single-cell level. To this end, we used fluorescent reporters and flow cytometry to track the stochastic transitions between the uninduced and induced states over a wide range of inducer concentrations [1, 2].

For the transition to the induced state, our experiments provide a stringent test of the analytic switching rate expression.

By measuring the fraction of cells that remain in the uninduced state as a function of time, we estimated the switching rate for inducer concentrations spanning several orders of magnitude. The resulting data show excellent agreement with the theoretical predictions, both in terms of the absolute switching rates and their dependence on the inducer concentration. This agreement validates the key assumptions underlying our model, such as the identification of operator unbinding as the rate-limiting step and the role of inducer accumulation in driving the transition.

In the case of the reverse transition to the uninduced state, the extremely long predicted lifetimes of the induced state pose a challenge for direct experimental verification. For inducer concentrations above a critical threshold, our model predicts mean switching times that far exceed the typical duration of an experiment. Nevertheless, by measuring the stability of the induced state over a limited range of sub-threshold inducer concentrations, we were able to place lower bounds on the switching times that are consistent with the theoretical predictions. Further experiments with larger populations of cells and longer observation times could help to quantify these slow switching rates more precisely.

5.5. Conclusions and outlook

In conclusion, this thesis presents a comprehensive theoretical and experimental investigation of the stochastic dynamics of the *lac*-gene regulatory network. By combining detailed mechanistic modeling with novel computational methods and quantitative experiments, we have elucidated the key factors governing the transitions between alternative phenotypic states. Our results provide new insights into the molecular mechanisms of phenotypic variability and the design principles of multistable gene regulatory systems.

The smoothening procedure introduced in this work offers a general and powerful tool for identifying the rate-limiting fluctuations in complex regulatory networks. By selectively modulating the amplitude of fluctuations *in silico*, this approach allows us to dissect the stochastic mechanisms of phenotypic transitions without the need for challenging experimental

perturbations. As the smoothening can be applied to any model component, it could be used to probe the role of fluctuations in a wide range of cellular processes, from gene expression and signal transduction to metabolism and cell fate decisions.

Moreover, our analytic theory for the switching dynamics illustrates how complex regulatory networks can be reduced to tractable stochastic models based on their rate-limiting fluctuations. The key steps in this approach are (i) identifying the relevant molecular species and reactions through smoothening, (ii) deriving effective transition rates that capture the essential feedback loops, and (iii) formulating a simplified stochastic process that reproduces the dynamics of the original system. This strategy could be generalized to other multistable networks, providing a systematic way to derive coarse-grained models of phenotypic variability.

Finally, the *lac*-operon with its well-characterized molecular components provides an ideal platform for the rational design of synthetic gene circuits with desired stochastic properties. Our quantitative understanding of the switching dynamics could guide the engineering of novel regulatory architectures with customized noise characteristics, memory timescales, and sensitivity to environmental signals. Such endeavors will not only advance our understanding of the fundamental principles of gene regulation, but also open new avenues for the control and exploitation of biological variability in biotechnology and medicine.

A. Appendix: Experiments

The experiments described here were performed by Robin A. Sorg in the group of J. W. Veening, and have been published in joint work with the present author [1]. We include a description of them here for convenience and completeness.

A.1. Determining phenotypic switching rates

To assess expression of the *lac* genes at the single-cell level we used flow cytometry on a population of *E. coli* strain CH458, which contains a *gfp-cat* cassette inserted downstream of the *lac*-operon [39]. To determine the switching rate from the uninduced to the induced state, cells were first grown overnight for approximately 12 generations in the absence of the inducer (TMG). Then cells were adapted to a state of steady state exponential growth by re-diluting the growth culture to optical density (OD) 0.04 every hour for four hours, resulting in the pre-culture. OD values were thus kept in a narrow range between 0.03 and 0.08. Cells from the pre-culture were transferred to media with different inducer concentrations and cultivated in constant conditions of exponential growth. Cell cultures were diluted by a factor 2 per hour since the strain CH458 doubled in 60 minutes under our experimental conditions. See [1]

for details.

We also looked at the switch from the induced state to the uninduced state, by growing cells overnight and pre-culturing them at an inducer concentration of 250 μM as described above for switching to the induced state. However, the induced state is very stable and we only observed switching to the uninduced state in a very narrow range of low inducer concentrations.

Cell populations were grown at various inducer concentrations between 0 μM and 250 μM . Growth cultures were analyzed by flow cytometry on an hourly basis (additional 0.5 hour steps during the first two hours). For a range of inducer concentrations between 10 μM to 200 μM we found two peaks in the fluorescence distribution of the population, corresponding to the uninduced and to the induced expression state respectively (see Fig. 3.1). The fluorescence intensity distribution measured at different intervals yields the fraction of induced cells at various time points, for each value of external TMG concentration we probed.

A.2. Experimental conditions

We used the non-metabolizable thio-methylgalactoside (TMG) as an inducer. M9 minimal salts supplemented with thiamine, MgSO_4 , CaCl_2 , and casamino acids were chosen as growth medium for the CH458 strain used in our experiments. We used succinate instead of glucose as carbon source to reduce catabolite repression yet maintain sufficient growth. Chloramphenicol (10 $\mu\text{g/ml}$) was added to reduce the risk of contamination during sampling. Plasmid pREP4 (Qiagen) was transformed to strain CH458 using CaCl_2 transformation and selecting for kanamycin resistance, resulting in strain CH458+pREP4.

For rapid and robust optical density (OD) determination, cultures of 2ml were grown in 5ml tubes fitting directly into the spectrophotometer. Overnight cultures were grown at different TMG concentrations for 16 hours (approximately 12 generations) at 37°C while shaking. In the morning, uninduced cells from 0 μM TMG and induced cells from 250 μM TMG were diluted to OD 0.04 and grown in the particular TMG concentration for four additional hours. Cultures were re-diluted every hour to ensure constant exponential growth within a narrow OD range between

0.03 and 0.08. After this adaptation phase, cells were spun down and washed for the change of medium to the desired final TMG concentration. In the following eight hours, samples were taken every hour for measurement and cultures were rediluted as described above to maintain steady state. Fluorescence of individual cells was determined by flow cytometry of 10^5 cells at a time. The fluorescence intensity was measured with a BD FACS Canto Flow Cytometer of BD Bioscience at medium flow with a forward scatter (FSC) of 200V and side scatter (SSC) of 400V. A threshold of 500V was set to exclude recording of particles that are smaller than normal *E. coli* cells. The fluorescence detector FL-1 was set to 800V for a maximal separation of induced versus uninduced cells. We found it crucial to maintain constant growth conditions by dilution to keep intra and extra-cellular parameters stable.

Time-lapse microscopy was carried out by spotting single cells on a M9 polyacrylamide (10%) slide containing TMG inside a Gene Frame (Thermo Fisher Scientific). A Nikon Ti-E microscope equipped with a CoolsnapHQ2 camera and an Intensilight light source was used in an Okolab climate incubator at 37°C. Images with cells expressing the green fluorescent protein (GFP) were taken with the following protocol and filter set: 200ms exposure time for phase contrast and 0.5s exposure for fluorescence at 450-490 nm excitation via a dichroic mirror of 495nm and an emission filter at 500-550 nm. Pictures were taken every 30 minutes.

Bibliography

- [1] P. M. Bhogale, R. A. Sorg, J-W. Veening, and J. Berg. What makes the *lac*-pathway switch: identifying the fluctuations that trigger phenotype switching in gene regulatory systems. Nucleic Acids Research, 42(18):11321-11328, 2014.
- [2] P. M. Bhogale, R. A. Sorg, J-W. Veening, and J. Berg. Switching off: The phenotypic transition to the uninduced state of the lactose uptake pathway. Biophysical Journal, 121:183-192, January 2022.
- [3] B. Müller-Hill. The *lac* Operon: A Short History of a Genetic Paradigm. Walter de Gruyter, 1996.
- [4] A. Novick and M. Weiner. Enzyme induction as an all-or-none phenomenon. PNAS, 43:553-566, 1957.
- [5] E. M. Ozbudak, M. Thattai, H. N. Lim, B. I. Shraiman, and A. van Oudenaarden. Multistability in the lactose utilization network of *Escherichia coli*. Nature, 427:737-740, 2004.
- [6] P. J. Choi, L. Cai, K. Frieda, and X. S. Xie. A stochastic single-molecule event triggers phenotype switching of a bacterial cell. Science, 322(5900):442-446, Oct 2008.
- [7] Crispin W Gardiner. Handbook of stochastic methods, volume 3. Springer Berlin, 1985.
- [8] N.G. van Kampen. Stochastic Processes in Physics and Chemistry. Elsevier Science Publishers, Amsterdam, 1992.

- [9] T. B. Kepler and T. C. Elston. Stochasticity in transcriptional regulation: origins, consequences, and mathematical representations. Biophys. J., 81(6):3116–3136, 2001.
- [10] Irina Smirnova, Vladimir Kasho, Junichi Sugihara, and H. Ronald Kaback. Opening the periplasmic cavity in lactose permease is the limiting step for sugar binding. PNAS, 108(37):15147–15151, September 2011.
- [11] P. C. Maloney and T. H. Wilson. Quantitative aspects of active transport by the lactose transport system of *Escherichia coli*. Biochim. Biophys. Acta, 330(2):196–205, 1973.
- [12] A. Kepes. Kinetic studies on galactoside permease of *Escherichia coli*. Biochim. Biophys. Acta, 40:70–84, 1960.
- [13] B. Volkmer and M. Heinemann. Condition-dependent cell volume and concentration of *Escherichia coli* to facilitate data conversion for systems biology modeling. PLOS One, 6(7), 2011.
- [14] H. E. Kubitschek and J. A. Friske. Determination of bacterial cell volume with the Coulter counter. J. Bacteriol., 168(3):1466–1467, 1986.
- [15] B. Müller-Hill, L. Crapo, and W. Gilbert. Mutants that make more *lac* repressor. PNAS, 59:1259–1264, 1968.
- [16] M. Brenowitz, N. Mandal, A. Pickar, E. Jamison, and S. Adhya. DNA-binding properties of a *lac* repressor mutant incapable of forming tetramers. J. Biol. Chem., 266(2):1281–1288, 1991.
- [17] X. S. Xie, P. J. Choi, G-W. Li, N. K. Lee, and G. Lia. Single-molecule approach to molecular biology in living bacterial cells. Annual Review of Biophysics, 37:417–444, 2008.
- [18] M. Dunaway, J. S. Olson, J. M. Rosenberg, O. B. Kallai, R. E. Dickerson, and K. S. Matthews. Kinetic studies of inducer binding to *lac* repressor-operator complex. J. Biol. Chem., 255(21):10115–10119, 1980.
- [19] J. Elf, G. W. Li, and X. S. Xie. Probing transcription factor dynamics at the single-molecule level in a living cell. Science, 316(5828):1191–1194, 2007.

- [20] J. T. Mettetal, D. Muzzey, J. M. Pedraza, E. M. Ozbudak, and A. van Oudenaarden. Predicting stochastic gene expression dynamics in single cells. PNAS, 103(19):7304–7309, 2006.
- [21] E. Roberts, A. Magis, J. O. Ortiz, W. Baumeister, and Z. Luthey-Schulten. Noise contributions in an inducible genetic switch: a whole-cell simulation study. PLoS Comput. Biol., 7(3):e1002010, 2011.
- [22] M. Stamatakis and K. Zygorakis. Deterministic and stochastic population-level simulations of an artificial *lac* operon genetic network. BMC Bioinformatics, 12:301–318, 2011.
- [23] T. E. Kuhlman and E. C. Cox. Gene location and DNA density determine transcription factor distributions in Escherichia coli. Mol. Syst. Biol., 8:610, 2012.
- [24] J. Sugihara, I. Smirnova, V. Kasho, and H. R. Kaback. Sugar recognition by CscB and LacY. Biochemistry, 50:11009–11014, 2011.
- [25] Irina Smirnova, Vladimir Kasho, Junichi Sugihara, and H. Ronald Kaback. Opening the periplasmic cavity in lactose permease is the limiting step for sugar binding. Proceedings of the National Academy of Sciences, 108(37):15147–15151, 2011.
- [26] D. W. Selinger, R. M. Saxena, K. J. Cheung, G. M. Church, and C. Rosenow. Global RNA Half-Life Analysis in Escherichia coli Reveals Positional Patterns of Transcript Degradation. Genome Research, 13:216–223, 2003.
- [27] Y. Taniguchi, P. J. Choi, G. W. Li, H. Chen, M. Babu, J. Hearn, A. Emili, and X. S. Xie. Quantifying E. coli proteome and transcriptome with single-molecule sensitivity in single cells. Science, 329(5991):533–538, 2010.
- [28] L. Cai, N. Friedman, and X. S. Xie. Stochastic protein expression in individual cells at the single molecule level. Nature, 440(7082):358–362, 2006.
- [29] M. B. Elowitz, A. J. Levine, E. D. Siggia, and P. S. Swain. Stochastic gene expression in a single cell. Science, 297(5584):1183–1186, 2002.

- [30] I. Golding, J. Paulsson, S. M. Zawilski, and E. C. Cox. Real-time kinetics of gene activity in individual bacteria. Cell, 123(6):1025–1036, 2005.
- [31] M. Stamatakis and N. V. Mantzaris. Comparison of deterministic and stochastic models of the *lac* operon genetic network. Biophysical Journal, 96:887–906, 2009.
- [32] R. B. Winter, O. G. Berg, and P. H. von Hippel. The Escherichia coli *lac* repressor-operator interaction: Kinetic measurements and conclusions. Biochemistry, 20:6961–6977, 1981.
- [33] A. M. Khoury, H. J. Lee, M. Lillis, and P. Lu. Lac repressor-operator interaction: DNA length dependence. Biochim. Biophys. Acta, 1087(1):55–60, 1990.
- [34] A. M. Khoury, H. S. Nick, and P. Lu. In vivo interaction of Escherichia coli *lac* repressor N-terminal fragments with the *lac* operator. J. Mol. Biol., 219(4):623–634, 1991.
- [35] D. Colquhoun, K. A. Dowsland, M. Beato, and A. J. Plested. How to impose microscopic reversibility in complex reaction mechanisms. Biophys. J., 86(6):3510–3518, 2004.
- [36] O. G. Berg. A model for the statistical fluctuations of protein numbers in a microbial population. J. Theor. Biol., 71:587–603, 1978.
- [37] C. Gupta, J. M. Lopez, W. Ott, K. Josic, and M. R. Bennett. Transcriptional delay stabilizes bistable gene networks. Phys. Rev. Lett., 111(5):058104, 2013.
- [38] D. T. Gillespie. A general method for numerically simulating the stochastic time evolution of coupled chemical reactions. Journal of Computational Physics, 22:403–434, 1976.
- [39] A. J. Gordon, J. A. Halliday, M. D. Blankschien, P. A. Burns, F. Yatagai, and C. Herman. Transcriptional infidelity promotes heritable phenotypic change in a bistable gene network. PLoS Biol., 7(2):e44, Feb 2009.

- [40] M. Kim, Z. Zhang, H. Okano, D. Yan, A. Groisman, and T. Hwa. Need-based activation of ammonium uptake in *Escherichia coli*. Mol. Syst. Biol., 8:616–626, 2012.
- [41] R. A. Fasani and M. A. Savageau. Molecular mechanisms of multiple toxin-antitoxin systems are coordinated to govern the persister phenotype. Proc. Natl. Acad. Sci. U.S.A., 110(27):E2528–2537, Jul 2013.
- [42] S. D. Santos, R. Wollman, T. Meyer, and J. E. Ferrell. Spatial positive feedback at the onset of mitosis. Cell, 149(7):1500–1513, 2012.
- [43] R. Losick and C. Desplan. Stochasticity and cell fate. Science, 320(5872):65–68, 2008.
- [44] F. J. Isaacs, J. Hasty, C. R. Cantor, and J. J. Collins. Prediction and measurement of an autoregulatory genetic module. Proc. Natl. Acad. Sci. U.S.A., 100(13):7714–7719, 2003.
- [45] W. K. Smits, O. P. Kuipers, and J. W. Veening. Phenotypic variation in bacteria: the role of feedback regulation. Nat. Rev. Microbiol., 4(4):259–271, 2006.
- [46] G. Neuert, B. Munsky, R. Z. Tan, L. Teytelman, M. Khammash, and A. van Oudenaarden. Systematic identification of signal-activated stochastic gene regulation. Science, 339(6119):584–587, 2013.
- [47] H. H. McAdams and A. Arkin. Stochastic mechanisms in gene expression. Proc. Natl. Acad. Sci. U.S.A., 94(3):814–819, 1997.
- [48] E. Kussell, R. Kishony, N. Q. Balaban, and S. Leibler. Bacterial persistence: a model of survival in changing environments. Genetics, 169(4):1807–1814, 2005.
- [49] W. J. Blake, M. Kærn, C. R. Cantor, and J. J. Collins. Noise in eukaryotic gene expression. Nature, 422(6932):633–637, 2003.
- [50] E. Levine and T. Hwa. Stochastic fluctuations in metabolic pathways. Proc. Natl. Acad. Sci. U.S.A., 104(22):9224–9229, 2007.

- [51] J. Paulsson. Summing up the noise in gene networks. Nature, 427(6973):415–418, 2004.
- [52] A. D. Weinberger and L. S. Weinberger. Stochastic fate selection in HIV-infected patients. Cell, 155(3):497–499, 2013.
- [53] H. Maamar, A. Raj, and D. Dubnau. Noise in gene expression determines cell fate in *Bacillus subtilis*. Science, 317(5837):526–529, 2007.
- [54] J. A. Megerle, G. Fritz, U. Gerland, K. Jung, and J. O. Rädler. Timing and dynamics of single cell gene expression in the arabinose utilization system. Biophysical Journal, 95:2103–2115, 2008.
- [55] T. Cagatay, M. Turcotte, M. B. Elowitz, J. Garcia-Ojalvo, and G. M. Süel. Architecture-dependent noise discriminates functionally analogous differentiation circuits. Cell, 139(3):512–522, 2009.
- [56] C. Zong, L. H. So, L. A. Sepulveda, S. O. Skinner, and I. Golding. Lysogen stability is determined by the frequency of activity bursts from the fate-determining gene. Mol. Syst. Biol., 6:440–452, 2010.
- [57] P. J. Johnsen, D. Dubnau, and B. R. Levin. Episodic selection and the maintenance of competence and natural transformation in *Bacillus subtilis*. Genetics, 181(4):1521–1533, 2009.
- [58] M. J. Morelli and P. R. ten Wolde. Reaction Brownian dynamics and the effect of spatial fluctuations on the gain of a push-pull network. J Chem Phys, 129(5):054112, 2008.
- [59] A. M. Walczak, J. N. Onuchic, and P. G. Wolynes. Absolute rate theories of epigenetic stability. PNAS, 102(52):18926–18931, 2005.
- [60] M. J. Morelli, S. Tanase-Nicola, R. J. Allen, and P. R. ten Wolde. Reaction coordinates for the flipping of genetic switches. Biophys. J., 94(9):3413–3423, 2008.

- [61] J. Jaruszewicz, M. Kimmel, and T. Lipniacki. Stability of bacterial toggle switches is enhanced by cell-cycle lengthening by several orders of magnitude. Phys. Rev. E, 89:022710-022720, Feb 2014.
- [62] S. Oehler, E.R. Eismann, H. Krämer, and B. Müller-Hill. The three operators of the lac operon cooperate in repression. The EMBO journal, 9(4):973-9, 1990.
- [63] M. Santillan and M. C. Mackey. Why the lysogenic state of phage lambda is so stable: a mathematical modeling approach. Biophysical Journal, 86(1 Pt 1):75-84, January 2004.

